TIME DOMAIN COMPUTER SIMULATION AND ITS APPLICATIONS TO TRANSIENT EMC PROBLEMS AND VLSI INTERCONNECTION SYSTEMS

by

Xiao-Ding CAI

Supervisor: Dr. G.I.Costache

A thesis
submitted to the School of Graduate Studies and Research
in partial fulfillment of the requirements for the degree of
Doctor of Philosophy

Department of Electrical Engineering
University of Ottawa, Ottawa, Ont. K1N 6N5, Canada

Sep.28, 1994

ISBN 0-612-04896-9

Abstract

The time domain computer simulation presented in this Ph.D. thesis is composed of three parts. The first part is an introduction of a novel finite element formulation in the Laplace domain and its applications to the technical area of electromagnetic compatibility (EMC). The second part presents a new time domain resistance (skin effect) model and its applications to the analysis of VLSI interconnection systems. The applications include two topics: time domain analysis of lossy VLSI interconnects with a time domain skin effect model; and time domain analysis of interconnect discontinuities. In the last part of this thesis, a numerical modelling approach of the partial inductance, which is of great importance in ground noise problems, is provided.

All the analysis models in this thesis are finalized in the time domain, though some of them start in the Laplace domain or space domain. Original contributions are summarized in **Section 1.3**.

Acknowledgements

I wish to express my sincere gratitude to Professor George I. Costache (Chairman, Department of Electrical Engineering, University of Ottawa), Ph.D. thesis supervisor, for providing exceptional supervision throughout the research in the form of technical guidance, thought provoking suggestions to solve practical problems, patience, friendship and generous assistance in any other aspects necessary for the completion of the thesis.

I would also like to thank the thesis examiners who have carefully reviewed the thesis manuscript and made valuable comments. They are: Dr. Satish Kashyap (Electronic Warfare Division, Department of National Defense), Professor Michel Nakhla (Department of Electronics, Carleton University), Professor T.K.Sarkar (Department of Electrical and Computer Engineering, Syracuse University), and Professor D.Gibbons (Department of Electrical Engineering, University of Ottawa).

I am grateful to many of the staff and colleaques in the Department of Electrical Engineering, University of Ottawa, for various technical discussions.

Last but not the least, I would like to mention my family: Mom, Dad (who died with his wish unrealized for my degree), aunt, sister for encouraging education. Most importantly, I wish to thank my wife Hong and son Charles, for their unending support and love.

I hereby declare that I am the sole author of this document. I authorize the University of Ottawa to lend this document to other institutions for the purpose of scholarly research.

Xiao – Ding Cai

I further authorize the University of Ottawa to reproduce this document by photocopying or by any other means, in total or in part, at the request of other institutions or individuals for the purpose of scholarly research.

Xiao – Ding Cai

Contents

List of Figures

List of Tables

Chapter 1

INTRODUCTION

1.1 MOTIVATION

In electrical engineering, numerical modeling or computer simulation has been constantly actively involved in static and dynamic analyses of electromagnetic problems. In regard to the dynamic analysis, which is the most concerned part of this Ph.D. thesis, numerical modeling approaches are traditionally divided into two categories: one in the time domain, and the other in the frequency domain. These two distinct approaches were developed independently, especially in the early years. While appearing as a technical phenomenon, both approaches have had a tendency to be merged in recent years. This tendency has resulted in several new hybrid methods, such as **Transmission Line Matrix (TLM)** method, **Finite Difference Time Domain(FDTD)** method, and some other time domain finite element methods (see **Section1.4**).

One of the major features of these methods mentioned above is that, they provide time domain results in a direct way. Thus, they could be called *time domain methods*. However, most applications of these methods are in the frequency domain, where utilization of the Fast Fourier Transforms (FFT) becomes an indispensable means. In terms of applications, these methods could be considered as *frequency domain methods*. The bridge between the time and frequency domain approaches appears solely to be the FFT, and nothing else whatsoever. (Here, a Laplace domain method is considered to be new and will be excluded from the traditional time/frequency domain methods.)

The methodology adopted in these hybrid approaches follows a special numerical arrangement called the Time-Stepping Schemes (TSS). The TSS features an easy and straightforward realization of time domain results, but suffers from numerical instability and long computing time. On the other hand, to recover frequency domain results with the use of the TSS approach, the FFT algorithm that must be engaged in requires full coverage of the transient process. This full coverage may often result in a large number of time steps. Thus, the ineffeciency of adopting the TSS and FFT is, in general, evident.

To avoid the stability and efficiency problems that are inherently related with the existing numerical methods, a new approach has to be sought. A Laplace domain finite element method (LDFEM), which takes the advantage of many meritorious properties of the Laplace transforms, is proposed here for both diffusion and propagation problems. It is seen that the present method is not restrained by any stability conditions. Hence, the inefficiency that is associated with the stability conditions is evaded by using the LDFEM. The LDFEM is thereupon applied to some transient EMC/EMI problems, where analysis needs to be curried out in either time domain or frequency domain, or in both.

Time domain analysis has another important application area — VLSI interconnection systems. In this technical area, time/frequency dependent distributed parameters have recently become a major concern. Historically, distributed parameters, such as, resistance R, conductance G, inductance L and capacitance C of transmission lines modeled for the interconnects, have long been treated as time/frequency independent ones, or at most as frequency domain models. For instance, the resistance of a transmission line is modeled in proportion to the square root of the frequency. This frequency domain model is restricted by the rise time of signal, which is interpreted in terms of a frequency bandwidth. As the signal speed changes beyond the prescribed bandwidth, the frequency domain model becomes incapable of revealing a real resistance change in the line corresponding to a wider frequency range.

In this thesis, a time domain resistance model is derived for any strip-like conductor with a ground plane by making use of the Laplace transforms. Application of this model to high speed interconnects with multiconductors is presented. Advantages of the present time domain model over conventional frequency domain models are: 1) no frequency limit related to the signal rise time or signal speed; 2) no FFT process and associated problems; and 3) complete suitability to high speed signal analysis.

1.2 STATE OF THE ART OF TIME DOMAIN NUMERICAL SIMULATION

An overview of the development of time domain numerical modeling in the areas of applied electromagnetics and applied mechanics, which is most relevant to the objective of this Ph.D. thesis, is presented here. More detailed review will be provided in **Section1.4** and in the beginning of each Chapter, respectively.

Concerning the finite elements formulated in the Laplace domain, the first literature visible to public could be found in 1982 when K.Miya, M.Uesaka and F.C.Moon solved the vibration problem of toroidal field-coils in mechanical engineering [1]. Then, H.T.Chen, T.M.Chen and C.K.Chen put forward a systematic way of making a hybrid Laplace transform/finite element method in dealing with heat conduction problems [2]. Later, they extended their method from one dimension [2] to three dimensions [3]. It should be noted that their contribution to this hybrid method is limited to diffusion problems in the applications within the field of mechanical engineering. The final numerical results derived with these methods, though formulated in the Laplace domain, are eventually provided in the time domain.

With regard to general finite element analysis, until now, there has not been any published method that could solve both deterministic and eigenvalue problems with only one formulation. Traditionally, these two types of problems are formulated and solved independently. This survey conclusion applies to any finite element method (FEM) in any domain (time or frequency).

In analysis of VLSI interconnections, three approaches could be classified as: A) direct time domain solution, B) frequency-time domain solution, and C) Laplace-time domain solution. The following literature survey will be focused on these three groups.

1.2.1 Direct Time Domain Solution

A typical time domain approach in this area is called the **Method of Characteristics (MoC)** (please see Appendix B), which found its application to the field of electrical engineering in 1967 [4]. Later on, F.Y.Chang [5] and V.Dvorak [6] elaborated this method for more practical circuit applications. Until early the 90's, the MoC had been extended to treat complicated situations that allow nonuniform transmission lines, nonlinear terminations and frequency dependent distributed parameters to be involved in the circuit/network analysis. N.Orhanovic, V.K.Tripathi and P.Wang presented a **Generalized Method of Characteristics** (GMoC) [7] - [9]. J.-F.Mao and Z.-F.Li proposed a hybrid method called the **Method of Convolution – Characteristics** (MCC) [10] to tackle the frequency-dependent losses encountered in the VLSI interconnects. A more general approach similar to the one in [10] was also reported in [8].

1.2.2 Frequency-Time Domain Solution

A.R.Djordjevic, T.K.Sarkar and R.F.Harrington have offered typical solutions in the frequency domain [11] [12]. Other authors have also made contributions to the frequency domain solutions [13]-[15]. To convert their results into the time domain, the Inverse Fast Fourier Transforms (IFFT) must be resorted to.

1.2.3 Laplace-Time Domain Solution

R.Griffith and M.Nakhla presented an alternative method [16] to the above frequency-time domain solution. The modified nodal admittance (MNA) matrix and numerical inversion of Laplace transform (NILT) are adopted in their method, which make their solution more efficient and more accurate than the one with the IFFT. Their method has been improved [17]-[20] since the publication of [16] in 1990.

1.3 PRIMARY ORIGINAL CONTRIBUTIONS

Technical contributions originated in this Ph.D. thesis may attribute to two parts: the major and minor ones. The primary and important contributions are summarized as below:

i. Proposed a dual-domain finite element formulation — **the Laplace Domain Finite Element Method (LDFEM)** for propagation problems, which provides solutions in both time and frequency domains without using the Time-Stepping Schemes (TSS) or Fast Fourier Transforms (FFT). The efficiency and stability of the LDFEM is proved desirably to be better than that of the methods which employ the TSS and FFT.
(to appear in *Int. J. Numer. Model. - Electronic Net. Dev. Fields.*)

ii. Developed a new numerical modeling approach which solves both eigenvalue and deterministic problems in one run without reformulating the problem.
(to appear in *Int. J. Numer. Model. - Electronic Net. Dev. Fields.*)

iii. Explicitly expressed the field value at each node as a function of time in the finite element formulation.
(to appear in *IEEE Trans. on EMC, Nov. 1994 issue.*)

iv. Introduced an efficient approach — **Convolution Method** to handle complicated time domain excitations applied to the Laplace domain finite element formulation.
(to appear in *Int. J. Numer. Model. - Electronic Net. Dev. Fields.*)

v. Analyzed and derived a time domain resistance model for transmission lines modeled as VLSI interconnects with inclusion of ground plane corrections and partial inductances.
(submitted to *IEEE Trans. on Cir. Sys. Pt.I.*)

vi. Modified the **Method of Characteristics – Convolution(MCC)** with time dependent resistance models and applied to high speed interconnects with coupled structures. Called Modified MCC (MMCC).
(submitted to *IEEE Trans. on Cir. Sys. Pt.I.*)

vii. Constructed a mathematical interface between discrete time domain solutions derived from distributed parameters and a lumped RLC circuit. Based on this interface, the transferring voltage and current are both explicitly expressed in the time domain without resorting to the FFT.) (submitted to *1995 SBMO/IEEE MTT-S Int. Mic. Opt. Conf., Brazil.*)

viii. Numerically characterized the Triple-TEM (TTEM) cell in both static and dynamic aspects, and established a CAD guideline for the TTEM cell based on field distributions, characteristic impedance, TE and TM mode cutoff frequencies, and their longitudinal behavior versus frequency. (to appear in *IEEE Trans. on EMC, Nov. 1994 issue.*)

Minor contributions will be indicated in the conclusions of each Chapter.

1.4 RESEARCH BACKGROUND

A brief survey of the literature focusing on the thesis topic has been provided in **Section1.2**. Much broader review of the publications related to the research approach adopted in this thesis needs to be done in such a way that one would understand why the author motivated the two unique objectives (see **Section1.1**) to achieve. In this Section, the review will be provided in two aspects according to the two objectives, respectively :

A. Time domain simulation with a Laplace Domain Finite Element Method and its applications to transient EMC/EMI problems;

B. Time domain analysis of VLSI interconnects with a time dependent skin effect model.

1.4.1 Review of Time Domain Finite Element Methods

There are, in general, three types of the time domain finite element methods (TDFEM): traditional time domain, point-matched and finite volume FEMs.

A. Traditional Time Domain Finite Element Method (TDFEM):

Traditional TDFEM [21]-[26] uses well-established finite element formulation in the space domain and solves the problem in the time domain with time-stepping or time-marching schemes. Typical time-marching schemes include backward difference, Galerkin, Crank-Nicolson and forward difference algorithms, for which different stability conditions are to be satisfied [21].

B. Point-Matched Finite Element Method (PMFEM):

The Point-matched finite element method (PMFEM) is relatively new. The PMFEM was first proposed by A.C.Cangellaris, C.C.Lin and K.K.Mei [27] in 1987. This method combines the simplicity of the explicit integration scheme of the finite-difference time-domain (FDTD) method with the versatility of conventional finite element spatial discretization procedures. The computational domain is discretized using two complementary meshes, one for the electric and the other for the magnetic field, positioned in such a way that an element of each mesh encloses a node of the other. This type of discretization is quite similar to the one used in the FDTD and TLM methods. The major difference between PMFEM and FDTD is that the interpolation function in the space domain is exactly the same as the one employed in the nodal elements. The stability condition for the PMFEM resembles the one for the FDTD method. The usage of the PMFEM is rather less popular for some unknown reason. Quite a few applications can be found in [28]-[31]. It would be interesting if one noticed that the PMFEM has been applied to transmission line analysis [30] [31]. But, again, the stability condition has to be satisfied.

C. Time Domain Finite Volume Method (TDFVM):

The time domain finite volume method (TDFVM) is an alternative way to cope with the time dependent curl equations using the explicit integration technique. This method casts Maxwell's equations in a conservation form, according to the standard computational fluid dynamics procedures. A finite element treatment follows the semi-discrete conservation law form, which essentially relates the time derivatives of the electric and magnetic flux density at the centroid of a grid element to the values of the projections of the magnetic and electric fields, respectively, onto the edges of the element [28]. At interelement boundaries the appropriate boundary conditions on the tangential electric and magnetic fields are enforced. Finally, the Lax-Wendroff upwind scheme is used for the explicit integration of the spatially discretized time dependent equations. The potential of this method comes from the fact that its foundation consists of proven computational fluid dynamics procedures, which have been developed over the last two decades. A similar stability condition is also needed for the TDFVM. Applications of the TDFVM to electromagnetic problems are available in [32]-[34].

All of the above time domain finite element methods are able to provide frequency domain results by using the FFT procedures. To achieve this, a typical combination of the TSS and FFT is, however, not evadable.

1.4.2 Review of Frequency Dependent Skin Effect Models

Skin effect is a historical topic in the field of electrical engineering. A brief survey of the contributors to this area, from J.C.Maxwell, Kelvin (W.Thomson) to H.A.Wheeler, can be found in [35]. The skin effect phenomenon is also a concurrent engineering subject which is encountered in the VLSI designs. There are quite a few skin effect models in the frequency domain. Some key references concerning these models will be reviewed in **Chapter 4**, but relevant contributive papers are exhibited here as a part of the research background.

N.S.Nahman raised a problem of high frequency losses in coaxial cables concerning a frequency dependent skin effect model in 1962 [36]. Later, T.D.English and J.J.McNichol treated a similar problem for magnetic thin film memories [37] using the frequency techniques developed by C.L.Bertin [38]. Using lumped equivalent circuit to represent the frequency dependent skin effect, E.F.Miersch and A.E.Ruehli solved a lossy coupled transmission line problem with inclusion of a lossy groundplane [39]. References [40]-[43] have a common feature to cope with the frequency dependent losses. They all used transmission line theory to empirically model the skin effect, not much numerical work being involved. There is some frequency limit to their applications.

The first few cases of numerical treatment of the frequency domain skin effect can be traced back to 1960's [44]-[46] when the "filament technique" was availed. These filament methods are very good for low frequency situation.

Another class of methods involves solving the magnetic vector potential integral equation [47]-[50]. Numerical results obtained by these methods are discrete resistance and reactance values according to the prescribed frequencies. These skin effect models are considered as implicit models, which can not be incorporated into the concurrent time domain solutions discussed in **Section1.2**.

Recently, Q.Yu and O.Wing [51] proposed a comprehensive solution that allows the frequency dependent skin effect to be represented by the impedance of an RL ladder with no FFT or convolution being required. However, this method is based on the model of the square root of frequency, which is inherently restricted by a frequency limit corresponding to the rise time of a pulse.

1.4.3 Review of Time Dependent Skin Effect Models

It should be noted that the most common frequency domain skin effect model is the square root of the frequency. However, this model can only cover a frequency range from upper medium to a relatively high frequency. In order to cover a wider frequency range, several complicated but explicit models have been proposed [38] [43] [51] [52]. Up to now, only one full coverage is attained in an implicit model [35]. On the other hand, if the skin effect model is set up in the time domain, no frequency limits will be imposed.

The time domain skin effect model has long been established since 1960's, but not as well done as its counterpart in the frequency domain. Only a few publications [53]-[56] are committed to this model but they are of great importance to the thesis research (some key references will be mentioned in **Chapter 4**). A.Timotin could be thought of as one of the pioneers of the time domain skin effect model. He initiated the time domain model for round conductors over a ground plane [53] and he also devoted himself to an intensive study of the skin effect and transient analysis [54] [55]. The advantage of Timotin's model is the explicitness of the time domain function, which was not ascertained by C.-S.Yen *et al* [56] even ten years later.

1.5 ORGANIZATION OF THE THESIS

The thesis consists of three parts. The first part includes **Chapter 2** and **Chapter 3**. The second part contains **Chapter 4**. The last part has also one chapter — **Chapter 5**. The first chapter of the thesis is a general introduction to all three parts. The last chapter is an outline for the future work.

The first part (**Chapter 2** and **Chapter 3**) introduces a new time domain finite element method — the Laplace Domain Finite Element Method (LDFEM) in **Chapter 2**, and demonstrates its applications to transient EMC problems in **Section 2.5** and **Chapter 3**.

The second part (**Chapter 4**) proposes a new time domain skin effect model and incorporates this model into a newly formulated "Method of Convolution-Characteristics". Application of the new methodology to the transient analysis of lossy VLSI interconnects are included in **Section 4.5**. Another important application to analysis of VLSI interconnect discontinuities is included in **Chapter 6**.

The last part (**Chapter 5**) comprises an innovative approach to obtain the partial inductance of any package reference planes. The partial inductance is an important parameter when analyzing the VLSI interconnection systems. The procedure to obtain the self and mutual partial inductances is presented in **Section 5.3**. A numerical solution of the partial inductance of a gap in a printed wire board (PWB) is provided with theoretical and experimental verifications in **Section 5.3.3.**

Chapter 2

LAPLACE DOMAIN FINITE ELEMENT METHOD

2.1 INTRODUCTION

In the field of electrical engineering, problems analyzed with the finite element method (FEM) are commonly formulated in either space/frequency domain or space/time domain. In the former case, time domain results are difficult to derive, while in the latter, time domain solutions suffer from instability and long computing time.

Quite frequently, both frequency domain and time domain results are of interest in certain types of applications with the FEM. Space/time domain approaches with the FEM, as in [29] and [32], are able to provide such results with the aid of time-stepping schemes and the Fast Fourier Transform (FFT). Generally, a time-stepping scheme requires the satisfaction of the stability condition, that is, the ratio of spatial to temporal subdivision is to be greater than or equal to the speed of propagation [29]. This results in another problem, i.e., the finer the mesh, the smaller the time step that must be chosen [25]. In order to achieve a satisfactory resolution with the use of the FFT, longer computing time is needed; in other words, more time steps are involved. It is obvious that long computing time is one of the drawbacks of the time-stepping schemes. On the other hand, if the time step is not small enough, instability of numerical results occurs. The same numerical phenomenon happens in other space/time domain approaches [26] [21], where special numerical treatment, like the Crank-Nicolson algorithm, is involved.

Conventional time domain finite element approaches are restricted by computing time and the stability condition when both frequency domain and time domain results are required at the same time, as in the cases mentioned above. Hence a new method based on the finite element analysis needs to be sought. In circuit theory, there are many applications with Laplace transforms: in order to obtain time domain results, the Laplace transform and its inverse transform are used; in order to obtain frequency domain results, the Laplace transform can still be used with the substitution of the Laplace parameter s for $j\omega$. The same principle can also be applied to the problem formulation with the FEM.

In fields other than electrical engineering, finite element analysis combined with the Laplace transform has been proposed to solve the vibration problem in toroidal field coils [1]. A systematic approach of hybrid Laplace transform/finite element method has been proposed since 1987 [2] [62] - [63] for heat transfer problems. In these applications, the heat conduction equation, which describes the unsteady temperature distribution in a solid domain, together with proper initial/boundary conditions, is transformed to the Laplace domain and then solved by conventional node-based finite element method. This approach has been extended to three-dimensional problems [3] but is restricted to diffusion type partial differential equations, an important improvement being the adoption of the congruence transformation of matrices [59] [63].

In this thesis, we use the same approach but extend it to the wave equations. Our formulation is generated from a damped wave equation. Thus it can be used to deal with either diffusion or propagation problems. This extension of the hybrid Laplace transform/finite element method to propagation problems is especially necessary and important in the field of electrical engineering.

Because of the reason stated above, we shall call our approach a Laplace Domain Finite Element Method (LDFEM), differing from the approach used in the field of mechanical engineering. With this approach, some diffusion and propagation problems of electromagnetic fields can be formulated in the Laplace domain based on finite element analysis. The main procedure is as follows: first, the given problem in the form of damped wave equation associated with suitable initial and boundary conditions is transformed to the Laplace domain from the time domain and formulated with a conventional FEM scheme; secondly, the congruence transformation is used to deal with the matrices; finally, the numerical results derived in the Laplace domain are inverted into the time domain in either an analytical or numerical way. The major advantage of utilizing the Laplace domain instead of the frequency domain is that we can easily make use of numerous existing analytical expressions of the Laplace transform and its inverse transform, which are believed to be more numerous than those of Fourier transforms. Another prominent advantage of the proposed approach is that some typical time domain excitations, e.g., the unit step pulse and the ramp pulse, can be exactly modeled through the Laplace transform. Besides, for some complicated time domain excitations, the inverse transform process can be handled with the residue theorem or the numerical method as in [57]. In this thesis, we also propose a new method to deal with the time domain excitation by benefiting from the analytical property of the Laplace domain formulation. Through utilization of the *Duhamel* integral, which will be discussed in **Section 2.5**, tackling any complicated excitation would be greatly eased.

2.2 FORMULATION

For a homogeneous and source-free medium, the following damped wave equations are derived from the Maxwell equations:

$$\nabla^2 \vec{E} - \epsilon\mu \frac{\partial^2 \vec{E}}{\partial t^2} - \sigma\mu \frac{\partial \vec{E}}{\partial t} = 0 \tag{2.1}$$

$$\nabla^2 \vec{H} - \epsilon\mu \frac{\partial^2 \vec{H}}{\partial t^2} - \sigma\mu \frac{\partial \vec{H}}{\partial t} = 0. \tag{2.2}$$

Equations (2.1) and (2.2) can be applied to either a diffusion problem where the second term will be dropped or a propagation problem where the third term will be dropped. Solving one of the above equations with appropriate boundary and initial conditions will be enough to demonstrate our LDFEM algorithm. For simplicity, a one-dimensional problem is formulated here with this new method and we will not lose the generality to apply it to a multiple-dimensional system. Let us choose a transient magnetic field problem where the field to be solved is distributed in the x-direction while it is invariant in other two directions.

Applying the Laplace transform to Eqn.(2.2) in a one-dimensional case, we have

$$\frac{\partial^2 \tilde{H}}{\partial x^2} - \epsilon\mu s^2 \tilde{H} + \epsilon\mu s H(0^-) + \epsilon\mu H'(0^-) - \mu\sigma s \tilde{H} + \mu\sigma H(0^-) = 0 \tag{2.3}$$

and the associated boundary and initial conditions

$$\tilde{H}(x,s)\mid_{B_D} = f_D(x,s) \tag{2.4}$$

$$\frac{\partial \tilde{H}(x,s)}{\partial x}\mid_{B_N} = f_N(x,s) \tag{2.5}$$

$$H(x,0^-) = g_0(x) \tag{2.6}$$

$$H'(x,0^-) = g_1(x) \tag{2.7}$$

where $\tilde{H}$ represents the H-field in the Laplace domain. In Eqns.(2.4) and (2.5), the subscripts B_D and B_N denote *Dirichlet* and *Neumann* boundary conditions, respectively.

Using the finite element analysis based on the variational techniques [58], the final system of equations is obtained as

$$\{[A] + (\epsilon\mu s^2 + \mu\sigma s)[B]\}[\tilde{H}] = [\tilde{f}] \tag{2.8}$$

where

$$[A] = \sum_{e=1}^{N} \int_{x_i}^{x_j} [P^{(e)}]^T [P^{(e)}] dx \tag{2.9}$$

$$[B] = \sum_{e=1}^{N} \int_{x_i}^{x_j} [N^{(e)}]^T [N^{(e)}] dx \tag{2.10}$$

$$[\tilde{f}] = \sum_{e=1}^{N} \int_{x_i}^{x_j} \{\epsilon\mu s H(0^-)[N^{(e)}]^T + [\epsilon\mu H'(0^-) + \mu\sigma H(0^-)][N^{(e)}]^T\} dx + \sum_{e=1}^{N} [N^{(e)}]^T [\frac{\partial \tilde{H}}{\partial x} |_b - \frac{\partial \tilde{H}}{\partial x} |_a] \tag{2.11}$$

where N is the total number of the elements.

In Eqns.(2.9)-(2.11), $[N^{(e)}]$ is the vector of shape functions and $[P^{(e)}]$ is the vector of the first order derivative of $[N^{(e)}]$ with respect to x. The problem domain is defined in $x \in [a, b]$, which is divided into N finite elements. Only the inhomogeneous *Neumann* boundary condition is explicitly displayed in Eqn.(2.11) for reference while the *Dirichlet* boundary condition can be implemented through the algorithm. $H(0^-)$ and $H'(0^-)$ in Eqn.(2.11) represent $H(x, 0^-)$ and $H'(x, 0^-)$, respectively. Either global matrix $[A]$ or $[B]$ in Eqn.(2.8) should be symmetric and positive definite for the purpose of the following mathematical processing.

2.3 CONGRUENCE TRANSFORMATION

Solving Eqn.(2.8) with appropriate boundary conditions is not straightforward since it involves the unknown Laplace parameter s, a complex number, which exerts its influence on every element in matrix $[B]$ and is not separable as an independent unknown in the final system of equations. One possible way to the solution of Eqn.(2.8) is to reduce both $[A]$ and $[B]$ simultaneously to the canonical forms and then all the unknowns except for s could be decoupled.

A non-singular real transformation [59] can be applied to matrices $[A]$ and $[B]$ as long as either $[A]$ or $[B]$ is symmetric and positive definite. The congruence transformation of matrices has been successfully applied for this purpose in order to solve heat conduction problems [3] [63]. In our case of solving the finite element equations based on the damped wave equation, i.e. Eqn.(2.8), both $[A]$ and $[B]$ fortunately satisfy this condition after the formulation with the conventional node-based finite element scheme. However, since the final system of equations (2.8) must be associated with some boundary conditions and even with the inhomogeneity of the media involved in the problem domain, one more condition limiting the application of the non-singular real transformation to Eqn.(2.8) will be imposed and mentioned later.

Let us first describe the procedure of the non-singular real transformation applied to Eqn.(2.8) without considering the boundary conditions and inhomogeneity of the media. We will start to apply orthogonal transformations to $[A]$ and $[B]$ based on the following assumptions: i) both $[A]$ and $[B]$ are symmetric and positive definite; ii) the boundary conditions do not destroy the properties of these two matrices, i.e., symmetry and positive definiteness; and iii) the problem domain is filled with homogeneous medium. These assumptions can be modified or removed for the more general case. This will be discussed later in the Conclusions.

For the purpose of reducing $[A]$ and $[B]$ simultaneously to canonical forms, we first set

$$[\tilde{H}] = [Q][\tilde{H}'] \tag{2.12}$$

where $[Q]$ is an orthonormal modal matrix of $[B]$ and $\tilde{H}'$ is a new variable representing its original $\tilde{H}$ through the new transformation relationship Eqn.(2.12). Using the congruence transformation, we can write

$$[B'] = [Q]^T[B][Q]. \tag{2.13}$$

$[Q]$ is chosen to comprise normalized and orthogonal eigenvectors of $[B]$. $[B']$ is then expressed as

$$[B'] = \begin{bmatrix} \gamma_1 & & & & \\ & \gamma_2 & & & \\ & & .. & & \\ & & & \gamma_{n-1} & \\ & & & & \gamma_n \end{bmatrix} \tag{2.14}$$

where $\gamma_1, \gamma_2, ..., \gamma_n$ are the eigenvalues of $[B]$ and n is the number of unknowns. $[Q]^T$ can be written as

$$[Q]^T = \begin{bmatrix} e_1 \\ e_2 \\ : \\ e_{n-1} \\ e_n \end{bmatrix} \tag{2.15}$$

where $e_1, e_2, ..., e_n$ are the eigenvectors of $[B]$.

Since $[B]$ is a positive definite matrix and $\gamma_1, \gamma_2, ..., \gamma_n$ are all positive eigenvalues, $[Q]^T$ can be normalized by using these eigenvalues as

$$[Q']^T = \begin{bmatrix} e_1/\sqrt{\gamma_1} \\ e_2/\sqrt{\gamma_2} \\ : \\ e_{n-1}/\sqrt{\gamma_{n-1}} \\ e_n/\sqrt{\gamma_n} \end{bmatrix}. \tag{2.16}$$

Replacing $[Q]$ with $[Q']$ in Eqn.(13), we obtain a unit matrix

$$[B''] = [Q']^T[B][Q'] = \begin{bmatrix} 1 & & & & \\ & 1 & & & \\ & & .. & & \\ & & & 1 & \\ & & & & 1 \end{bmatrix} = [I]. \tag{2.17}$$

We will use a new variable $\tilde{H}'$ which satisfies

$$[\tilde{H}] = [Q'][\tilde{H}'] \tag{2.18}$$

instead of Eqn.(2.12). Substituting $[\tilde{H}]$ in Eqn.(2.8) yields

$$\{[A] + (\epsilon\mu s^2 + \mu\sigma s)[B]\}[Q'][\tilde{H}'] = [\tilde{f}]. \tag{2.19}$$

Premultiplying Eqn.(2.19) with $[Q']^T$, we obtain

$$\{[Q']^T[A][Q'] + (\epsilon\mu s^2 + \mu\sigma s)[Q']^T[B][Q']\}[\tilde{H}'] = [\tilde{f}'] \tag{2.20}$$

where

$$[\tilde{f}'] = [Q']^T[\tilde{f}]. \tag{2.21}$$

According to Eqn.(2.17), Eqn.(2.20) can be written as

$$\{[Q']^T[A][Q'] + (\epsilon\mu s^2 + \mu\sigma s)[I]\}[\tilde{H}'] = [\tilde{f}']. \tag{2.22}$$

We define

$$[C] = [Q']^T[A][Q'] \tag{2.23}$$

and further set

$$[\tilde{H}'] = [W][\tilde{H}''] \tag{2.24}$$

where $[W]$ is an orthonormal modal matrix of $[C]$. In the same fashion as we obtain $[B']$, we have

$$[C'] = [W]^T[C][W] \tag{2.25}$$

where [W] is chosen to comprise normalized and orthogonal eigenvectors of $[C]$.

Since the above equation represents a congruence transformation, we have

$$[C'] = \begin{bmatrix} \lambda_1 & & & & \\ & \lambda_2 & & & \\ & & \ddots & & \\ & & & \lambda_{n-1} & \\ & & & & \lambda_n \end{bmatrix} \tag{2.26}$$

where $\lambda_1, \lambda_2, ..., \lambda_n$ are the eigenvalues of $[C]$. Substituting Eqns.(2.23) and (2.24) in Eqn.(2.22) and premultiplying Eqn.(2.22) with $[W]^T$, we obtain

$$\{[W]^T[C][W] + (\epsilon\mu s^2 + \mu\sigma s)[W]^T[I][W]\}[\tilde{H}''] = [\tilde{f}''] \tag{2.27}$$

where

$$[\tilde{f}''] = [W]^T[\tilde{f}']. \tag{2.28}$$

Since $[W]$ is an orthonormal modal matrix, it is easily seen that the following equation holds

$$[W]^T[I][W] = [I]. \tag{2.29}$$

Thus we finally have

$$\{[C'] + (\epsilon\mu s^2 + \mu\sigma s)[I]\}[\tilde{H}''] = [\tilde{f}'']. \tag{2.30}$$

We notice that the above equation is solved since all the unknowns in $[\tilde{H}'']$ are decoupled. The nodal solutions for $[\tilde{H}'']$ can be written, for example, as

$$\tilde{H}_i''(s) = \frac{\tilde{f}_i''(s)}{\lambda_i + (\epsilon\mu s^2 + \mu\sigma s)} \qquad (i = 1, 2, ..., n). \tag{2.31}$$

The original unknowns $[\tilde{H}]$ can be traced back by Eqns.(2.24) and (2.18) and the time domain results of $H_i(x,t)$ can be obtained with the inverse Laplace transform. It is seen that the inversion of the Laplace transform could be easily performed on the analytical expressions like Eqn.(2.31).

2.4 NUMERICAL RESULTS AND VALIDATION

In this section, we will solve a one-dimensional diffusion problem as a test problem to validate the above proposed algorithm. The test problem is shown in Fig.2.1 , where a time-dependent current $i(t)$ is flowing through a a slot in a metallic structure of infinite length. The side and bottom walls of the slot are made of magnetic walls. The current is produced by the H-field uniformly excited on the top surface of the slot, which can be any function of the time. As depicted in Fig.2.1, the direction of the H-field on the top is right-pointed producing a current (normal to the transverse plane of the slot). Since the metal in the slot has finite conductivity σ and finite permeability μ and all three walls have infinite permeability, this is obviously a one-dimensional diffusion problem under given excitation.

The analytical solution for the given problem is provided in the Appendix. In fact, to solve it numerically, the problem formulation has been established through Eqns.(2.3)-(2.11) while the term with s^2 can be dropped due to omission of the displacement current. Assuming only when $t \geq 0$, the excitation field is applied to the top of the slot. Thus the initial condition related with $H(0^-)$ and $H'(0^-)$ are set to be zero. Since only the *Dirichlet* boundary condition is involved, the right-hand side term of the final system of equations, i.e., $[\tilde{f}]$ in Eqn.(2.11), should be modified with the appropriate contribution from the top-exciting H-field.

There are two ways to apply the inhomogeneous *Dirichlet* boundary condition:

i. Direct method — if the time function is simple, that is, if the Laplace transform of the excitation and the related inverse Laplace transform of the expression (2.31) are easily found, we can simply apply the original time domain excitation with its form in the Laplace domain on the boundary without involving any convolution process.

ii. Convolution method — if the time function is complicated, we can first use the unit step pulse function as the excitation, and then, after finding out the response of the simple excitation, we will use the *Duhamel* integral to retrieve the original response to the complicated excitation.

In general, either method can be implemented since we always have the explicit expressions, e.g., Eqn.(2.31), to perform the inverse Laplace transform or to utilize the *Duhamel* integral. This advantage may not be taken over by other time domain methods, such as the Time-Domain Finite-Difference (FDTD) method, the Transmission-Line Matrix (TLM)

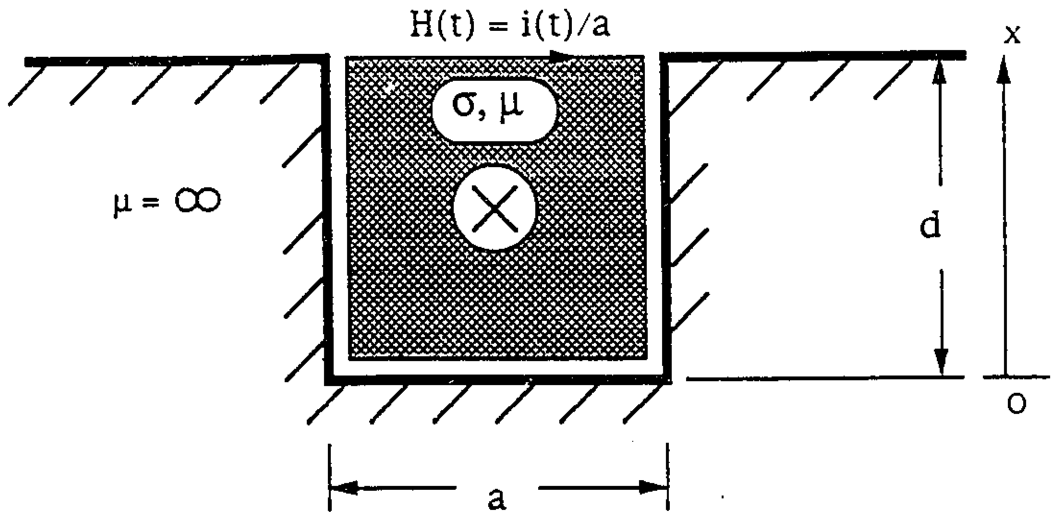

Figure 2.1: The physical structure of the test problem.

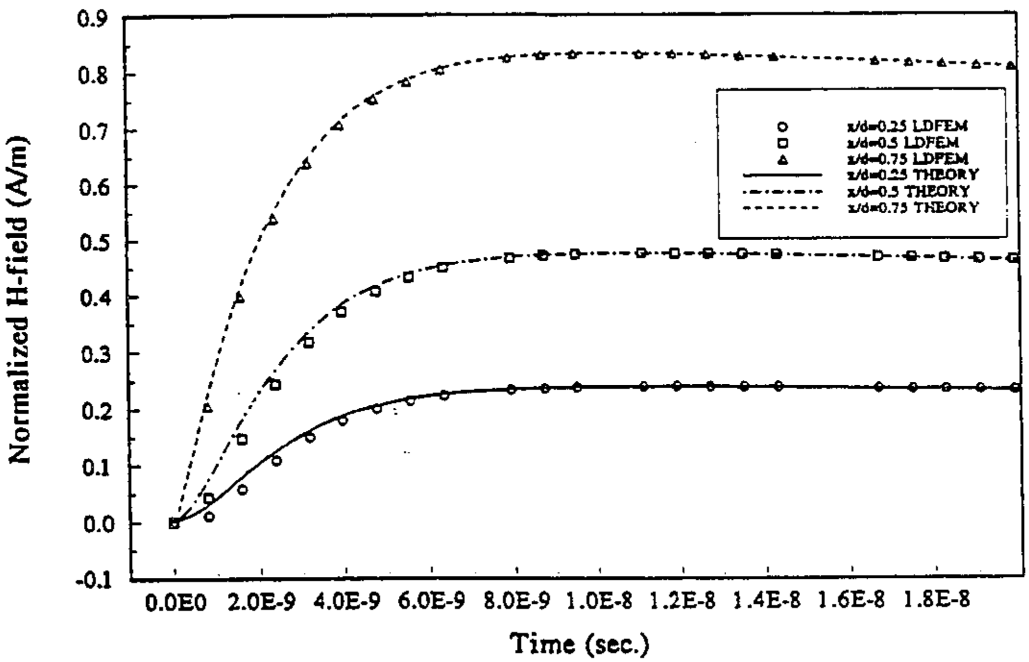

Figure 2.2: Time-history of magnetic field distributions excited by a double-exponential EMP.

method and the afore-mentioned time domain finite element methods.

Fig.2.2 illustrates the comparison between the numerical results derived with the LD-FEM algorithm and the analytical solutions in the time domain for the given problem shown in Fig.2.1. The excitation of the H-field on the top of the slot is chosen to be in the following form

$$H(t) = A_0(e^{-\alpha t} - e^{-\beta t}) \qquad (x = d). \tag{2.32}$$

This is an electromagnetic pulse (EMP) type of excitation featuring a steep rise slope if both α and β are properly set. We choose α and β to be $4.0 \cdot 10^6(1/s)$ and $4.76 \cdot 10^8(1/s)$, respectively, for the purpose of checking the early time response. For the results shown in Fig.2.2, the physical parameters are $A_0 = 1.0(A/m)$, $d = 1.0 \cdot 10^{-4}(m)$, $\mu = 4\pi \cdot 10^{-7}(H/m)$ and $\sigma = 5.76 \cdot 10^5(S/m)$. Another boundary condition is

$$H(t) = 0 \qquad\qquad (x = 0). \tag{2.33}$$

The direct method mentioned above is used to obtain the LDFEM results in this test problem. Good agreement has been found in the comparison (Fig.2.2) even though the number of the uniform elements is only 8 and the linear basis functions are used [58]. No early time oscillation (numerical) is observed at different locations. Table 2.1 shows the peak-time at different locations in the problem domain $x \in [0, d]$ due to the double-exponential EMP excitation Eqn.(2.32).

Table 2.1: The peak-time at different locations

Locations	Theory (sec.)	LDFEM (sec.)
$x/d = 0.25$	$11.13 \cdot 10^{-9}$	$11.41 \cdot 10^{-9}$
$x/d = 0.50$	$10.96 \cdot 10^{-9}$	$11.16 \cdot 10^{-9}$
$x/d = 0.75$	$10.38 \cdot 10^{-9}$	$10.91 \cdot 10^{-9}$

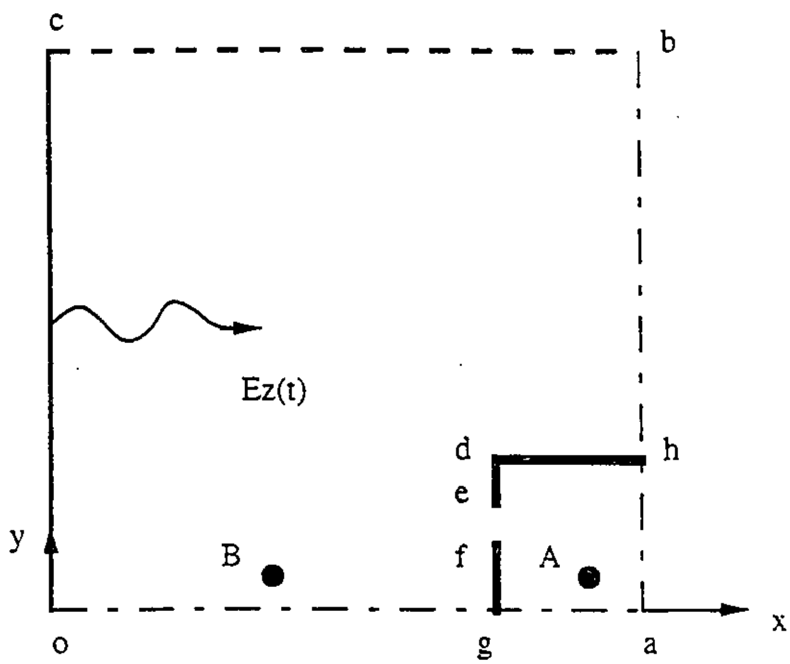

Figure 2.3: A two-dimensional shielding problem (TM wave case).

2.5 APPLICATION TO A 2-D SHIELDING PROBLEM

As discussed in **Section 2.2**, the application of the LDFEM algorithm to a propagation problem is straightforward if we follow the generalized approach described earlier. We can simply drop the terms involving $\sigma\mu$ due to omission of the conduction current. This will cause some modifications in the problem formulation (in a general sense) with the LDFEM. For example, if the term involving $\sigma\mu$ in Eqn.(2.31) is dropped, the solution of $H_i(x,t)$ is known to correspond to that of a wave equation. This is why we started with the damped wave equations in **Section 2.2**.

In this Section, we present a demonstration of the application of the LDFEM algorithm, where both frequency domain and time domain results are needed. Consider a two-dimensional (2-D) shielding problem: two TM plane-waves, independent of z-coordinate, oppositely impinge on a rectangular metallic cylinder serving as a electromagnetic shield, in which four slots or apertures are symmetrically located(Fig.2.3). Owing to the symmetry of the problem, only a quarter of the geometric structure is shown in Fig.2.3. The boundary conditions for the problem are as follows:

$$E_z(t) = 2\sqrt{\frac{a_2}{\pi}}e^{-a_2t^2} \qquad (on \quad \bar{co}) \tag{2.34}$$

$$\frac{\partial E_z(t)}{\partial y} = 0 \qquad (on \quad \bar{cb} \quad and \quad \bar{oa}) \tag{2.35}$$

$$\frac{\partial E_z(t)}{\partial x} = 0 \qquad (on \quad \bar{ba}). \tag{2.36}$$

For the excitation on the boundary $\bar{co}$, we choose Gaussian pulse (Eqn.(2.34)) such that the spectral components of the TM waves are under control. The Laplace transform of the given form of the Gaussian pulse is

$$\tilde{E}_z(s) = e^{\frac{s^2}{4a_2}}erfc(\frac{s}{2\sqrt{a_2}}) \tag{2.37}$$

where the complex error functions are defined as

$$erfc(y) = 1 - erf(y) \tag{2.38}$$

$$erf(y) = \frac{2}{\sqrt{\pi}}\int_0^y e^{-\omega^2}d\omega \ . \tag{2.39}$$

It is found that numerical implementation of the Gaussian pulse excitation with the LDFEM is difficult. One possible way to tackle this problem is to use the *Duhamel* integral, that is, the convolution method mentioned in the previous section. The *Duhamel* integral is written as

$$\phi(x,t) = \psi(x,t)b(0) + \int_0^t \psi(x,t-\tau)b'(\tau)d\tau \qquad (t > 0) \tag{2.40}$$

where $\psi(x,t)$ is the system response to the excitation of $b(t) = u(t)$, a unit step pulse.

When $b(t)$ is chosen to be any other function, e.g., $E_z(t)$ given by Eqn.(2.34) or $H(t)$ given by Eqn.(2.32), $\psi(x,t)$ is always in the form of the system response to the unit step pulse. This offers a great flexibility. As long as the problem is solved with the LDFEM to the excitation of the unit step pulse, one of the simplest excitation functions, any other system response $\phi(x,t)$ to any other complicated excitation $b(t)$ is ready to be given by the *Duhamel* integral. This feature of the convolution method also eases the process of obtaining the time domain results since no numerical inverse Laplace transform would be needed for the complicated excitations. It is noted that the way of using the numerical inverse Laplace transform is highlighted in [2], which is different from our approach.

Considering numerical implementation of the *Duhamel* integral, there are two ways to accomplish it: i) in combination with time-stepping schemes, Eqn.(2.40) can be numerically modeled by the first order approximation in the time domain [26]; ii) in combination with the LDFEM algorithm, both $\psi(x,t)$ and $b(t)$ have analytical expressions, e.g., Eqns.(2.34) and (2.31), and then Eqn.(2.40) can be solved in either an analytical or numerical way. By taking the advantage of many sophisticated numerical integral packages, the second method is believed to yield more accurate results than those of the first one. It is apparent that we benefit from the analytical property pertinent to the LDFEM algorithm.

Fig.2.4 shows the time domain response at Location A (Fig.2.3) to a Gaussian pulse excitation

$$E_z(t) = \frac{A_0}{\sqrt{\pi}} e^{-a_2(t-t_0)^2} \qquad (on \quad \bar{co}) \tag{2.41}$$

where $A_0 = 2.0(V/m)$, $a_2 = 2.65 \cdot 10^{16}(1/s^2)$, and the time shift $t_0 = 20.0 \cdot 10^{-9}(s)$.

Fig.2.5 illustrates the frequency domain responses at different locations (A and B in Fig.2.3). The physical structure of the problem shown in Fig.2.3 is as follows: the 2-D shield with slots is made of perfect conductor; the excitation source has no spatial variation in z-direction, i.e., the propagation constant $k_z = 0$; $\bar{oa} = 1.0(m)$, $\bar{ga} = 0.2(m)$, $\bar{ha} = 0.2(m)$, $\bar{ba} = 1.0(m)$, $\bar{de} = 0.05(m)$, and the slot width $\bar{ef} = 0.05(m)$. Locations A and B are given in the rectangular coordinates shown in Fig.2.3 as $x_A = 0.9571(m)$, $y_A = 0.05(m)$ and $x_B = 0.4(m)$, $y_B = 0.05(m)$. For the results shown in Fig.2.4 and Fig.2.5, we have 364 nonuniform elements with 181 nodal unknowns. The frequency domain results are obtained with the use of the FFT. Instead, the frequency domain results can also be obtained by justifying the eigenvalues derived in the congruence transformation [60]. The latter facilitates the process of obtaining both frequency domain and time domain results

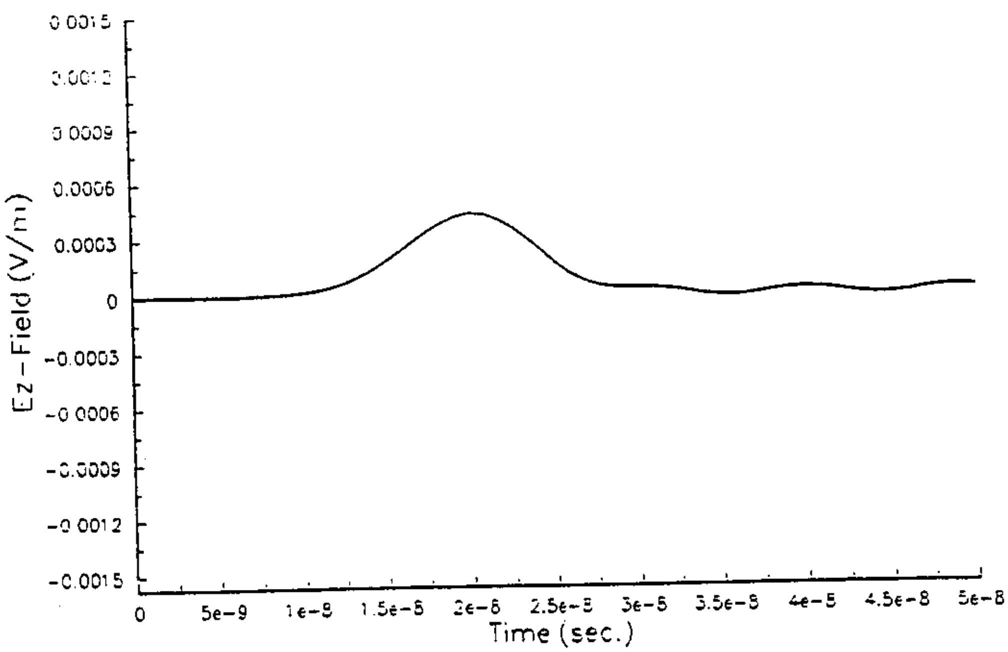

Figure 2.4: Time domain response of the penetrating E_z-field inside the shield (Location A).

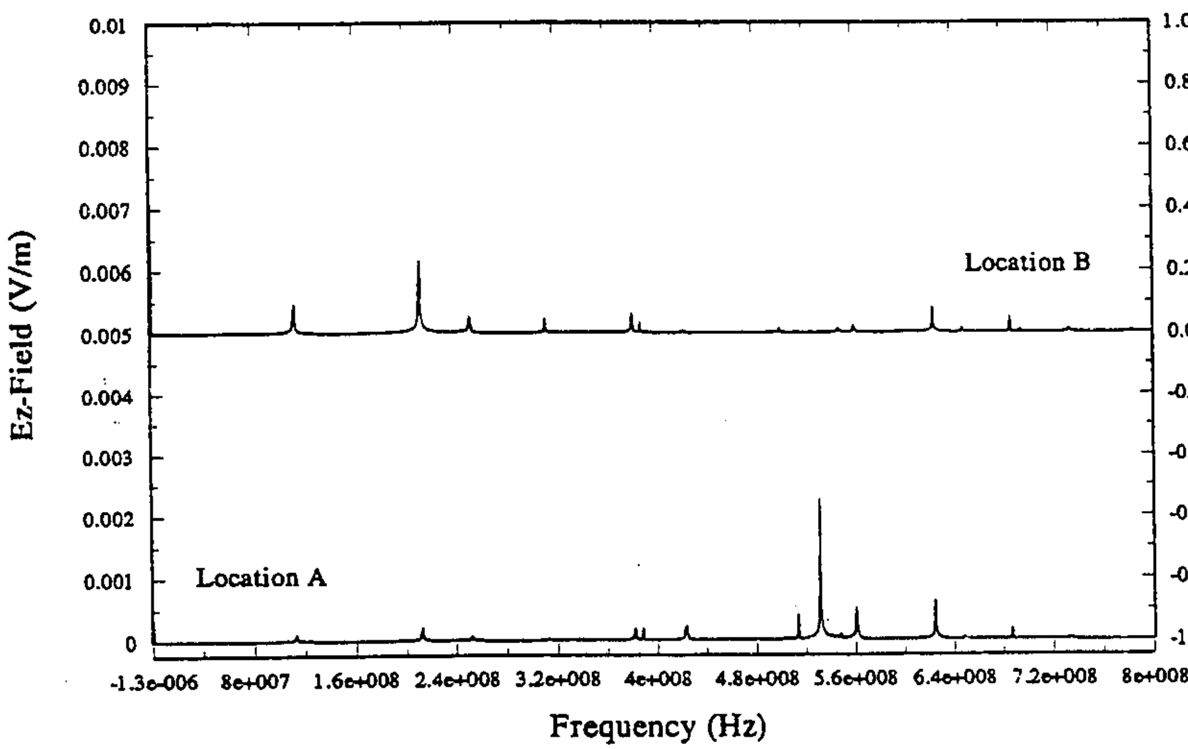

Figure 2.5: Frequency domain responses of the E_z-field inside the shield (Location A) and outside the shield (Location B).

without formulating two different problems: one deterministic and the other eigenvalue, respectively.

A brief discussion on the results given in Fig.2.4 and Fig.2.5 is needed. The shielding structure in Fig.2.3 is like a rectangular waveguide. Under the TM wave excitation through the slots, the transverse resonances of the higher order modes would occur in the shield. In the 2-D case, the transverse resonance frequency happens to be the corresponding cutoff frequency of an infinitely long waveguide [61]. For the given dimensions of the shield and the specified excitation, the transverse resonance frequency of the first higher order mode, i.e., TM_{11}, is easily determined as $530.3(MHz)$. The numerical result shown on the curve of "Location A" in Fig.2.5 displays this resonance at $531.9(MHz)$ with a strong contrast while this resonance is not observed outside the shield, i.e., on the curve of "Location B". Table 2.2 displays a comparison between the theoretical and numerical results for the first few higher order modes (TM) excited at Location A in the shielding. In this comparison (Table 2.2), the theoretical results are derived for a rectangular wave guide with perfect walls (no apertures). Since the dimension of the apertures in the numerical model is small compared to the one of the walls and the location of the apertures does not cause large distortion of the excited modes, we would trust this comparison to an acceptable degree of accuracy.

Table 2.2: The higher order modes (TM) at Location A

Mode	Theory (MHz)	LDFEM (MHz)	Error (%)
TM_{11}	530.33	531.90	0.30
TM_{12}	838.53	894.50	6.67
TM_{22}	1060.66	1132.00	6.73

Other minor resonances on both curves (Fig.2.5) are caused by the interaction between the shield and the boundaries since neither the far-field condition nor the absorbing boundary condition is imposed. These minor resonances also cause small disturbances in the time domain results as one can find that small ripples follow the main pulse (Fig.2.4). In addition, one can observe the peak-time of the pulse at $t_{peak} = 20.224 \cdot 10^{-9}(s)$ since the time shift of the Gaussian pulse is $t_0 = 20.0 \cdot 10^{-9}(s)$.

2.6 CONCLUSIONS

The algorithm of the Laplace domain finite element method is presented in this thesis including its validations. Satisfactory numerical results are found in a one-dimensional diffusion problem and, therefore, validate the algorithm. In principle, the LDFEM algorithm is limited neither to one-dimensional problems nor to diffusion problems. Thus it is applied to a 2-D propagation problem and reasonable results corresponding to the specified physical structure are obtained in **Section 2.5**.

The application in **Section 2.5** is chosen in such a way that one can understand better the applicability and limitations of the LDFEM. First of all, the LDFEM can be used in multiple-dimensional systems for either diffusion or propagation problems. Without any time-stepping scheme, the resultant numerical solutions derived with this method can be given in both time domain and frequency domain at almost the same computing time, especially for propagation problems. Using the inverse Laplace transform or the convolution method, time domain results are obtained straight away. Justification of the eigenvalues derived in the congruence transformation provides useful frequency domain results, such as cutoff frequencies of a waveguide. This means that the frequency information about the system to be solved has already existed in the process of the LDFEM solution even though the FFT is not used. We can utilize this property of the LDFEM in other applications [60]. It is evident that the LDFEM combines both deterministic and eigenvalue problems together, and, therefore, it provides either or both solutions depending upon the applications.

Two limitations pertinent to the present LDFEM algorithm should be addressed if the congruence transformation is used. It is seen in **Section 2.3** that the property of symmetry of the two matrices $[A]$ and $[B]$ is a preliminary requirement for positive definiteness. To ensure the symmetry, boundary conditions are restricted to the *Dirichlet* and *Neumann* boundary conditions, either homogeneous or inhomogeneous. No mixed boundary conditions, such as *Cauchy* boundary condition, are allowed because mixed boundary conditions would destroy the required properties of the matrices. This means that the far-field condition and the absorbing boundary condition could not be used with the present LDFEM algorithm. However, this limitation might be removed if some other method, for example, the "Double Dire :: G..ussian Elimination" approach [2], is applied to deal with those matrices. Another limitation is related to the inhomogeneity of the media in the problem domain. Examining the coefficient of matrix [B] in Eqn.(2.8), i.e., $\epsilon\mu s^2 + \mu\sigma s$, one can find that if the media are filled partially with ϵ (other than ϵ_0) or partially with σ (other than $\sigma = 0$) while both ϵ and σ are present at the same time in the problem domain, the congruence transformation is not a successful treatment to the Laplace domain finite element formulation. Otherwise, inhomogeneity is allowed in either pure diffusion or pure propagation problems.

The convolution method proposed in this thesis is an efficient and versatile way of tackling complicated time domain excitations. It also assures excellent accuracy of the numerical results because explicit analytical expressions can always be found when necessary in the LDFEM algorithm.

Since no time-stepping scheme is involved, instability and long computing time are avoided with the LDFEM.

Chapter 3

LDFEM APPLIED TO ANALYSIS OF A TRIPLE-TEM CELL

3.1 INTRODUCTION

Recently, a new type of TEM cell having two separately perpendicular inner conductors (septums) has been proposed [64]. Called the "Triple-TEM (TTEM) cell", this new device features an additional electric field polarization in the transverse plane compared to conventional TEM cells and GTEM cells.

The TTEM cell (Fig.3.1) has a GTEM cell-like configuration in appearance but the two perpendicular septums distinguish it from the latter one. Alternative exposures can be achieved when one of the septums is set to a higher voltage while the other as well as the outer conductor are at the same voltage. It is evident that the equipment under test (EUT) is exposed to either a y-polarized or an x-polarized electric field (Fig.3.1) with only an electrical switching between these conductors. By using a turntable [64] on which the EUT is placed, the equipment can be better illuminated in the specified electromagnetic environment established in the TTEM cell. Compared with traditional test procedures, in which the EUT has to be positioned in several orientations [65], the TTEM cell setup facilitates the measurement of the EUT inside the cell.

Conventional TEM cells and GTEM cells have the same transverse configuration: only one inner conductor either symmetrically located or offset, in the y-direction, for instance. Analysis of symmetric and asymmetric TEM cells can be carried out by resorting to semi-analytical or analytical methods [66]-[70] for better accuracy. In some other cases, numeri-

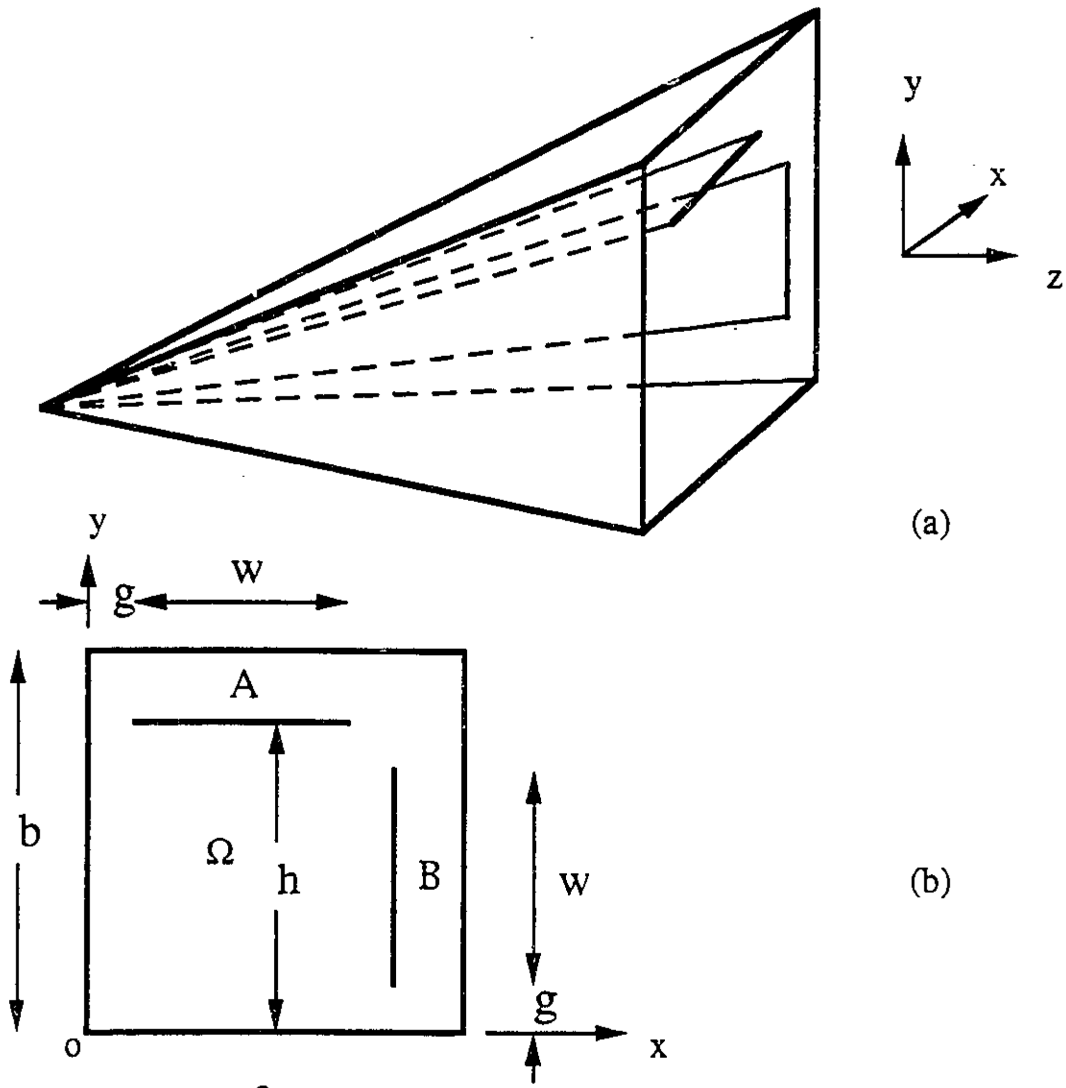

Figure 3.1: Triple-TEM cell: (a) 3-D configuration; (b) cross-sectional area.

cal methods have also been applied to two-dimensional (2-D) and three-dimensional (3-D) analyses of TEM cells [71]-[73]. Besides, experimental methods [74]-[75] have long been employed ever since the invention of the TEM cell. A hybrid theoretical/empirical method has also been used in the evaluation of the longitudinal variations of the field and the line impedance in the TEM cell [76]. Based on all these results, a set of engineering design approaches has been established for the these conventional cells.

It has been seen that the existing design approaches are not applicable to the design of the TTEM cell due to its unusual septum geometry (Fig.3.1). An essential analysis of the TTEM cell should include all basic characteristics (static and dynamic), such as the TEM field distributions, characteristic impedance and cutoff frequencies of the higher order modes (TE and TM). Of all the aforementioned methods, numerical methods would be the best choice for the required analysis. In this chapter, the conventional finite element method (FEM) is chosen to determine the first two static characteristics, i.e. the TEM field distributions and characteristic impedance. Concerning the high frequency performance of a TEM cell-like structure, Das and Sinha [71] used a finite element formulation to treat the symmetric TEM cell and reported corresponding TE and TM modes cutoff frequencies. However, their method is restricted to the symmetric geometry of the inner conductor location and can not be extended to obtain TE mode cutoff for the unusual arrangement of the septums like the one in the TTEM cell. The newly proposed finite element approach — Laplace Domain Finite Element Method (LDFEM) [77] is adopted here for the analysis of the dynamic characteristics of the TTEM cell. In combination with a special numerical treatment for perfectly conducting boundaries, which is a difficulty in the TE mode case, the LDFEM algorithm is able to tackle the problem of both TE and TM modes in the TTEM cell without generating spurious modes.

The LDFEM is a dual-domain method, with which both time domain and frequency domain results can be obtained in the numerical process [77]. Since no time-stepping scheme is involved, the LDFEM provides stable solutions in the time domain. Without resorting to the Fast Fourier Transform (FFT), the LDFEM algorithm also yields useful information in the frequency domain, for example, the cutoff frequencies of a waveguide structure. The latter property of the LDFEM is fully utilized in the present numerical analysis. In addition to the elaborate discussion [77] on the problem formulation with the LDFEM in a one-dimensional case, this chapter will provide an extension of the algorithm to a 2-D formulation in detail.

Even though the TTEM cell has a structure which would require a 3-D analysis, it is still possible to carry out the analysis in two dimensions. All the numerical computations will only involve the transverse plane since the geometric ratios in the cross-sectional area of the TTEM cell are not a function of the longitudinal coordinate, say the z-coordinate (Fig.3.1). However, the local higher order modes will start to propagate at different longitudinal positions [67]. According to [67], the propagation properties of the local higher order modes will be determined by the dynamic characteristics of a corresponding uniform structure.

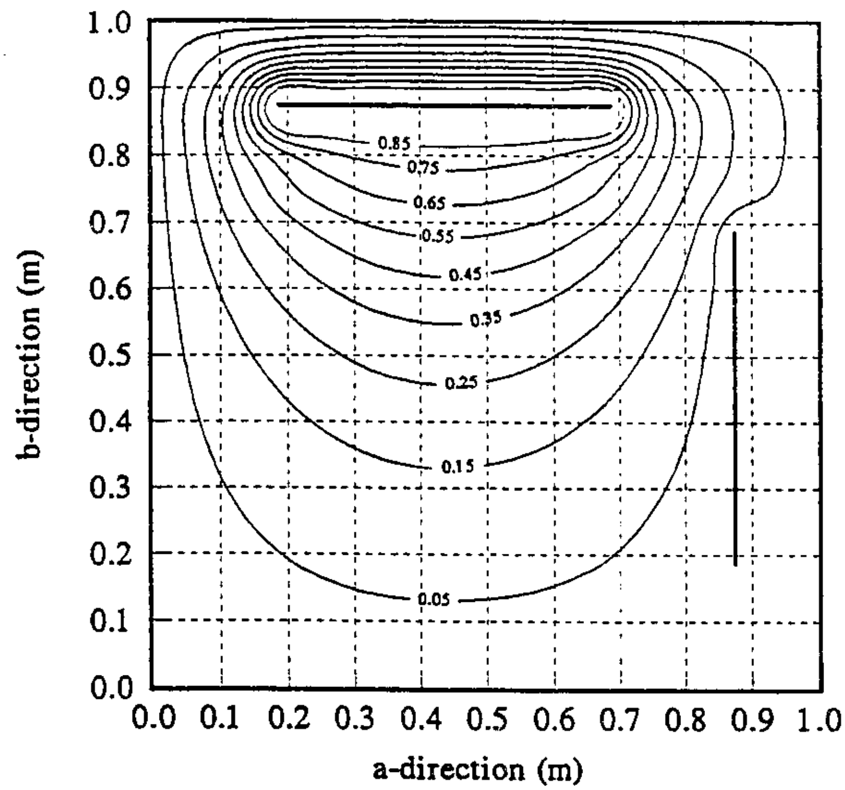

Figure 3.2: Potential distribution in a Triple-TEM cell.

3.2 TEM MODE ANALYSIS

The TTEM cell is a multiple-conductor system that will support pure TEM fields at frequencies below the cutoff of its first higher order mode. To obtain its basic characteristics, such as the TEM field distributions and the characteristic impedance, a TEM mode analysis can be carried out based on the assumption that the concerned frequency is below the first cutoff. A conventional node-based finite element method [78] is chosen here and the TEM mode analysis can start with the Laplace equation for the sourceless cross-sectional area of the TTEM cell.

In the transverse plane shown in Fig.3.1 (b), the problem domain Ω is bounded by the

Dirichlet boundary conditions, either homogeneous or inhomogeneous, depending on the excitations. For simplicity, two cases are specified as follows:

Case 1: septum A is set to 1 Volt while septum B is at 0 Volt;

Case 2: septum A is set to 0 Volt while septum B is at 1 Volt.

In both cases, the outer conductor is always set to 0 Volt. The same value of the characteristic impedance can be found when dealing with either case.

The two-dimensional electric potential $\Phi(x, y)$ distribution is governed by the following Laplace equation

$$\frac{\partial^2\Phi(x,y)}{\partial x^2} + \frac{\partial^2\Phi(x,y)}{\partial y^2} = 0 \tag{3.1}$$

and the associated boundary conditions mentioned above.

The problem is to find the potential distribution first. In the quasi-static analysis, the TEM fields can be obtained via the potential distribution, and then the characteristic impedance is resolved by the electric energy stored per-unit length in the system. Using the finite element procedure, the appropriate functional to be minimized for (3.1) is

$$F(\Phi) = \int_\Omega [(\frac{\partial\Phi(x,y)}{\partial x})^2 + (\frac{\partial\Phi(x,y)}{\partial y})^2] dxdy \tag{3.2}$$

where the problem domain Ω is divided into finite elements.

By introducing the linear interpolation functions in each element and minimizing the functional (3.2), we have the following final system of equations

$$[K][\Phi] = [f] \tag{3.3}$$

where $[K]$ is a symmetric matrix by virtue of the self-adjointness of the Laplacian operator describing the potential distribution, and $[f]$ contains the contributions from the inhomogeneous *Dirichlet* boundary condition. Fig.3.2 illustrates the potential distribution in the cross section of the TTEM cell.

Once the potential distribution is obtained, the TEM field distributions in the cross-sectional area are ready to be obtained numerically from

$$\vec{E}(x,y) = E_x(x,y)\vec{a}_x + E_y(x,y)\vec{a}_y = -\nabla\Phi(x,y) \tag{3.4}$$

and for each element, we have

$$E_x = -\frac{1}{2A}[(y_j - y_m)\Phi_i + (y_m - y_i)\Phi_j + (y_i - y_j)\Phi_m] \tag{3.5}$$

$$E_y = -\frac{1}{2A}[(x_m - x_j)\Phi_i + (x_i - x_m)\Phi_j + (x_j - x_i)\Phi_m] \tag{3.6}$$

where A is the area of each element, and $\Phi_{i,j,m}$ represent the electric potentials at three vertices (i, j, m) of each triangular element, respectively.

Fig.3.3 and Fig.3.4 show the dominant electric field component distributions for *Case* 1 and *Case* 2 in a TTEM cell. The field centers in Fig.3.3 and Fig.3.4 are the geometric center of the uniform E−field area. The dot-dashed line in both figures indicates the "one-third-area" rule of the cell's lower usable space.

The "one-third-area" rule was recommended in [74] as a reference to justify the uniform distribution of the electric field in the referred space in the TEM cell, which consists of a third the lower chamber height and width. In fact, the field uniformity varies with both position and operating frequency when an empty cell is concerned. As the frequency increases, the higher order modes will perturb the well-established dominant (TEM) mode distribution and field variation due to non-ideal termination match will occur [76]. However, if the cell is well matched over the prescribed frequency range and a reasonable termination absorber is used, the higher order modes are only weakly excited and are not highly resonant. Thus, this will result in a very uniform field versus frequency [79]. Based on these conditions, field uniformity versus position is of our concern in this chapter. Since the TTEM cell has a tapered structure, the TEM mode propagates as a spherical wave front. Therefore, Fig.3 and Fig.4 are really a projection. Reference [79] reported that the projection introduces variations of less than ± 0.1 dB. The "one-third-area" rule defined here and the normalized electric field distributions in Fig.3 and Fig.4 are then referred to the TEM mode field uniformity versus the transverse plane position.

For the geometric structure chosen, the characteristic impedance is obtained as $Z_0 = 49.36\Omega$, which is derived from

$$Z_0 = \frac{V^2}{c\int_\Omega \epsilon |\vec{E}(x,y)|^2 dxdy} \tag{3.7}$$

where c is the velocity of light and ϵ is the dielectric constant (air assumed here). In either *Case* 1 or *Case* 2, the voltage V is always 1 Volt. The integral in the denominator of (3.7) represents the electric field energy stored per-unit length in the multiple-conductor system, which can be numerically determined. The total number of the triangular elements involved in the calculations for the field and the impedance is 512, i.e. 16 uniform divisions on each side. The characteristic impedance obtained here can only be taken as a reference for engineering design of the TTEM cell since the calculation of Z_0 is based on a uniform transmission line. More rigorous work concerning the static analysis may resort to a 3-D analysis or other numerical methods as in [73].

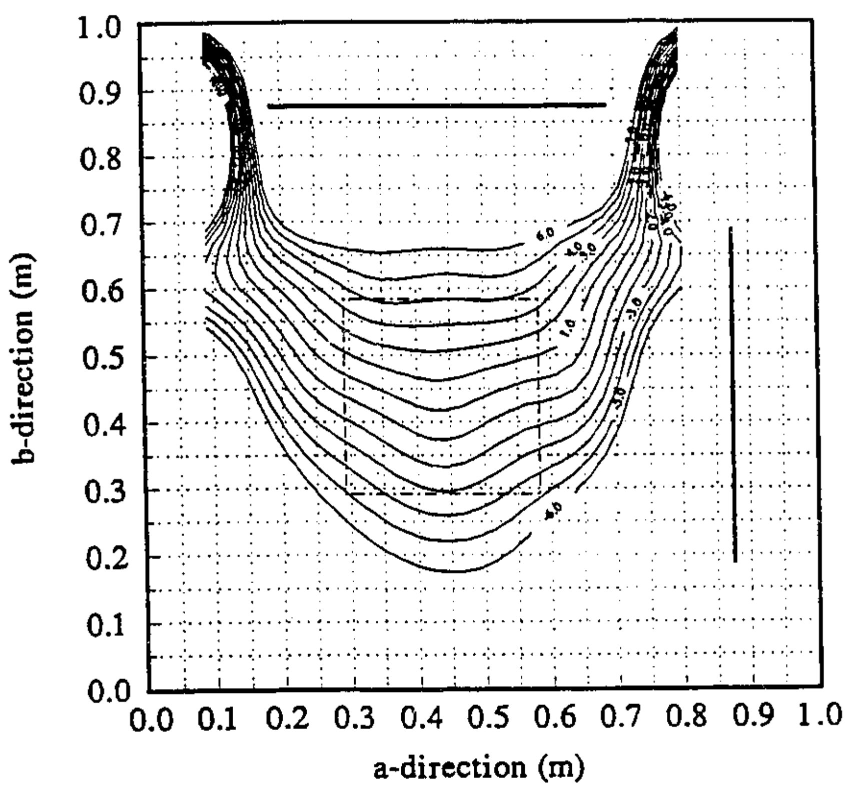

Figure 3.3: *Case* 1: Variation of the vertical electric field (E_y) distribution in a Triple-TEM cell. The figures on each curve indicate the normalized variations in dB to the value of E_y at the field center. ($a = 1.0m, b = 1.0m, w = 0.5m, h = 0.875m, g = 0.1875m$; field center: $x_c = 0.4375m, y_c = 0.4375m$.)

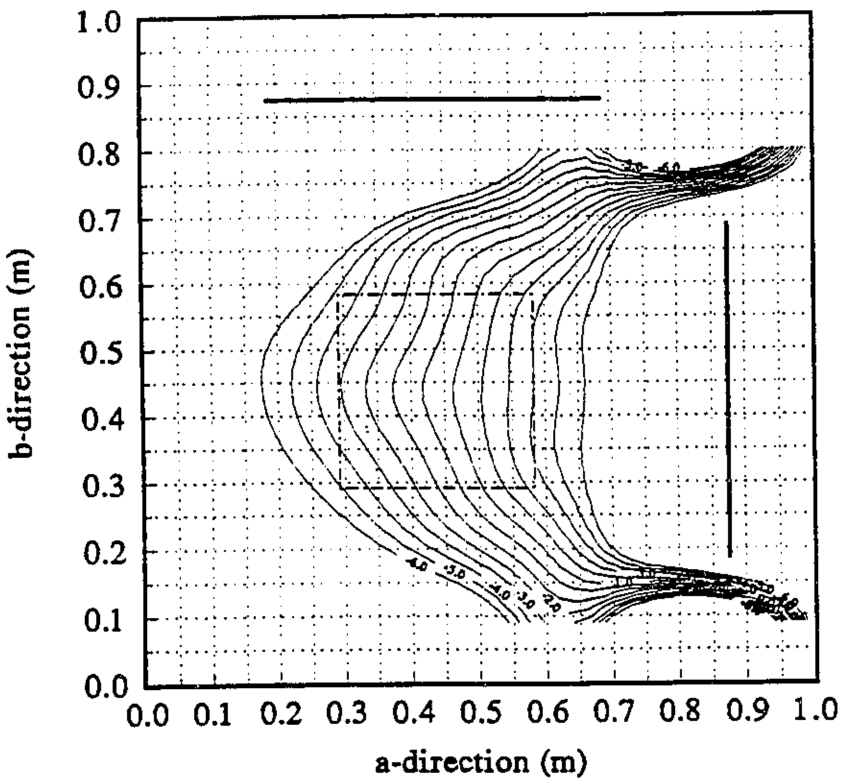

Figure 3.4: *Case* 2: Variation of the horizontal electric field (E_x) distribution in a Triple-TEM cell. The figures on each curve indicate the normalized variations in dB to the value of E_x at the field center. ($a = 1.0m, b = 1.0m, w = 0.5m, h = 0.875m, g = 0.1875m$; field center: $x_c = 0.4375m, y_c = 0.4375m$.)

3.3 HIGH FREQUENCY PERFORMANCE

The significance of investigating the behavior of the TE and TM modes is well known to TEM cell users and designers. Since the TTEM cell has a tapered structure like the GTEM cell, the analysis procedure described in [67] for the nonuniform transmission line will be partially adopted here. This procedure is as follows: first, the cutoff frequencies of the higher order modes in the uniform structure with the same geometric ratios are determined; then, the "local mode concept" [67] is applied to obtain the distributions of the higher order modes in the longitudinal (z-) direction. The uniform cross section analysis carried out here is a numerical one which differs from the analytical approach used in [67].

3.3.1 The LDFEM Formulation For 2-D Structure

Consider a 2-D scattering problem in a domain that is bounded by a homogeneous *Dirichlet* boundary. The assumed excitation could be a line source of E_z-field for the TM modes or H_z-field for the TE modes, which could be located anywhere in the bounded domain. For this two-dimensional case, it is also assumed that the fields have no variations along the z-coordinate (Fig.3.1). The problem formulation with the LDFEM will be the same for either the TE mode case or the TM mode case. Thus, only the TM mode formulation is presented here as a demonstration. Being different from conventional FEM formulations, the LDFEM algorithm first starts in the time domain, and then solves the problem in the Laplace domain, and finally provides the results in the frequency and/or time domain.

The following wave-equation is derived from Maxwell equations for the TM mode case:

$$\frac{\partial^2 \vec{E}}{\partial x^2} + \frac{\partial^2 \vec{E}}{\partial y^2} - \epsilon\mu \frac{\partial^2 \vec{E}}{\partial t^2} = 0 \tag{3.8}$$

where

$$\vec{E} = E_z(x, y, t)\vec{a}_z \qquad (TM\ mode)\ . \tag{3.9}$$

Applying a Laplace transform to (3.8) yields

$$\frac{\partial^2 \tilde{E}}{\partial x^2} + \frac{\partial^2 \tilde{E}}{\partial y^2} - \epsilon\mu s^2 \tilde{E} + \epsilon\mu s E(0^-) + \epsilon\mu E'(0^-) = 0 \tag{3.10}$$

where $\tilde{E}$ is the E_z-field in the Laplace domain with s being the Laplace parameter and $E'(0^-)$ representing the first derivative of $E_z(x, y, t)$ $(t = 0^-)$ with respect to time t. Since only the results in the frequency domain are of concern in this specific application, the initial conditions for (3.10) are assumed as follows

$$E(0^-) = E(x, y, 0^-) = 0 \tag{3.11}$$

$$E'(0^-) = E'(x, y, 0^-) = 0\ . \tag{3.12}$$

Applying the finite element procedure to (3.10)-(3.12) and the associated boundary conditions stated previously, we have the following functional

$$F(\tilde{E}) = \int_\Omega (\nabla\tilde{E})^2 dxdy + \int_\Omega \epsilon\mu s^2 \tilde{E}^2 dxdy \tag{3.13}$$

where the problem domain Ω is divided into triangular finite elements, and an implicit inhomogeneous *Dirichlet* condition due to the excitation is assumed. If proper shape functions are introduced in each element, we obtain the finite element equations as

$$\{[C] + \epsilon\mu s^2[D]\}[\tilde{E}] = [\tilde{f}] \tag{3.14}$$

in which both $[C]$ and $[D]$ are symmetric and positive definite, and $[\tilde{f}]$ contains the forced terms attributed to the time domain excitation.

Solving (3.14) is not straightforward because of the complex parameter s that is not separable as an independent parameter in the final system of equations. One possible way to solve (3.14) is to reduce both $[C]$ and $[D]$ simultaneously to canonical forms and then all the unknowns except s can be decoupled. To fulfil this, the congruence transformation [77] is introduced.

The final decoupled system of equations of (3.14) after the congruence transformation can be written as

$$\{[C''] + \epsilon\mu s^2[I]\}[\tilde{E}''] = [\tilde{f}''] \tag{3.15}$$

where $[C'']$ is a diagonal matrix that is made of the eigenvalues ($\lambda_1, \lambda_2, ..., \lambda_n$; n is the total number of the unknowns) of the system to be studied and $[I]$ is a unit matrix with $[\tilde{E}'']$ and $[\tilde{f}'']$ being the counterparts of $[\tilde{E}]$ and $[\tilde{f}]$ in (3.14), respectively.

It is noted that the system of equations (3.15) has already been solved since all unknowns in $[\tilde{E}'']$ are decoupled. The nodal solution for $[\tilde{E}'']$ can be expressed, for instance, as

$$\tilde{E}''_j(s) = \frac{A_0}{s}\,[\frac{r''_a(j) + \epsilon\mu s^2 r''_b(j)}{\lambda_j + \epsilon\mu s^2}] \qquad (j = 1, 2, ..., n) \tag{3.16}$$

where $r''_a(j)$ and $r''_b(j)$ are the forced terms after the transformation, and A_0 is the amplitude of a unit-pulse excitation. $\tilde{E}''_j(s)$ can be inverted into the time domain via the inverse Laplace transform

$$E''_j(t) = A_0 r''_b(j)\,[\frac{a_j}{\omega_j^2} - (\frac{a_j - \omega_j^2}{\omega_j^2})cos(\omega_j t)] \tag{3.17}$$

where

$$\omega_j = \sqrt{\frac{\lambda_j}{\epsilon\mu}} \tag{3.18}$$

$$a_j = \frac{r''_a(j)}{r''_b(j)\epsilon\mu} \qquad (j = 1, 2, ..., n)\ . \tag{3.19}$$

Then, $E_j(t)$ $(j = 1, 2, ..., n)$ can be traced back through the relationships developed in the process of the congruence transformation (**Section 2.3**). Negative values of λ_j $(j = 1, 2, ..., n)$ are not expected to appear for (3.18) since the finite element system is positive definite.

3.3.2 Double Defined Nodes (DDN)

It should be noted from (3.9) that the electric field $E_j(t)$ ($j = 1, 2, ..., n$) derived from (3.17) stands for the z-component of the total electric field, i.e. E_z in the TM mode case. The development for the TE mode formulation will be the same only with a substitution of E_z for H_z. However, the treatment of the boundary conditions in the TE and TM mode formulations will be very different, especially for the problem domain bounded merely by perfect conductors. In the TM mode case, the perfect conductor can be replaced with a homogeneous *Dirichlet* boundary condition. This replacement can be easily achieved with the FEM formulations. In the TE mode case, the perfect conductor must be replaced with a homogeneous *Neumann* boundary condition. However, this is not straightforward for the inner conductors, like conductors A and B in Fig.3.1. To avoid this difficulty, Das and Sinha [71] made use of the symmetry of the problem to be solved with the FEM. Thus, their formulation can not be extended to any generally asymmetric case like the TTEM cell.

In this subsection, we introduce a special type of node — Double Defined Nodes (DDN), which will overcome the inconvenience mentioned above. The DDN is based on the concept that the field value at a node on the homogeneous *Neumann* boundary should be treated as an unknown. Furthermore, the DDN is restricted to the TE mode analysis and can be applied to the node which resides on the surface of a zero-thickness perfect conductor that must be an inner conductor in the problem domain. In conventional FEM formulations, the node on an inner perfect conductor with zero thickness is shared by the elements on each side of the conductor. Thus, the field value at that node will be affected by the field contributions coming from the two elements opposite to the conductor such that the homogeneous *Neumann* boundary condition will not be satisfied. In order to separate the influences from the two elements, the node joining the two elements has to be divided into two while the nodes are still at the same position. Fig.3.5 shows the new arrangement of the nodes and the elements connecting to the zero-thickness perfect conductor. In Fig.3.5, nodes $2', 3', 4'$ and $5'$ are the replicas of nodes $2, 3, 4$ and 5. Nodes $2', 3', 4'$ and $5'$ are called "Double Defined Nodes" since they keep the original positions of their counterparts. The zero-thickness conductor appears to have thickness due to this special arrangement (Fig.3.5). Then, the orders of the nodes belonging to the related elements ($e1, e2, ..., e19$)

shall be rearranged while elements $i1$ and $i2$ are two imaginary ones that will not be counted.

3.3.3 Numerical Results And Validations

The LDFEM formulation developed above has three prominent features. First, the eigenvalues determined in (3.15) already reveal the frequency domain information pertinent to the system without solving for each of the nodal unknowns, say $E_j(t)$. Secondly, at each node there exists an explicit expression for the unknown, like (3.16), and thus, the inversion of the Laplace transform is easy to perform in either an analytical or a numerical way. It is noted that the LDFEM algorithm provides solutions for both eigenvalue and deterministic problems at the same time if proper excitation is used. Lastly, it is possible to obtain an explicit time domain expression, like (3.17), for the physical quantity to be known at any location in the problem domain even though the problem can not be solved analytically.

Concerning the present application, the LDFEM algorithm is utilized here for an eigenvalue problem formulation in most cases. However, we will compare the frequency domain results derived from both eigenvalue and deterministic solutions later.

A symmetric TEM cell (Fig.3.6) is taken here as a test problem for this 2-D formulation with the LDFEM. A group of typical geometric parameters of the TEM cell, for which the cutoff frequencies of the first few higher order modes are reported in the literature [70] - [72] [74], is given in Table 3.1. Table 3.1 also shows a comparison of the TE mode cutoff frequencies derived from the present method (LDFEM) and other methods. The cutoff frequencies for the TE modes are obtained directly from the eigenvalues $(\lambda_1, \lambda_2, ..., \lambda_n)$ in (3.15) as

$$f_{c_j} = \frac{c}{2\pi}\sqrt{\lambda_j} \qquad (j = 1, 2, ..., n) \tag{3.20}$$

where f_{c_j} refers to different higher order mode as j changes. Good agreement is found in Table 3.1. The numerical results of LDFEM are obtained by using the above-proposed DDN scheme. Thus, the whole problem domain is treated and a full set of cutoff frequencies are yielded. No spurious modes are found in the numerical solutions even though the conventional nodal elements instead of edge elements are used. The number of the elements involved in the calculations shown in the LDFEM (DDN) group (Table 3.1) is 336 and 14 by 12 nonuniform divisions are used. Only the homogeneous *Neumann* boundary condition is involved for this TE mode analysis in the whole problem domain.

For the TM mode case, the same calculation is performed. However, in order to test the LDFEM with hybrid boundary conditions, as *Dirichlet/Neumann* boundary conditions, the symmetry of the problem [71] is taken into account for the TM mode analysis. Table 3.2 shows the numerical results obtained with different methods. Good agreement is also found in Table 3.2. Only a quarter of the symmetric TEM cell is involved in the calculations and the same number of elements as in the TE mode case is used. It should be noted that four different groups of the boundary conditions have to be arranged to account for $TM_{odd,odd}$, $TM_{odd,even}$, $TM_{even,odd}$, and $TM_{even,even}$ modes [71]. Four more mode data that can not be verified with the reported ones in the literature are given, for reference, in Table 3.2.

The above validations of the LDFEM algorithm are only for the eigenvalue problem approach. We are also able to get the cutoff frequencies through a deterministic problem approach. That is, we can solve the problem by placing a time domain excitation inside the problem domain and then find the time domain response at any location inside the same region with the LDFEM algorithm. Using the FFT, the cutoff frequencies can be obtained for the same system. The column at the far right in Table 3.1 indicates the data derived from the FFT, where the symmetry of the problem is introduced in the calculation, as in [71]. Fairly good agreement can be found when comparing with other data in the same table. The data for the TE_{32} mode in the FFT group is missing because the output location is not sensitive to that mode. The deviations found in the data of the FFT group may be due to the following sources: i) the locations of the excitation point and the output point; ii) the resolution of the FFT process; iii) the boundary conditions involved. Experience shows that if the excitation point is chosen to be close to the *Dirichlet* boundary, good results will be yielded. However, since the excitation is introduced as an inhomogeneous *Dirichlet* boundary condition inside the problem domain, the eigenstructure of the system would more or less deviate from the original one depending on the location of the excitation. Anyhow, this deviation can be controlled within an acceptable range for most eigenmodes as shown in Table 3.1.

It should be noticed that the results of the FFT group are obtained at the same time while the DDN results (Table 3.1) are yielded. This means that the LDFEM algorithm solves the problem in both eigenvalue and deterministic approaches. Thus no reformulation is needed. This is especially important when dealing with the following case: an EMP wave impinges on an electromagnetic shield with apertures; using the LDFEM, the high peaks of the wave surges due to the resonances inside the shield (which represent the eigenmodes) can be detected, and the time domain behaviour of the pulse (which reflects the deterministic process) is still traced. A computational example for this case has been given in **Section 2.5**.

Table 3.1: The first few TE mode cutoff frequencies (MHz) in sequence

The symmetric TEM cell: $a = 3.05m,\ b = 3.65m,\ w = 2.03m$						
Mode	LDFEM (DDN)	[71]	[72]	[75]	[70]	LDFEM (FFT)
TE_{01}	14.9	15.3	15.1	15.2	15.5	15.85
TE_{10}	24.6	24.6	24.6	24.6	24.6	25.02
TE_{11}	31.0	31.2	31.0	31.3	31.9	31.70
TE_{02}	41.4	41.1	41.1	41.1	41.1	44.21
TE_{21}	45.7	45.5	45.4	45.4	52.9	45.88
TE_{12}	48.6	47.8	47.8	47.8	47.8	48.38
TE_{20}	49.6	49.2	49.2	49.2	49.2	53.39
TE_{03}	54.5	54.2	-	-	-	55.05
TE_{13}	61.6	62.1	-	-	-	63.40
TE_{22}	65.7	64.1	-	-	-	72.57
TE_{23}	73.8	73.2	-	-	-	74.24
TE_{30}	75.5	73.8	-	-	-	75.07
TE_{31}	77.7	76.9	-	-	-	76.74
TE_{32}	84.9	84.4	-	-	-	-
TE_{33}	87.7	87.2	-	-	-	87.59

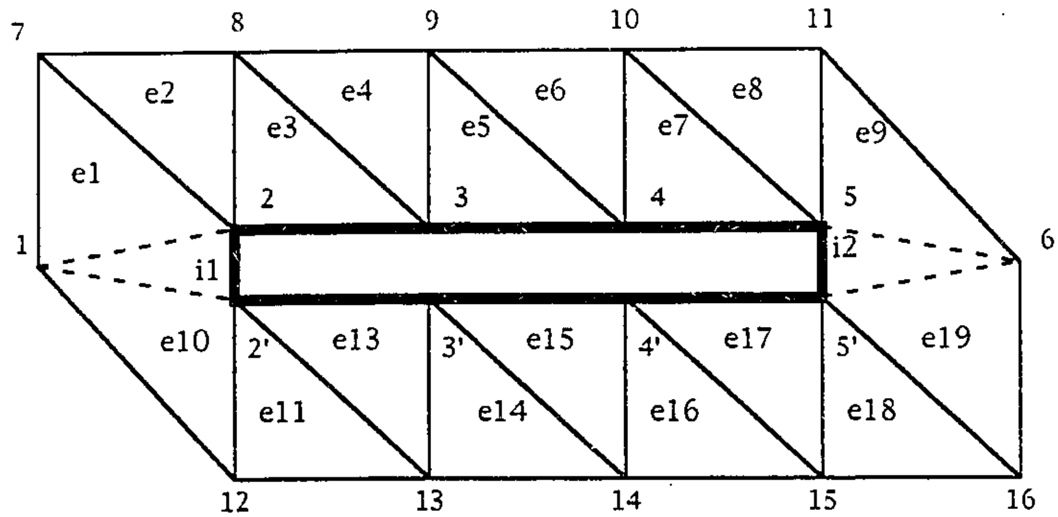

Figure 3.5: Double defined nodes on a perfect conductor for TE mode calculations (the rectangular box represents a zero-thickness perfect conductor.).

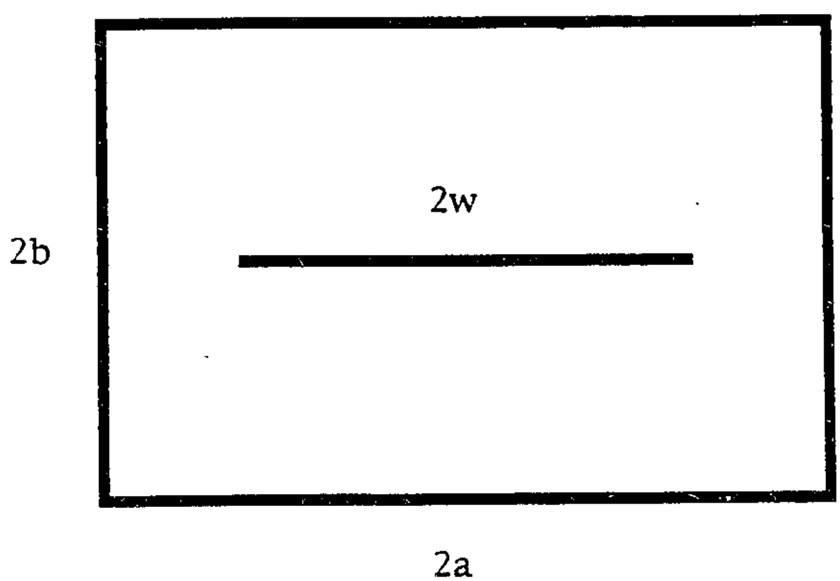

Figure 3.6: A symmetric TEM cell as a test problem of the higher order modes.

Table 3.2: The first few TM mode cutoff frequencies (MHz) in sequence

The symmetric TEM cell: $a = 3.05m$, $b = 3.65m$, $w = 2.03m$					
Mode	LDFEM	[71]	[72]	[75]	[70]
TM_{11}	47.95	47.9	47.6	47.5	54.2
TM_{12}	48.07	47.8	47.8	47.8	47.8
TM_{21}	64.19	64.3	-	-	-
TM_{22}	64.56	64.1	-	-	-
TM_{32}	85.38	-	-	-	-
TM_{33}	84.76	-	-	-	-
TM_{41}	96.01	-	-	-	-
TM_{42}	97.26	-	-	-	-

3.4 THE TRIPLE-TEM CELL

3.4.1 Higher Order Mode Cutoffs

The LDFEM algorithm that is established above and tested for the symmetric TEM cell can be directly applied to the TTEM cell with only changes to the input data because of the special geometry of the septums. The model dimensions chosen here are the same as the ones used in **Section 3.2** such that the 50 Ω impedance match can be guaranteed.

Table 3.3 shows the cutoff frequencies of the first few higher order modes (TE and TM) in a TTEM cell (Fig.3.1: $a = 1.0m$, $b = 1.0m$, $w = 0.5m$, $h = 0.875m$, and $g = 0.1875m$). In the calculation of TE modes, the DDN scheme is used and the number of elements is 512 (16 by 16 uniform divisions). The small numerical difference (Table 3.3) (less than 1.8%) between the cutoff frequencies of the two degenerate modes is caused by using non-symmetric meshes according to the physical structure. All the numerical results indicated in Table 3.3 are obtained using the eigenvalue problem approach described in the previous subsection. We have also obtained similar results (not shown here) using the deterministic problem approach.

It appears that the cutoff frequency of the first higher order mode in Table 3.3 is higher than that of a standard symmetric TEM cell with comparable outer dimensions. This may be due to the following reasons. First, theoretical calculations [70] of the first cutoff frequency of an asymmetric TEM cell show that the first cutoff increases as a parabolic function instead of a linear function of the location coordinate when the septum (for instance, septum A in Fig.1) is offset in the y-direction. Secondly, the two septums are simultaneously offset with a quite large ratio ($2h/b = 1.75$) in our calculating model. Thus, the offsetting effects on our numerical results would be doubly enhanced when compared with the symmetric septum case. In fact, we have calculated the cutoff frequencies for an asymmetric TEM cell and the program developed by us was proved to be working well.

Table 3.3: TE and TM modes cutoff frequencies (MHz) for a TTEM cell

The Triple-TEM cell: $a = 1.0m$, $b = 1.0m$, $w = 0.5m$ $h = 0.875m$, $g = 0.1875m$	
TE Mode	TM Mode
136.27	242.52
138.79	381.21
203.64	388.89
216.17	484.72
220.75	545.28
324.23	555.00
324.52	606.04
344.73	640.66

Further results about the local higher order modes are reported in [80] and will be included in the next subsection.

3.4.2 Local Modes And Longitudinal Behaviour

Up till now, we have calculated the cutoff frequencies in a cross-sectional area of the TTEM cell. It is found that the cutoff frequency of each mode is inversely proportional to the longitudinal coordinate (z-coordinate) because of the tapered structure [67]. Then, according to the "local mode concept" [67], the propagation properties of the local modes can be expressed as:

$$\beta_k = k_0\sqrt{1 - (\frac{z_{end} f_{c_k}|_{end}}{zf})^2} \tag{3.21}$$

where k_0 is the propagation constant of free space. Using (3.21), we can also determine the position where a higher order mode enters into propagation (Fig.3.7 - Fig.3.10). The

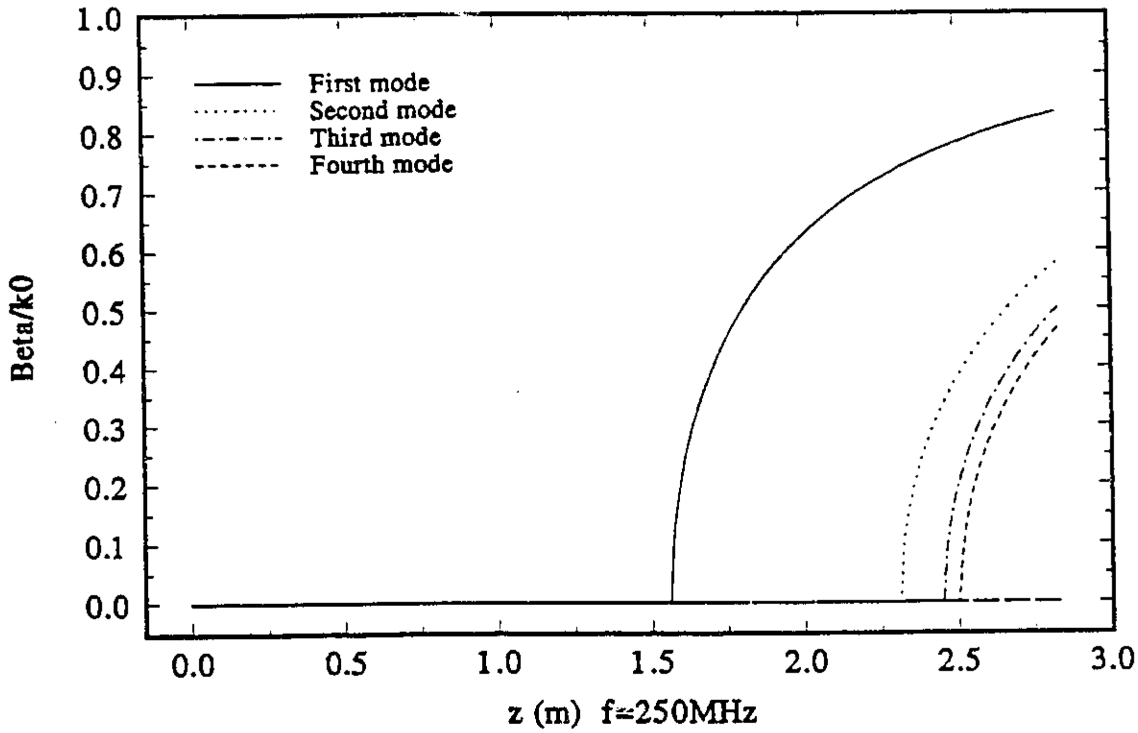

Figure 3.7: Normalized propagation constants of higher order TE modes in z-direction (f = 250MHz).

calculating model is as follows: the length of the TTEM cell $z_{end} = 2.836m$; the conical angle $\alpha = 20$ *degrees* [64]; the geometric parameters that belongs to the far end section, i.e., a, b, w, h, g, are the same as those given in Table 3.3.

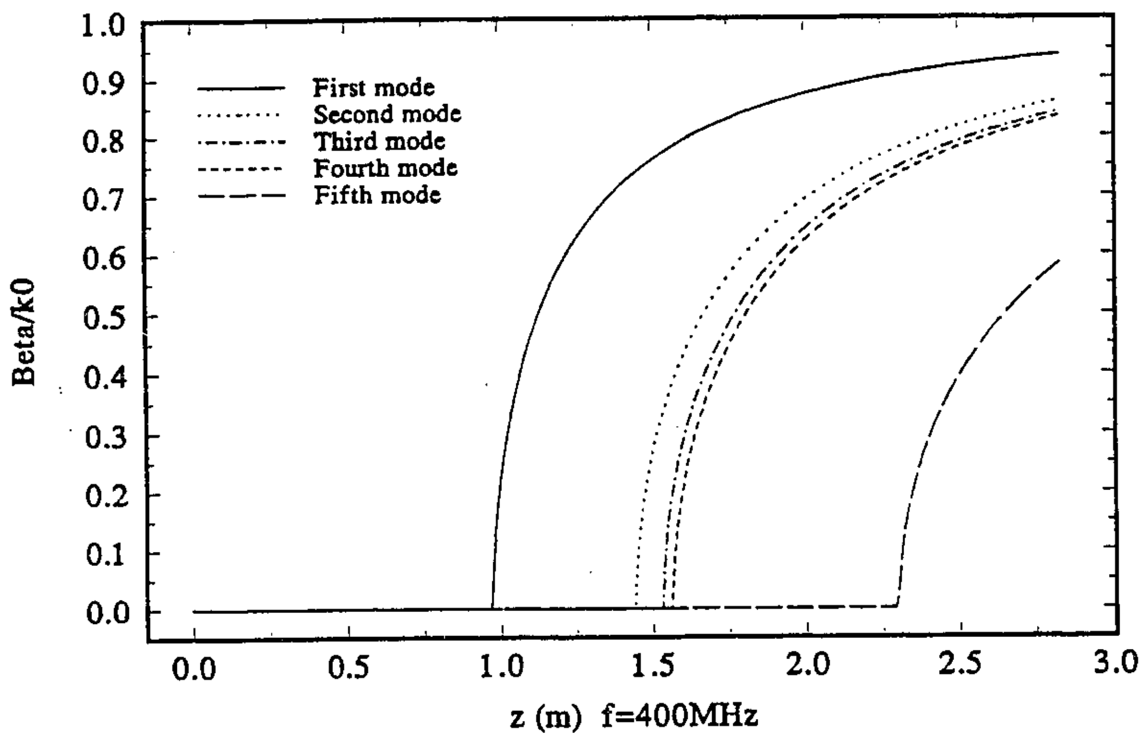

Figure 3.8: Normalized propagation constants of higher order TE modes in z-direction (f = 400MHz).

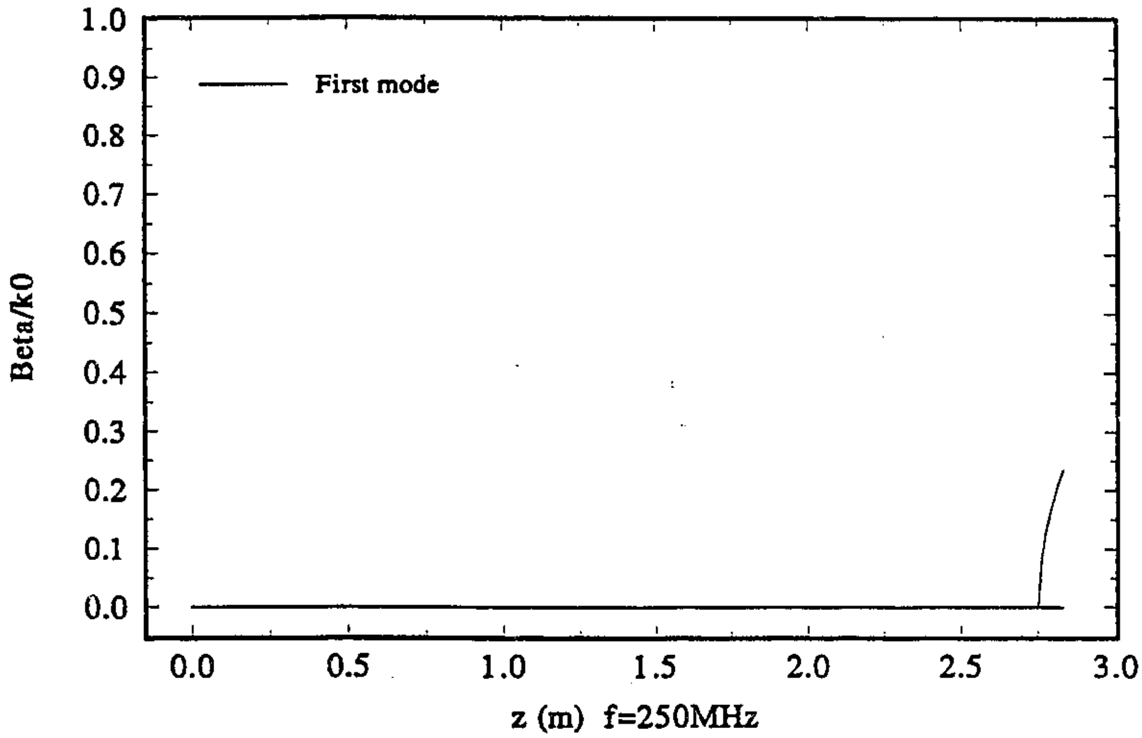

Figure 3.9: Normalized propagation constants of higher order TM modes in z-direction (f = 250MHz).

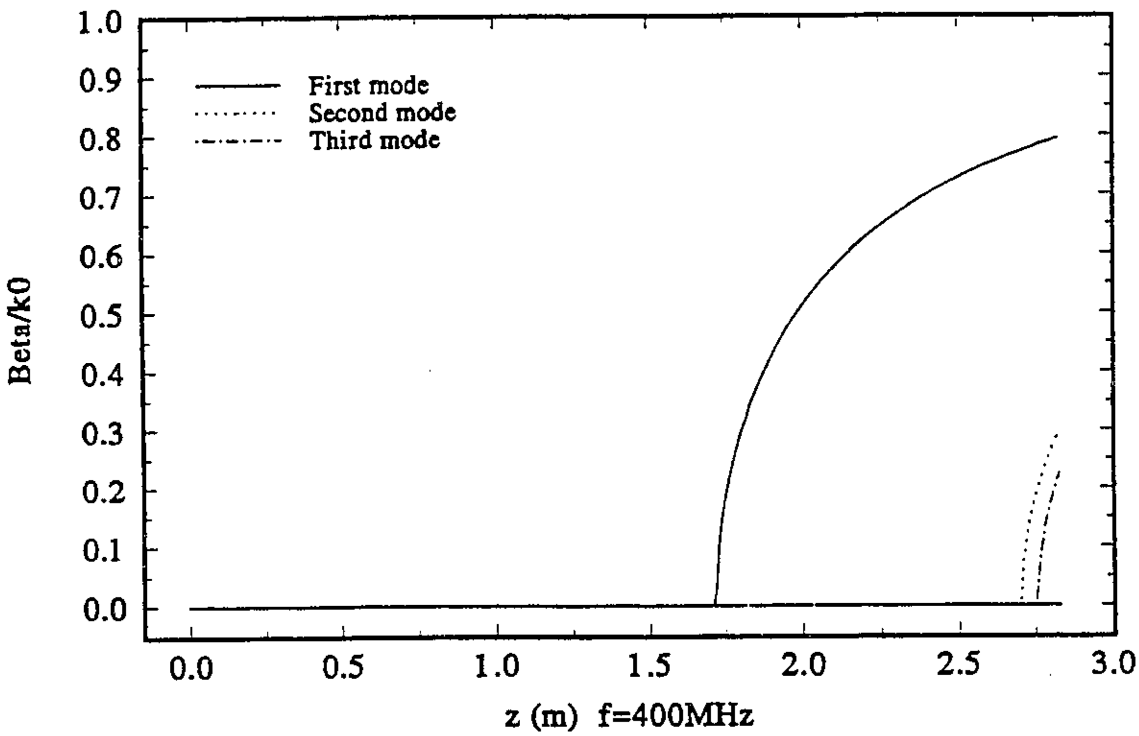

Figure 3.10: Normalized propagation constants of higher order TM modes in z-direction (f = 400MHz).

3.5 COMPUTER-AIDED ENGINEERING DESIGN

The main factors of an engineering design of the Triple-TEM cell could be thought of as follows: *A. Electrical aspects* : 1) impedance matching, 2) uniform field area, and 3) higher order modes; *B. Mechanical aspects*. In this chapter, the computer-aided-design (CAD) approach is confined to the *Electrical aspects* only. The proposed CAD approach is based upon the software developed for the three electrical design factors mentioned above. A brief description of the software packages is given as below:

$Software\ TTEM-A$: Calculation of field distribution and characteristic impedance;

$Software\ TTEM-B$: Calculation of TE mode cutoff frequencies;

$Software\ TTEM-C$: Calculation of TM mode cutoff frequencies.

Using the above software packages, an optimum design of the TTEM cell can still be achieved even though a synthesis software has not been developed yet. The initial input data will be chosen based on the size of the EUT and the frequency range that would be used for EMC testing. Generally, the EUT size should satisfy the "one-third-area" requirement, and then the dimensions of the outer conductor can be estimated. Using these as initial input data, the first round calculations with $Software\ TTEM-A$ could provide the value of the characteristic impedance corresponding to the initial structure.

Usually, several adjustments are needed to achieve the 50Ω matching condition. Then, the uniform field area will be checked up to meet both size and uniformity requirements. Adjustments of the geometry of the septums are necessary in the above processes. Finally, the properties of the higher order modes will be obtained with the use of the $Software\ TTEM-B$ and $Software\ TTEM-C$.

3.6 CONCLUSIONS

A numerical 2-D analysis is presented in this chapter for the 3-D structure of the Triple-TEM cell. Basic static and dynamic characteristics of the TTEM cell are obtained by using the conventional finite element method and a novel finite element method — LDFEM.

The "Double Defined Nodes" (DDN) proposed in the present analysis provides efficient way to deal with the inner conductors with zero-thickness in the problem domain for the TE mode case. As a convention, the thickness of the septum in the TEM cell can be ignored [66] - [73]. In fact, if the thickness of the septum is needed to be taken into account, the DDN can still be extended to this case without difficulty.

The LDFEM can be used for either eigenvalue or deterministic problems and provides either time domain or frequency domain results. In this chapter, the LDFEM is fully utilized as an approach to an eigenvalue problem and only frequency domain results are yielded. We have presented several time domain applications with the LDFEM in [77]. However, one example of using time domain results to obtain frequency domain ones through the solution to a deterministic problem is provided in Table 3.1 (the FFT group). In this case, it is suggested that the unit-step pulse as the time domain excitation be applied since it has a wide spectrum. With the Laplace transform, there is no difficulty to tackle the unit-step pulse. Thus, we are able to obtain as many resonances, which are interpreted as cutoff frequencies [77], as possible. Even though the LDFEM is not a time-stepping method, it is necessary to have sufficient time domain results provided by many time divisions such that good resolution is achieved with the use of the FFT if we use the LDFEM as a deterministic approach.

On the other hand, the LDFEM itself yields frequency domain information such as cutoff frequencies, without any time divisions or involvement of the FFT, as developed in this chapter. Having implemented the analyses of the static and dynamic characteristics, a reasonable physical structure of the TTEM cell could then be resolved. Further experimental work is needed to construct a real TTEM cell based on the present computer simulation.

Chapter 4

TIME DOMAIN ANALYSIS OF LOSSY VLSI INTERCONNECTS WITH A TIME DEPENDENT SKIN EFFECT MODEL

4.1 INTRODUCTION

The skin effect phenomenon mainly concerned in the analysis of transmission lines has been studied for many years. There are several skin effect models proposed in this technical area. These models could be classified into two categories: frequency domain model and time domain model.

The most popular model in the frequency domain is the representation of the square root of the frequency, i.e. $R(f) \sim \sqrt{f}$, which was introduced by Wigington and Nahman [81] in 1957. Another variety of this form includes a more general model like $A + B\sqrt{s}$ (s is the Laplace parameter) [82], which could be used for a wider frequency range. There are also some other frequency domain models that are represented by more complicated relationships with the physical properties associated with the conductor under study [8] [83] [120] [121]. Recently, a more comprehensive frequency domain model has been proposed by Djordjevic and Sarkar [52], which was derived with a quasi-static approach. This model can be applied to the case that the skin effect may not be pronounced even at frequencies in the gigahertz region [52].

Of the time domain models, Timotin introduced a transient line-resistance to the time domain transmission line equations [84]. A successful application of this model to practical EMC problems can be found in [85]. Their model is limited to the case in which a conductor with round cross-section and a ground plane are involved. For a strip conductor with rectangular cross-section, an implicit form of the time domain resistance accounting for the skin effect was presented by one of the authors in [8].

To solve the skin effect problems, implicit and numerical methods have been adopted [87] [88]. In [87], Graneau's numerical method was used to tackle the resistive and inductive skin effect in rectangular conductors in the mid-range of frequencies. A finite element method (FEM) formulation was proposed for the situations where the skin depth is greater than the thickness of the conductor [88].

In this chapter, we propose a new time domain skin effect model for a conductor with rectangular cross-section and a ground plane. Based on some approximations, the skin effect is taken into account separately in the rectangular conductor and the ground plane by two different time domain resistances. It should be noted that here the term of time domain resistance refers to the concept of impedance. It could be rather called time domain impedance since it includes both resistive and inductive parts of a transmission line. However, for historical reasons [84] [10], we prefer to call it time domain resistance [10] or transient resistance [84]. Both strip and ground plane resistances are represented with explicit expressions in the time domain to form a new skin effect model. It is easier to accommodate this time domain model directly in the transient analysis of interconnects used in VLSI systems than any other frequency domain models, where the Inverse Fast Fourier Transform (IFFT) is an indispensable tool. Naturally, the contribution of the new model to the time domain analysis of coupled lines takes into account the time/frequency dependent losses and dispersion of the subjects under study.

Uniform and nonuniform coupled transmission lines are used to model the interconnection lines in high speed digital circuit packages, integrated circuits, packaging and chip modules. Both time domain and frequency domain techniques have been developed in recent years for the analysis of such single or coupled line structures that are lossless or lossy, or even dispersive with frequency. A good list of the references in this technical area can be found in [9]. Two references have recently addressed a method of using numerical convolution in conjunction with the method of characteristics [8] [10]. By making use of the modal analysis techniques, coupled uniform and nonuniform lines can be analyzed with this method. Concerning the Method of Convolution-Characteristics (MCC) [10], it is noticed that several restrictions are applied to this method. For example, the line structures should be identical and only adjacent lines are taken into account [10]. In this chapter, a modified MCC is proposed and the above restrictions are removed. Furthermore, the new time domain skin effect model is employed in this modified method, for which any aliasing problem associated with the IFFT will be eliminated.

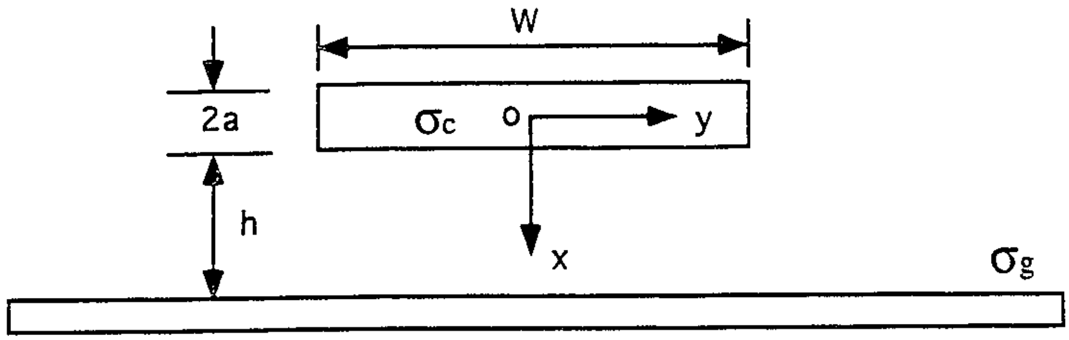

Figure 4.1: A rectangular conductor with the width much lager than the thickness.

4.2 TIME DOMAIN SKIN EFFECT MODEL

Considering a rectangular conductor (Fig.4.1, the ground plane in the figure is not taken into account when Eqn.(4.1) is established.) whose width is much larger than the thickness, the magnetic ($H-$) field inside the conductor can be approximated based on the following assumptions: 1) the $H-$field is a function of the $x-$coordinate while it is invariant in $y-$direction; 2) the $H-$field along the edges of the cross-section of the conductor is constant. The $H-$field is then governed by the following equation in the Laplace domain:

$$\frac{d^2\tilde{H}(x,s)}{dx^2} - \sigma\mu s\tilde{H}(x,s) = 0 \tag{4.1}$$

and the associated boundary conditions

$$\tilde{H}_1(x,s)\mid_{x=a} = \tilde{f}_D(s) \tag{4.2}$$

$$\tilde{H}_2(x,s)\mid_{x=-a} = -\tilde{f}_D(s) \tag{4.3}$$

$$\tilde{f}_D(s) = \frac{\tilde{I}(s)}{2(w+2a)} \tag{4.4}$$

where $\tilde{I}(s)$ is the total current flowing through the conductor, and $\tilde{H}(x,s)$ represents the $H-$field in the Laplace domain. In Eqn.(4.4), w is the width of the conductor and $2a$ the thickness of the same conductor. The two assumptions mentioned above imply that only the skin effect is considered while the edge effect has been neglected. The solution to the above equation is

$$\tilde{H}(x,s) = \tilde{H}_y(x,s) = \frac{\tilde{f}_D(s)}{sinh(\beta a)} sinh(\beta x) \tag{4.5}$$

where

$$\beta = \frac{\sqrt{s\tau_c}}{a} \tag{4.6}$$

and

$$\tau_c = \mu \sigma_c a^2. \tag{4.7}$$

In Eqn.(4.7), σ_c is the conductivity of the signal conductor. From Maxwell's equations, the electric field can be found as

$$\tilde{E}(x,s)\mid_{x=a} = \tilde{E}_z(s) = \frac{\beta}{\sigma_c} \frac{\tilde{f}_D(s)}{sinh(\beta a)} cosh(\beta a). \tag{4.8}$$

It should be noted that βa is independent of a with regard to Eqn.(4.6).

The voltage induced on the per unit length loop between the strip conductor and a current return that consists of the same conductor can be expressed as

$$\tilde{V}(s) = 2\tilde{E}_z(s) + s\tilde{I}(s)L_{ext} \tag{4.9}$$

where L_{ext} is the external inductance of the structure. The line impedance can be expressed as

$$\tilde{Z}(s) = \frac{\tilde{V}(s)}{\tilde{I}(s)} = 2\frac{\tilde{E}_z(s)}{\tilde{I}(s)} + sL_{ext}. \tag{4.10}$$

Substituting Eqn.(4.8) into the impedance, one obtains

$$\tilde{Z}(s) = \frac{\sqrt{s\tau_c}cosh(\sqrt{s\tau_c})}{\sigma_c awsinh(\sqrt{s\tau_c})} + sL_{ext}. \tag{4.11}$$

It is noticed that the first term on the right hand side of Eqn.(4.11) bears a similar form of the internal inductance [121] (differing by a dimension of frequency). However, in our case the mathematical process is carried out in the Laplace domain, which would provide great facility in converting results into the time domain without resorting to the IFFT. By means of the inverse Laplace transform, the time domain resistance of the rectangular conductor is defined as [84]

$$r_c'(t) = L^{-1}[\frac{\tilde{Z}(s)}{s} - L_{ext}] \tag{4.12}$$

i.e.

$$r_c'(t) = L^{-1}[2r_{dc}\sqrt{\tau_c}\frac{coth(\sqrt{s\tau_c})}{\sqrt{s}}] \tag{4.13}$$

where the dc resistance of the conductor per unit length is

$$r_{dc} = \frac{1}{2a\sigma_c w}. \tag{4.14}$$

In fact, the inverse Laplace transform of Eqn.(4.13) can be performed analytically and it is found as [89]

$$r_c'(t) = 2r_{dc}[1 + \sum_{n_r=1}^{\infty} 2e^{-\frac{\pi^2 n_r^2}{\tau_c}t}]. \tag{4.15}$$

In regard to the time domain resistance established above, the return path is assumed to be the same conductor as the signal conductor. However, it would be more practical if we take into account the time domain resistance in a real ground plane composed of a larger conductor with finite conductivity. Thus we return back to the configuration depicted in Fig.4.1.

An indepth study of the ground plane resistance has been performed in the frequency domain [120], where the configuration of a strip conductor above a ground plane was taken as a research objective. Based on numerical calculations, an asymptotic expression which reveals the relationship between the ground plane ac resistance and the strip conductor resistance has been derived as [120]

$$R_g = 0.55 r_{dc} \frac{2a}{\delta}(1 - e^{-\frac{w}{1.2\pi h}}) \tag{4.16}$$

where δ is the skin depth and h is the separation between the strip conductor and the ground plane. Let us also consider another expression which is given as an ac resistance approximation for a single strip conductor [122]

$$R_{ac} = \frac{1}{\sigma_c \delta} \frac{l}{2w + 4a} \tag{4.17}$$

in which l the length of the conductor. Combining (4.14) (4.17) with (4.16) and assuming $l = 1m$ for per unit length consideration, we may have the following expression for the ground plane resistance

$$R_g = 1.1 R_{ac}(1 - e^{-\frac{w}{1.2\pi h}}). \tag{4.18}$$

There are several points that should be mentioned considering the application of (4.18) to our time domain resistance analysis. First, Eqn.(4.18) is derived from frequency domain but it does not explicitly display the dependancy of frequency. This means that if R_{ac} is given in the time domain, R_g may also be revealed in the time domain through Eqn.(4.18). Secondly, Eqn.(4.16) covers a wide range of the asymptotic behavior (from $w/h = 0$ to $w/h = 10$) of the ground plane resistance, and the error displayed by Eqn.(4.16) due to the frequency dependency (from $1GHz$ to $10GHz$) is very small for w/h up to 5 with a fixed thickness (referring to Fig.12 in [120]). Thirdly, in practice most applications would not require very large w to h ratio. This means that the strip conductor is relatively high above the ground plane in a realistic consideration. Thus Eqn.(4.17) could be reasonably applied to any case in which w/h is small, say $w/h < 5$, and so could Eqn.(4.18).

Based on the above justification, the resistance of the signal conductor and the resistance of the ground conductor can, in principle, be superimposed [83] [84] [120]. The global time domain resistance is expressed as $r(t) = r_c(t) + r_g(t)$, where $r_c(t)$ is half of $r'_c(t)$ and $r_g(t)$ is derived from Eqn.(4.18) in which R_{ac} should be replaced by $r_c(t)$.

4.3 MODAL ANALYSIS AND CONVOLUTION SOLUTION

The new skin effect model presented in the previous section can be applied to either a single line or multiconductor systems. To the latter, the model is approximated by ignoring the proximity effect caused by the adjacent lines. However, this model does take into account the geometric structure in the skin effect model while this information is not fully revealed in the traditional skin effect model, i.e. the square root of the frequency. In fact, the geometric structure of the conductors affects not only the dc resistance but also the decaying rate of the transient resistance in the early times when only the skin effect is considered (referring to Eqns.(4.15) and (4.18)).

The method of characteristics has been extensively used in the analysis of VLSI interconnects problems for years [9]. There is a way to directly adopt the time domain resistance into the method of characteristics [8] [10]. To do so a numerical convolution must be involved. The combination of the numerical convolution and the method of characteristics has been called "the Method of Convolution-Characteristics" [10]. We can call it the MCC for simplification. The MCC procedure proposed in [10] will be reformulated and fit in with our analysis. A generalized MCC should be a versatile way that is able to solve single/multiconductor, uniform/nonuniform and linear/nonlinear transmission line problems in the time domain. In addition, time/frequency dependent parameters, such as R, L, G , and C, can be well involved with the MCC.

For multiconductor systems, several modal analysis approaches have been attempted [5] - [7] to generalize the method of characteristics. In [10], Mao and Li adopted Romeo and Santomauro's approach [90] in their MCC for multiconductor transmission lines. Two assumptions have to be made for applying this approach [10]. The more crucial assumption results in truncating or eliminating the contributions coming from the fourth and farther away lines (see Fig.9 (c) in [91]) while this can be avoided by using another approach proposed in [7]. In this chapter, the more general approach used in [7] will be employed to decouple the multiconductor systems where the time/frequency dependent lossy properties are still retained.

4.3.1 Modal Analysis

The time domain analysis on m coupled lossy transmission lines can be carried out starting from the following generalized propagation equations [92]

$$\frac{\partial[v(z,t)]}{\partial z} = -[L_{ext}(z)]\frac{\partial[i(z,t)]}{\partial t} - \frac{\partial}{\partial t}\int_0^t [r(z,t-\tau)][i(z,\tau)]d\tau \tag{4.19}$$

$$\frac{\partial[i(z,t)]}{\partial z} = -[C(z)]\frac{\partial[v(z,t)]}{\partial t} - [G(z)][v(z,t)] \tag{4.20}$$

where $[v(z,t)]$ and $[i(z,t)]$ are $m \times 1$ voltage and current vectors, $[r(z,t)]$, $[L_{ext}(z)]$, $[G(z)]$ and $[C(z)]$ are $m \times m$ matrices per unit length, which characterize the transmission line system. It is assumed that the voltage and current vectors are initially zero everywhere on the lines. The boundary conditions of Eqns.(4.19) and (4.20) are given by

$$[v(z,t)] = F_1([v_s(t)],[i(z,t)],t) \qquad (z=0) \tag{4.21}$$

$$[v(z,t)] = F_2([v_L(t)],[i(z,t)],t) \qquad (z=D) \tag{4.22}$$

where $[v_s]$ and $[v_L]$ are two voltage vectors applied at the input $(z=0)$ and output $(z=D)$ of the network, respectively, and F_1 and F_2 represent two well behaved vector functions that can be extended to any arbitrary terminations.

The coupled system of equations (4.19) (4.20) should be first decoupled to accommodate the method of characteristics. Two transformed vectors are defined as below [7]

$$[v(z,t)] = [T_v(z)][v_T(z,t)] \tag{4.23}$$

$$[i(z,t)] = [T_i(z)][i_T(z,t)] \tag{4.24}$$

where $[T_v(z)]$ and $[T_i(z)]$ are $m \times m$ matrices, and $[v_T(z,t)]$ and $[i_T(z,t)]$ are transformed voltage and current vectors, respectively. Substituting (4.23)-(4.24) into (4.19)-(4.20), the decoupled system of equations are

$$\frac{\partial[v_T(z,t)]}{\partial z} = -[L_{ext_T}(z)]\frac{\partial[i_T(z,t)]}{\partial t} - \frac{\partial}{\partial t}\int_0^t [r_T(z,t-\tau)][i_T(z,\tau)]d\tau \tag{4.25}$$

$$\frac{\partial[i_T(z,t)]}{\partial z} = -[C_T(z)]\frac{\partial[v_T(z,t)]}{\partial t} - [G_T(z)][v_T(z,t)] \tag{4.26}$$

where

$$[r_T(z,t)] = [T_v(z)]^{-1}[r(z,t)][T_i(z)] \tag{4.27}$$

$$[L_{ext_T}(z)] = [T_v(z)]^{-1}[L_{ext}(z)][T_i(z)] \tag{4.28}$$

$$[G_T(z)] = [T_i(z)]^{-1}[G(z)][T_v(z)] \tag{4.29}$$

$$[C_T(z)] = [T_i(z)]^{-1}[C(z)][T_v(z)]. \tag{4.30}$$

The subscript T denotes "transformed". $[T_v(z)]$ and $[T_i(z)]$ are two special matrices that have to be determined by ensuring that $[L_{ext_T}(z)]$ and $[C_T(z)]$ are diagonalized. It can be found that $[T_v(z)]$ and $[T_i(z)]$ are the eigenvectors of $[L_{ext_T}(z)][C_T(z)]$ and $[C_T(z)][L_{ext_T}(z)]$, respectively. One would observe that neither $[L_{ext_T}(z)][C_T(z)]$ nor $[C_T(z)][L_{ext_T}(z)]$ is, in general, symmetric though $[L_{ext_T}(z)]$ and $[C_T(z)]$ are real and symmetric, respectively. Thus, the eigenvalue solver should be chosen from the real-general type rather than the real-symmetric type.

The boundary conditions (4.21) and (4.22) are also transformed using (4.23) and (4.24) as

$$[v_T(z,t)] = [T_v(z)]^{-1}F_1([T_v(z)]^{-1}[v_{s_T}(t)],[T_i(z)]^{-1}[i_T(z,t)],t) \qquad (z=0) \qquad (4.31)$$

$$[v_T(z,t)] = [T_v(z)]^{-1}F_2([T_v(z)]^{-1}[v_{L_T}(t)],[T_i(z)]^{-1}[i_T(z,t)],t) \qquad (z=D). \qquad (4.32)$$

Concerning a triple-line structure shown in Fig.4.2, we assume that no nonlinear circuit elements are involved in the terminations at the moment. The terminal resistances at the near and far ends, $[R_s]$ and $[R_L]$, have to be transformed according to (4.31) and (4.31) and they take the form of the following transformation

$$[R_{s_T}] = [T_v(z)]^{-1}[R_s][T_i(z)] \qquad (z=0) \qquad (4.33)$$

$$[R_{L_T}] = [T_v(z)]^{-1}[R_L][T_i(z)] \qquad (z=D). \qquad (4.34)$$

In principle, $[R_{s_T}]$ and $[R_{L_T}]$ are expected to be diagonal matrices. However, this will not be always true. Some conditions have to be imposed and they will be mentioned later in the Discussion and Conclusions. In Fig.4.2, the transformed voltage sources $[V_{s_T}]$ have, in general, all non-zero elements even though there is only one source as designated (Fig.4.2).

4.3.2 Convolution Solution

The convolution term in Eqn.(4.25) can be numerically realized. Tripathi and Orhanovic have used a first order approximation to deal with a similar convolution term [8]. In our case, a more convenient feature by using the new skin effect model is prominent. Since the time domain resistance is explicit in expression, no IFFT is needed and the related error can be avoided. As calculations showed that the first order approximation is good enough to do the job, we present our formulation adopting the same order of approximation.

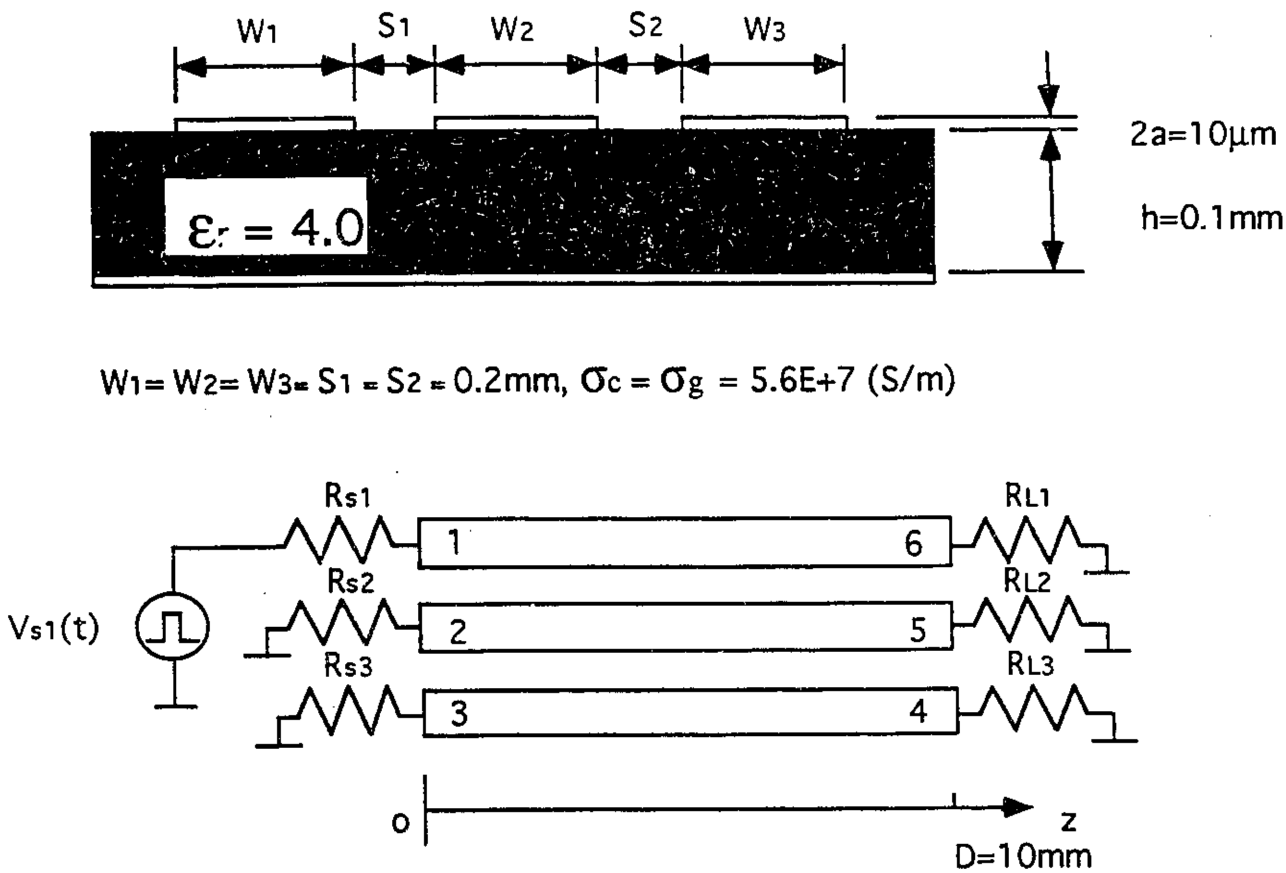

Figure 4.2: A triple-line structure with terminations.

$$\frac{\partial}{\partial t}\int_0^t [r_T(z,t-\tau)][i_T(z,\tau)]d\tau = [r_T(z,0)]\Delta t\frac{\partial[i_T(z,t]}{\partial t} + [Q(z,t)] \tag{4.35}$$

where

$$[Q(z,t)] = [r_T(z,t)][i_T(z,0)] + \sum_{l=1}^{n-1}[r_T(z,t)]\frac{[i_T(z,(n-l+1)\Delta t)] - [i_T(z,(n-l-1)\Delta t)]}{2} \tag{4.36}$$

and $t = n\Delta t$ (Δt is the time step that will be taken in the numerical analysis using the method of characteristics.). Eqn.(4.25) has to be reformulated as

$$\frac{\partial[v_T(z,t)]}{\partial z} = -([L_{ext_T}(z)] + [r_T(z,0)]\Delta t)\frac{\partial[i_T(z,t)]}{\partial t} - [Q(z,t)]. \tag{4.37}$$

It is noticed that $r(t)$ tends to infinity when t is close to zero. Thus some approximation approach [26] can be applied. For instance, the value of $r_c(z,t)$ at $t = 0$ for a single transmission line may be given by

$$r_c(z,0) \approx \frac{4r_{dc}(z)}{\Delta t}\sum_{n_r=1}^{N}[\frac{\tau_c(z)}{\pi^2 n_r^2} - (\frac{\tau_c(z)}{\pi^2 n_r^2} + \frac{\Delta t}{2})e^{-\frac{\pi^2 n_r^2}{\tau_c(z)}\Delta t}] + r_{dc}(z) \tag{4.38}$$

where

$$\tau_c(z) = \mu\sigma_c a^2(z) \tag{4.39}$$

$$r_{dc}(z) = \frac{1}{2a(z)\sigma_c w(z)}. \tag{4.40}$$

N is the number of terms after truncation from the infinity. The term $[r_T(z,0)]\Delta t$ in Eqn.(4.37) represents the transformed internal inductance and it causes a small amount of phase shift in the time domain due to the time/frequency dependent properties which have been taken into account.

4.4 NUMERICAL FORMULATION

The hyperbolic system of partial differential equations of the first order (4.25) and (4.26) together with the boundary conditions (4.31) and (4.31) can be solved with the method of characteristics [9] [4] [6]. Replacing (4.25) with (4.37), a new MCC formulation called *Modified MCC* (*MMCC*) is presented as below

$$\Delta([v_T] + [\rho_T][i_T]) \big|_{z_k,t_n}^{z_{k+1},t_{n+1}} = -([v_T]\frac{[G_T]}{[C_T]} + [Q]\frac{[\rho_T]}{[L_T]}) \big|_{ave} \Delta t' + [F_T][i_T] \big|_{ave} \Delta t' \quad (4.41)$$

$$\Delta([v_T] - [\rho_T][i_T]) \big|_{z_k,t_n}^{z_{k-1},t_{n+1}} = -([v_T]\frac{[G_T]}{[C_T]} - [Q]\frac{[\rho_T]}{[L_T]}) \big|_{ave} \Delta t' + [F_T][i_T] \big|_{ave} \Delta t' \quad (4.42)$$

where

$$[v_T] = [v_T(z,t)], \qquad [i_T] = [i_T(z,t)], \qquad [Q] = [Q(z,t)] \quad (4.43)$$

$$[L'_T] = [L'_T(z)] = [L_{ext_T}(z)] + [r_T(z,0)]\Delta t \quad (4.44)$$

$$[G_T] = [G_T(z)], \quad [C_T] = [C_T(z)], \quad [\rho_T] = [\rho_T(z)] = \sqrt{\frac{[L'_T(z)]}{[C_T(z)]}} \quad (4.45)$$

$$[F_T] = [F_T(z)] = \frac{1}{2[L'_T(z)]}\frac{d}{dz}\frac{[L'_T(z)]}{[C_T(z)]}. \quad (4.46)$$

The subscript "*ave*" means taking the average value when $t_n \leq t \leq t_{n+1}$. Eqns.(4.41) and (4.42) are the representations of forward and backward wave processes, respectively. According to the principle of the method of characteristics, the voltage and current at any point $0 < z_k < D$ at any time $t > 0$ are the contributions from both forward and backward waves. Then we end up with

$$\begin{bmatrix} W_{11}^j & W_{12}^j \\ W_{21}^j & W_{22}^j \end{bmatrix} \begin{bmatrix} v_T^j(z_k, t_{n+1}) \\ i_T^j(z_k, t_{n+1}) \end{bmatrix} = \begin{bmatrix} U_1^j \\ U_2^j \end{bmatrix} \qquad (j = 1, 2...m) \tag{4.47}$$

where

$$W_{11}^j = W_{21}^j = 1 + B_T^j(z_k) \tag{4.48}$$

$$W_{12}^j = \rho_T^j(z_k) - D_T^j(z_k) \tag{4.49}$$

$$W_{22}^j = -\rho_T^j(z_k) - D_T^j(z_k) \tag{4.50}$$

$$\begin{aligned} U_1^j = {} & (1 - B_T^j(z_{k-1}))v_T^j(z_{k-1}, t_n) + (\rho_T^j(z_{k-1}) + D_T^j(z_{k-1}))i_T^j(z_{k-1}, t_n) - \\ & A_T^j(z_k)Q_1^j(z_k, t_{n+1}) - A_T^j(z_{k-1})Q^j(z_{k-1}, t_n) \end{aligned} \tag{4.51}$$

$$\begin{aligned} U_2^j = {} & (1 - B_T^j(z_{k+1}))v_T^j(z_{k+1}, t_n) + (-\rho_T^j(z_{k+1}) + D_T^j(z_{k+1}))i_T^j(z_{k+1}, t_n) + \\ & A_T^j(z_k)Q_1^j(z_k, t_{n+1}) + A_T^j(z_{k+1})Q^j(z_{k+1}, t_n) \end{aligned} \tag{4.52}$$

and

$$A_T^j(z_k) = \frac{\Delta t'}{2} \frac{\rho_T^j(z_k)}{L_T^j(z_k)} \tag{4.53}$$

$$B_T^j(z_k) = \frac{\Delta t'}{2} \frac{G_T^j(z_k)}{C_T^j(z_k)} \tag{4.54}$$

$$D_T^j(z_k) = \frac{\Delta t'}{2} F_T^j(z_k) \tag{4.55}$$

$$\begin{aligned} Q_1^j(z_k, t_{n+1}) = {} & -\frac{1}{2} r_T^j(z_k, \Delta t') i_T^j(z_k, (n-2)\Delta t') + \\ & \sum_{l=2}^{n-1} r_T^j(z_k, l\Delta t') \frac{i_T^j(z_k, (n-l+1)\Delta t') - i_T^j(z_k, (n-l-1)\Delta t')}{2} \end{aligned} \tag{4.56}$$

$$Q^j(z_k,t_n) = \sum_{l=1}^{n-2} r_T^j(z_k, l\Delta t')\frac{i_T^j(z_k,(n-l)\Delta t') - i_T^j(z_k,(n-l-2)\Delta t')}{2}$$

$$(j = 1, 2...m). \qquad (4.57)$$

From Eqns.(4.41) to (4.57), Δt has been changed to $\Delta t'$ due to the introduction of the internal inductance term $[r_T(z,0)]\Delta t$. The new time step is given by

$$\Delta t' = \int_0^D \sqrt{L_T'^j(z)C_T^j(z)}dz/M^j \qquad (4.58)$$

and

$$t_n = (n-1)\Delta t', \qquad t_{n+1} = n\Delta t'$$

where M^j is the number of segments on the jth line. $\Delta t'$ must be the same for all lines in the system. The original voltage and current vectors on the lines can be traced back by using Eqns.(4.23) and (4.24).

4.5 SIMULATION RESULTS

Further implementation of the numerical formulation presented in the previous section needs concerns about the terminations, i.e. the boundary conditions. Seeing from Eqns.(4.21) and (4.22) or Eqns.(4.31) and (4.31), we would notice that there is no unified formula for any arbitrary terminations. In other words, different terminations cause different treatment of the numerical implementation that will be involved in the core analysis described earlier. For an easy access to the method developed in this chapter, an example of the numerical treatment of linear terminations is provided.

Displayed in Fig.4.2, the near end or sending end termination of line 1 is a conventional type of voltage generator. Other terminations are linear resistive loads without additional voltage generators. Due to the transformation made by (4.23) and (4.24), the transformed voltage generators will be nonzero exhibiting at the sending ends of line 2 and 3. The derivation of the terminal conditions will be related with the forward and backward wave processes as shown in Eqn.(4.41) and (4.42). Further development may involve an evaluation of U_1^j and U_2^j expressed by (4.51) and (4.52). Taking both U_1^j and U_2^j as functions of time and z−coordinate on each line, respectively, we would rather have

$$U_1^j = U_1^j(z_{k-1}, z_k, t_n, t_{n+1}) \tag{4.59}$$

$$U_2^j = U_2^j(z_k, z_{k+1}, t_n, t_{n+1}). \tag{4.60}$$

The voltage and current at the sending ends are obtained as

$$v_T^j(0, t_{n+1}) = \frac{R_{s_T}^j U_2^j(0, z_2, t_n, t_{n+1}) - W_{22}^j(0) v_{s_T}^j(t_{n+1})}{R_{s_T}^j W_{21}^j(0) - W_{22}^j(0)} \qquad (j = 1, 2, 3) \tag{4.61}$$

$$i_T^j(0, t_{n+1}) = \frac{U_2^j(0, z_2, t_n, t_{n+1}) - W_{21}^j(0) v_{s_T}^j(t_{n+1})}{W_{22}^j(0) - W_{21}^j(0) R_{s_T}^j} \qquad (j = 1, 2, 3) \tag{4.62}$$

where $v_{s_T}^j(t)$ are transformed voltage sources according to (4.31) and $R_{s_T}^j$ ($j = 1, 2, 3$) are the elements of $[R_{s_T}]$ given by (4.33).

The voltage and current at the receiving ends are obtained as

$$v_T^j(D,t_{n+1}) = \frac{R_{L_T}^j U_1^j(z_{M^j},D,t_n,t_{n+1})}{R_{L_T}^j W_{11}^j(D) + W_{12}^j(D)} \qquad (j=1,2,3) \tag{4.63}$$

$$i_T^j(D,t_{n+1}) = \frac{U_1^j(z_{M^j},D,t_n,t_{n+1})}{R_{L_T}^j W_{11}^j(D) + W_{12}^j(D)} \qquad (j=1,2,3) \tag{4.64}$$

where $v_{L_T}^j(t)$ are transformed voltage sources according to (4.32) and $R_{L_T}^j$ $(j=1,2,3)$ are the elements of $[R_{L_T}]$ given by (4.34). Since the delay times on each line are, in general, different, the integer numbers M^j $(j=1,2,3)$ will be different either. Suitable roundoff is necessary. We would suggest that the number of segments M on the active line be first set to be an integer. It is apparent that the numbers of segments on other lines without active sources will be rounded off. We have observed that no major numerical errors would attribute to this roundoff.

The triple-line structure (Fig.4.2) is taken as a testing problem and all necessary physical parameters are shown in the same figure. All three lines are assumed to be uniform and only linear terminations are involved . The matrix elements of L_{ext} and C are calculated using the software developed in [93]. They are obtained as

$$[L_{ext}] = \begin{bmatrix} 305.9 & 32.62 & 11.86 \\ 32.62 & 286.5 & 32.62 \\ 11.86 & 32.62 & 305.9 \end{bmatrix} \qquad (nH/m)$$

$$[C] = \begin{bmatrix} 103.9 & -4.475 & -1.1 \\ -4.475 & 113.1 & -4.475 \\ -1.1 & -4.475 & 103.9 \end{bmatrix} \qquad (pF/m)$$

and the resistive loads are

$$[R_s] = \begin{bmatrix} 50.0 & 0.0 & 0.0 \\ 0.0 & 75.0 & 0.0 \\ 0.0 & 0.0 & 50.0 \end{bmatrix} \qquad (\Omega)$$

$$[R_L] = \begin{bmatrix} 50.0 & 0.0 & 0.0 \\ 0.0 & 50.0 & 0.0 \\ 0.0 & 0.0 & 50.0 \end{bmatrix} \qquad (\Omega).$$

It is assumed here that the conductance matrix has no influence on the structure, i.e. $[G] = [0]$ (S/m). The time domain resistances of the structure are simulated using the model proposed in Section II. The voltage generator on Line 1 is given below

$$v_s^1(t) = \begin{cases} 100t & t < 0.01\ ns \\ 1 & 0.01\ ns \leq t < 0.05\ ns \\ 1 - 100(t - 0.05) & 0.05\ ns \leq t < 0.06\ ns \\ 0 & t \geq 0.06\ ns \end{cases}$$

where the unit for $v_s^1(t)$ is Volts.

Fig.4.3-4.6 show the simulation results against those from time/frequency independent parameters. In Fig.4.3-4.6, all dot-dashed curves are computed with only dc resistances and this is a special case of the method developed in this chapter; all dashed curves are provided for the same structure but with lossless transmission lines by using the software given in [94].

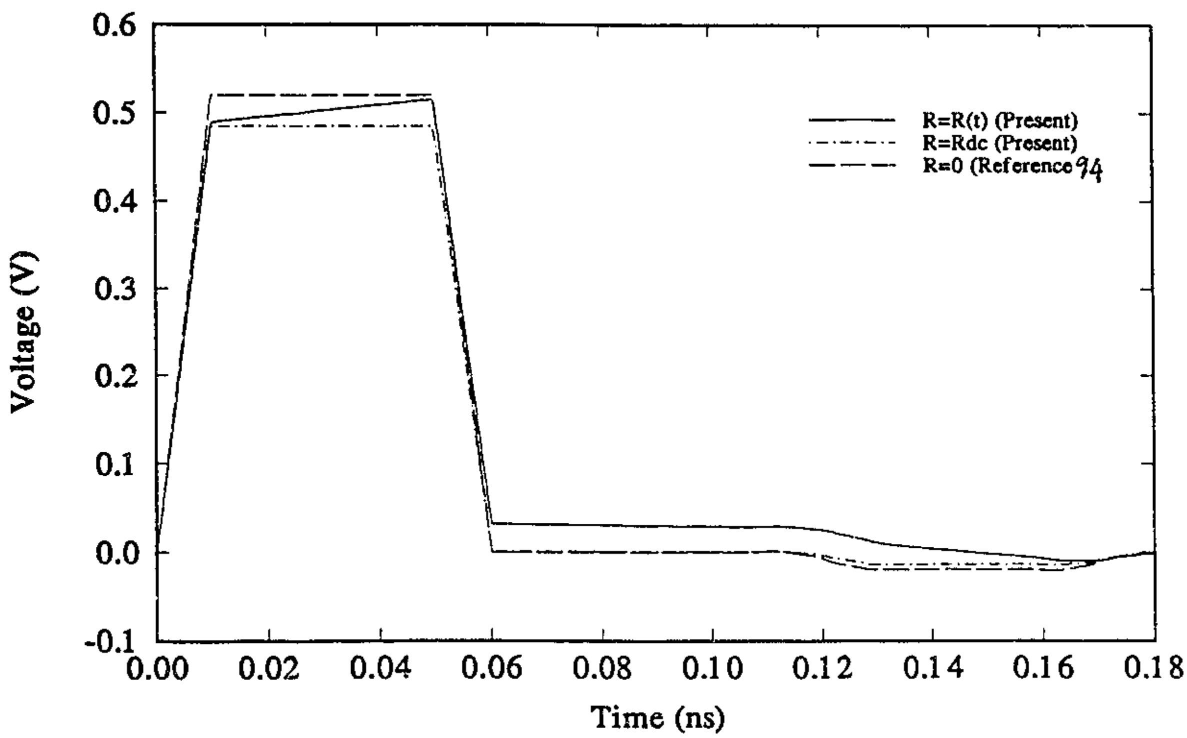

Figure 4.3: Time domain response of port 1 with and without time/frequency dependent losses. (—) represents time domain resistance case, (– · –) dc resistance case, (– – –) lossless case [94].

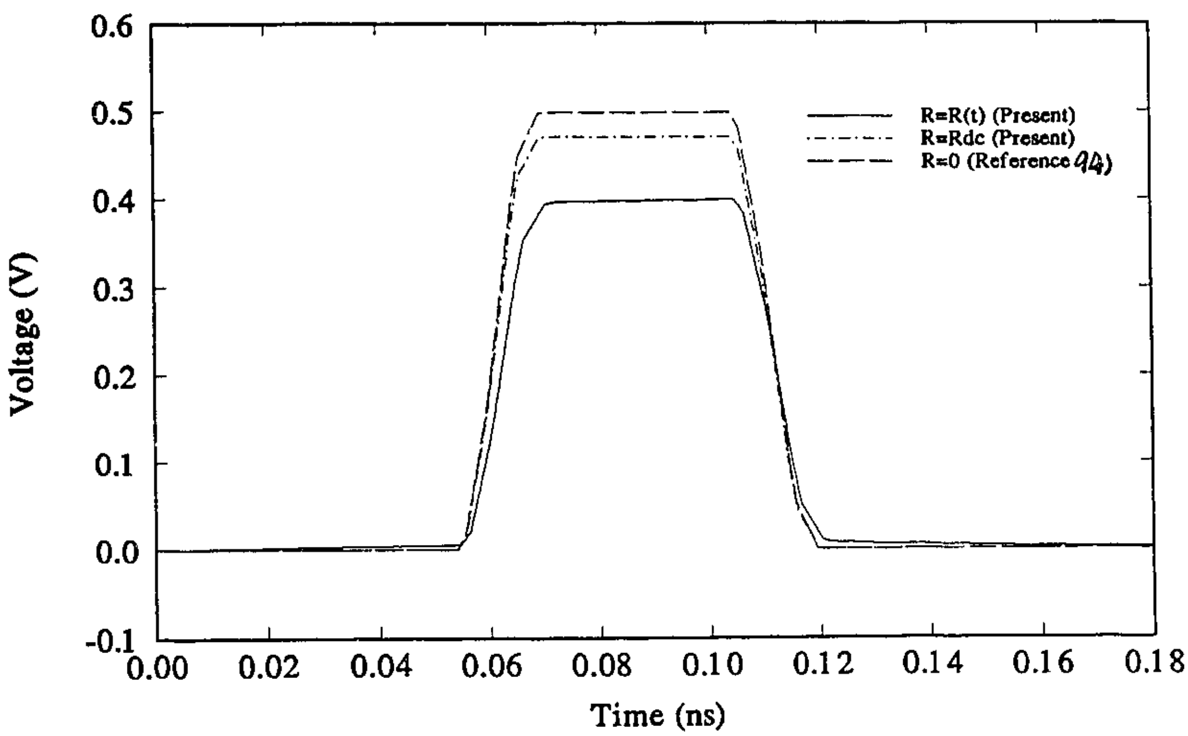

Figure 4.4: Time domain response of port 6 with and without time/frequency dependent losses. (—) represents time domain resistance case, (– · –) dc resistance case, (– – –) lossless case [94].

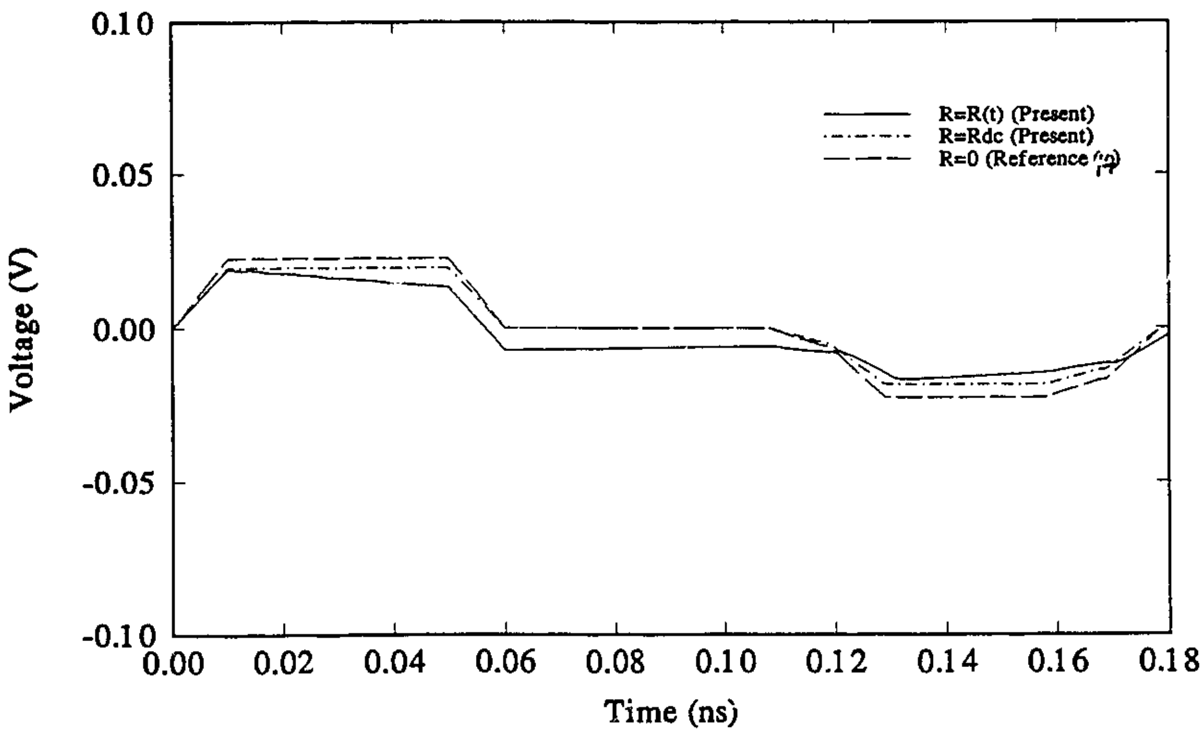

Figure 4.5: Time domain response of port 2 with and without time/frequency dependent losses. (—) represents time domain resistance case, (– · –) dc resistance case, (– – –) lossless case [94].

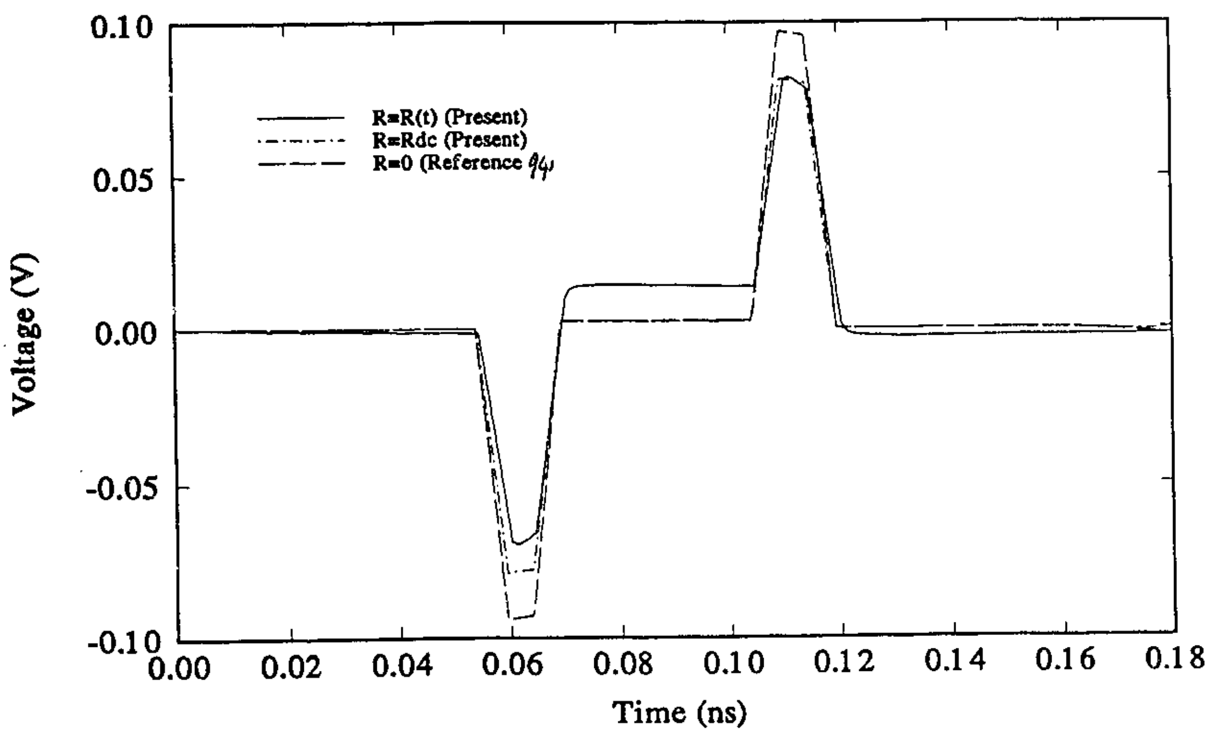

Figure 4.6: Time domain response of port 5 with and without time/frequency dependent losses. (—) represents time domain resistance case, (– · –) dc resistance case, (– – –) lossless case [94].

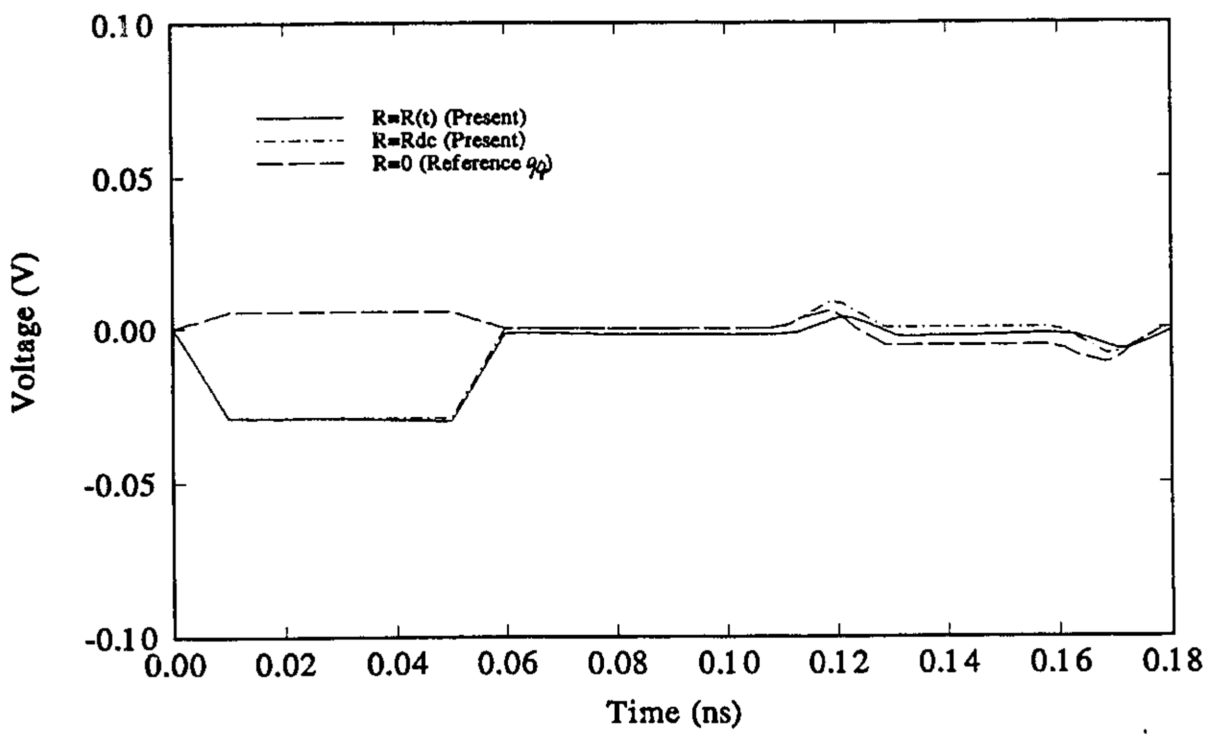

Figure 4.7: Time domain response of port 3 with and without time/frequency dependent losses. (—) represents time domain resistance case, (– · –) dc resistance case, (– – –) lossless case [94].

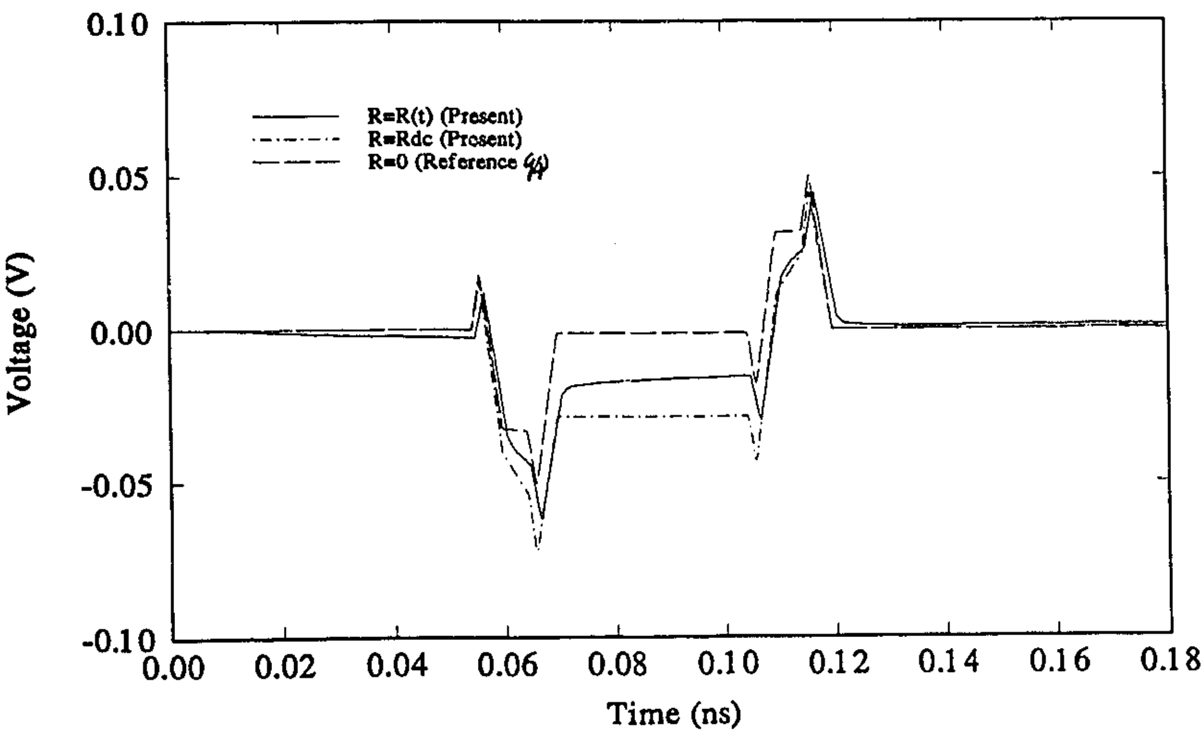

Figure 4.8: Time domain response of port 4 with and without time/frequency dependent losses. (—) represents time domain resistance case, (– · –) dc resistance case, (– – –) lossless case [94].

4.6 DISCUSSION AND CONCLUSIONS

The skin effect model explicit in the time domain is presented in this chapter. Compared with the widely used skin effect models given in the frequency domain, we would benefit from the avoidance of the IFFT process. In addition, more reasonable physical parameters are taken into account in this new skin effect model than the traditional model of the square root of the frequency. Hence, for nonuniform transmission lines this new model will be expected to provide more accurate prediction of the time/frequency dependent properties.

Like the frequency domain methods [81] [8], proper approximations have to be made in order to yield a simple but efficient skin effect model in the time domain. It is noticed that the skin effect models in the frequency domain are restricted to the frequency ranges that are related to different rise times of the pulse [82] [83] [52]. Thus, a more complicated skin effect model in the frequency domain, like the one in [52], is inspired such that a wider frequency range could be covered. However, this complication can be evaded if the skin effect model is established in the time domain. One may find, from the development of the new skin effect model, that a major approximation is made by neglecting of the edge effect as it was done in the widely used frequency domain model, i.e., the square root of the frequency. Another approximation is the requirement that the width of the rectangular conductor be much larger than the thickness. This may restrict the application of the present modeling.

For more generalized skin effect model, numerical methods are often used. In the time domain analysis, a commonly used technique is to utilize the Laplace transforms. A potential study on transient diffusion and propagation problems by using the Laplace Domain Finite Element Method (LDFEM) has been suggested [77]. The authors hope to continue the work in the future and extend to a more general analysis of the interconnects.

As found in [8] [10], the MCC approach is a versatile and accurate tool to time domain analysis of complicated interconnects terminated with any arbitrary loads. The Modified MCC (MMCC) formulation introduced in this chapter has the followoing new features compared with the MCC proposed in [10]: first, the physical contributions coming from non-adjacent lines are taken into account; secondly, adjacent lines can be non-identical and non-equally spaced; thirdly, the line resistances are given directly in the time domain with ground plane corrections and a new convolution treatment is provided.

As an introduction of the new skin effect model to the MMCC approach, a typical triple-line network has been analyzed. Reasonable results have been found in consistence with the responses derived from dc resistance and lossless cases, respectively. With regard to $[R_{s_T}]$ and $[R_{L_T}]$, one should note that there is some condition related to the original resistive terminations. In order to enhance the diagonal dominance of both $[R_{s_T}]$ and $[R_{L_T}]$, the diagonal elements of $[R_s]$ and $[R_L]$ should be symmetrically chosen. This condition can be stated in detail, for instance, that $R_{s_1} = R_{s_3} \leq R_{s_2}$ for a 3×3 matrix. The same condition applies to $[R_L]$.

The new skin effect model and the MMCC formulation have been implemented on workstations and 486PCs. Both numbers of the segments and time step samples are taken within the order of hundreds. Fast and accurate calculations are just as expected. In addition, since there is no limit on the rise time of the pulse, any higher switching speed signal designed to pass the interconnects in the VLSI systems can be applicable with the time domain skin effect model.

Chapter 5

COMPUTER SIMULATION OF PARTIAL INDUCTANCE OF PACKAGE REFERENCE PLANES

5.1 INTRODUCTION

As revealed by Eqn.(4.44) in **Section 4.4**, an equivalent inductance of the VLSI interconnects consists of both external and internal inductances:

$$L_{equ} = L_{ext} + L_{int} \tag{5.1}$$

where

$$L_{int} = r(0)\Delta t. \tag{5.2}$$

The internal inductance given above represents a part of the whole internal inductance of the strip-like conductor and the ground plane. This part of inductance is intentionally interpreted as the *internal inductance* because of its dimension and its position that comes after the external inductance L_{ext}. In fact, there exists another part of the internal inductance which mainly attributes to the ground plane, but we would not rather call it the internal inductance. A new term for this part of inductance is the *partial inductance*.

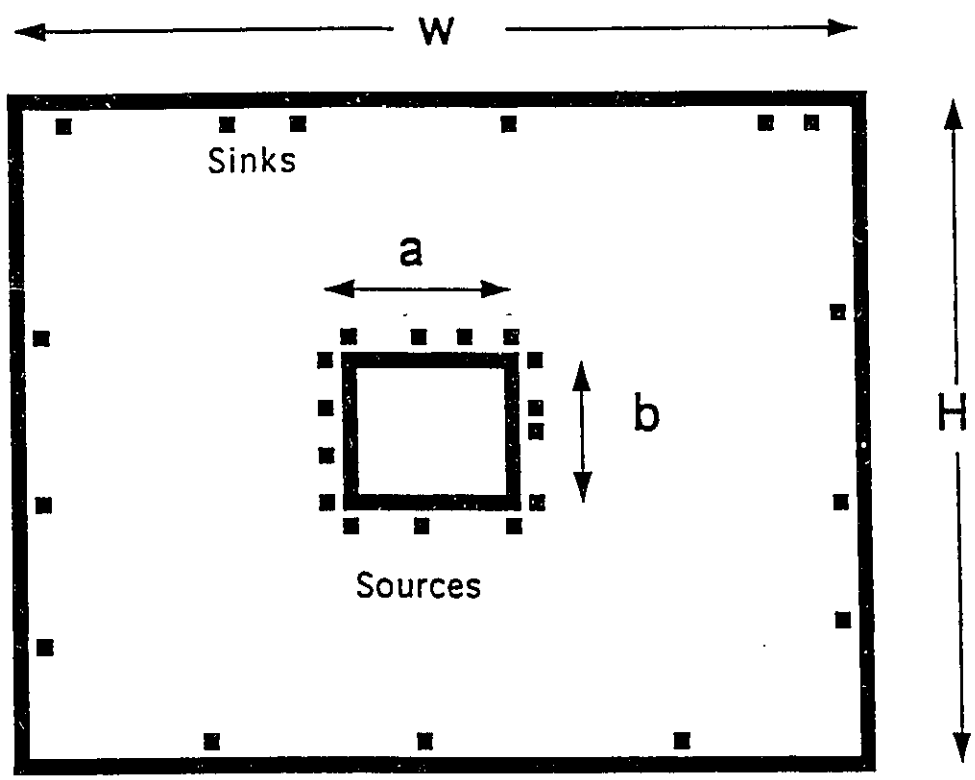

Figure 5.1: A package reference plane.

As pointed out by C.R.Paul in [95], the internal inductance, given by Eqn.(5.2), for instance, is frequency dependent, while the partial inductance is for practical purposes frequency independent.

The concept of partial inductance [95] is adopted to describe any lumped inductances originating from parasitic effects when currents flow between sources and sinks in the package reference (power and ground) planes shown in Fig.5.1. The computer simulation of lumped package parasitic models includes a major task, i.e. evaluation of the partial inductance in the early design and characterization of the output drivers.

There is only few literature related with extraction of the partial inductance from the parasitic effects in the reference planes [96] - [98]. A.C.Cangellaris *et al* described a numerical approach to obtain the effective inductance of power/ground planes [96]. Other references [97] [98] discussed the lumped effects due to the partial inductance.

Regarding to the complexity of the packages, which involves an arbitrary geometrical arrangement of the reference planes and locations of the sources and sinks, numerical solutions will be the only effective means to extract the parasitic models or the partial inductance. Among many commonly used numerical approaches, the Finite Element Method (FEM) is chosen as the major solution approach.

The extraction of the partial inductance in this chapter is based on the software described in [99]. There are two stages in the extraction procedure. The first stage is to calculate the electric scalar potential distribution in the specified plane, and then solve for the current distribution and the total magnetic field energy. The second stage is to obtain the self and mutual partial inductances. The FEM stage involved in the extraction procedure is not quite different from the one addressed in [96]. However, a simpler method is proposed for the second stage in this approach. With this method, the partial inductance can be solved for the particularly interesting points in the plane and no complicated inductance network [96] is involved.

5.2 THEORY AND NUMERICAL APPROACH

5.2.1 Definition of Partial Inductance

A general definition of the inductance can be expressed as

$$L = \frac{2W_m}{I^2} \tag{5.3}$$

where W_m is the magnetic field energy stored in the volume where the current I exists [100]. The current I which produces the magnetic field is given by

$$I = \oint_s \vec{J} \cdot d\vec{S} \tag{5.4}$$

where $\vec{J}$ is the current density vector in the cross section area s.

In regard to the partial inductance defined for the package reference planes, a similar definition can be given as below

$$L_p = \frac{2W_{m_p}}{I^2} \tag{5.5}$$

where the magnetic field energy W_{m_p} is stored in the volume where the current I exists.

In this analysis, the partial inductance is defined as the inductance between any two points in the reference planes, for instance, the ground plane. Usually, one of the two points is a source and the other a sink. However, the partial inductance can be extended to any two points that are not necessarily a source and a sink. For example, they may be the ground points of the sending (driving) end and receiving (loading) end of a transmission line, which represents a part of the interconnects in the VLSI circuitry.

The quantity of the partial inductance so defined can be used to determine how significant the inductive resistance is between these two points. It gives the circuit designer a quantitative idea of the design layout. In the analysis model, the reference planes are treated as practical metallic plates that have finite conductivity and finite thickness. Thus, the current flowing through the plate causes magnetic field inside and outside the plate. The partial inductance is somewhat related to the internal inductance. However, since it is defined between any two points in the plate, the partial inductance does not, in general, represent the whole internal inductance of a plate. As the general definition of the inductance, we also have self and mutual partial inductances.

Based on the above discussion, the integral contour in (5.4) will be a closed surface around one of the two points concerned. The magnetic field energy W_{m_p} in (5.5) can be obtained from [101]

$$W_{m_p} = \frac{1}{2}\int_v [\nabla \cdot (\vec{A} \times \vec{H}) + \vec{A} \cdot (\nabla \times \vec{H})] dv \tag{5.6}$$

where $\vec{A}$ is the magnetic vector potential given by

$$\vec{A} = \frac{\mu_0}{4\pi}\int_v \frac{\vec{J}}{R} dv \tag{5.7}$$

in which we have

μ_0 : *the magnetic permeability of the conducting plate*;

v : *the volume where the partial inductance is concerned*;

R : *the distance between the source and any observation point in the plate.*

The relationship between the magnetic field and the current is known from Maxwell equations

$$\nabla \times \vec{H} = \vec{J} \tag{5.8}$$

where

$$\vec{J} = -\sigma \nabla \Phi \tag{5.9}$$

in which Φ is the electric scalar potential.

5.2.2 Numerical Solution

It is seen that the electric scalar potential Φ is the only unknown to derive the partial inductance given by (5.5). For a given structure as in Fig.5.1, the electric potential distribution can be determined by the finite element method (FEM).

To model the structure shown in Fig.5.1 with the FEM, we assume that the current would flow uniformly in the cross section area of the conducting plate. Thus, it is possible to reduce the problem from three dimensions (3-D) to two dimensions (2-D).

The two-dimensional electric potential $\Phi(x, y)$ distribution is governed by the following Laplace equation

$$\frac{\partial^2\Phi(x,y)}{\partial x^2} + \frac{\partial^2\Phi(x,y)}{\partial y^2} = 0 \tag{5.10}$$

and the associated boundary conditions related with sources and sinks.

Using the finite element procedure, the appropriate functional to be minimized for (5.10) is

$$F(\Phi) = \int_\Omega [(\frac{\partial\Phi(x,y)}{\partial x})^2 + (\frac{\partial\Phi(x,y)}{\partial y})^2] dxdy \tag{5.11}$$

where the problem domain Ω is divided into finite elements. The finite elements can take the shapes of triangle or rectangular for the two dimensional area, for instance.

By introducing the linear interpolation functions in each element and minimizing the functional (5.11), we have the following final system of equations

$$[K][\Phi] = [f] \tag{5.12}$$

where $[K]$ is a symmetric matrix by virtue of the self-adjointness of the Laplacian operator describing the potential distribution, and $[f]$ contains the contributions from the inhomogeneous *Dirichlet* boundary condition. This FEM procedure is the same as the one described in **Section 3.2**, where a TEM mode analysis is curried out for a Triple-TEM cell.

Once the potential distribution is obtained, the magnetic field energy and the current can be obtained through numerical integration [99]. Finally, the partial inductance is derived from (5.5).

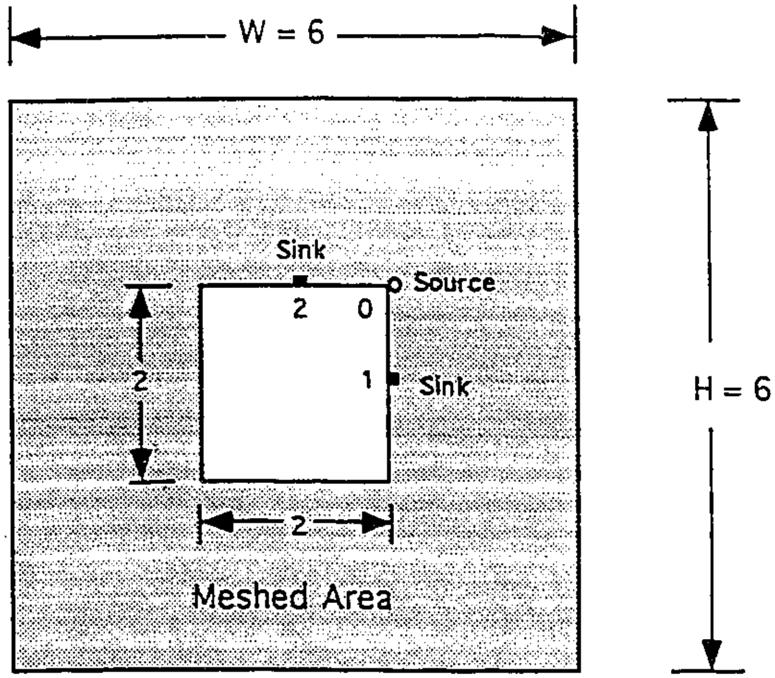

Figure 5.2: Simulation example for a package reference plane.

5.3 APPLICATIONS

According to the concept, the partial inductance only relates to two points/pins in the reference plane. However, it can be extended to an inductance between several pins located in the same plane Fig.5.2. Thus this partial inductance may be classified into two types: self and mutual partial inductances, as shown in Fig.5.3.

In this section, we will take the configuration displayed in Fig.5.2 as an example of the application. The procedures presented below may be used to deal with any other more complicated configurations of the package reference plane.

5.3.1 Self and Mutual Partial Inductances

Fig.5.4 shows an equivalent lumped element circuit consisting of three pins (one source and two sinks) in a reference plane. This circuit refers to the configuration depicted in Fig.5.3. The total equivalent partial inductance is given by

$$L_{ep} = \frac{L_{10p}L_{20p} - L_{12p}^2}{L_{10p} + L_{20p} - 2L_{12p}} \tag{5.13}$$

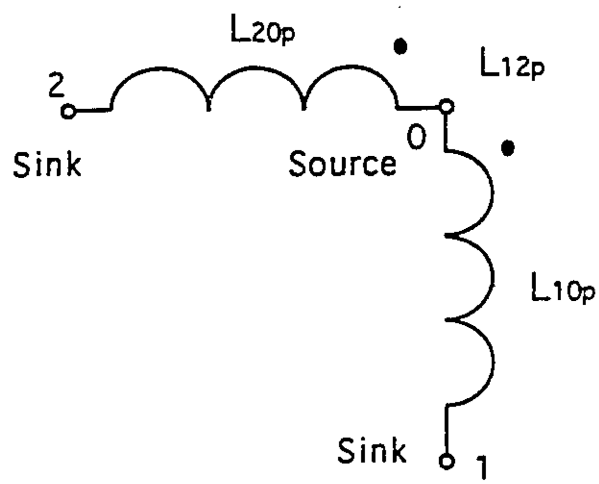

Figure 5.3: Self-/mutual-inductance related with sinks and sources.

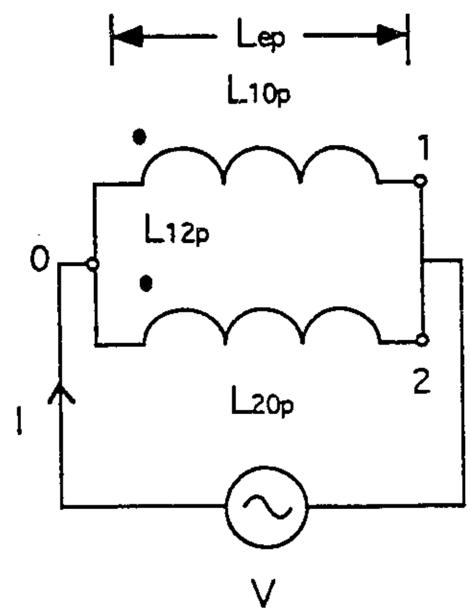

Figure 5.4: Lumped element equivalent circuit.

where L_{10p} and L_{20p} are the self partial inductances, and L_{12p} the mutual partial inductance. The mutual inductance can be derived as

$$L_{12p} = L_{ep} \pm \sqrt{L_{ep}^2 - [L_{ep}(L_{10p} + L_{20p}) - L_{10p}L_{20p}]}. \qquad (5.14)$$

Since the mutual inductance is less than the total equivalent inductance, the above formula can be written as

$$L_{12p} = L_{ep} - \sqrt{L_{ep}^2 - [L_{ep}(L_{10p} + L_{20p}) - L_{10p}L_{20p}]} \qquad (5.15)$$

where L_{ep}, L_{10p} and L_{20p} are all numerically determined.

5.3.2 Numerical Results

Numerical Results of Self Partial Inductance

A value of $L_{10p} = 0.287\ (nH/m)$ is obtained for the structure shown in Fig.5.3. To calculate L_{20p}, the same data file for the mesh can be reused with a change of the location of the sink. It is found that

$$L_{20p} = 0.290 \quad nH.$$

Numerical Results of Equivalent Partial Inductance

Following the same procedure for the self partial inductance, the total equivalent partial inductance L_{ep} can also be numerically determined. To solve for L_{ep}, one source and both sinks have to be properly set. The results are displayed for the current, magnetic field energy and inductance as:

it took: 22iterations!
the error residue is: 1.0618771129623D-15
statusis: 0
it used: 385storage locations for real
it used: 11storage locations for integer

and

TOTAL CURRENT IS 509838.77316000
TOTAL ENERGY IS 19974.980732438
INDUCTANCE 1.5369178121807D-07.

Using Eqn.(5.13) the equivalent partial inductance is determined as

$$L_{ep} = 0.154 \quad nH.$$

Calculation of the Mutual Partial Inductance

Having calculated L_{ep}, L_{10p} and L_{20p}, the mutual partial inductance is easily obtained from Eqn.(5.15) as

$$L_{12p} = 0.01891 \quad nH.$$

If more sources and sinks are involved, they can always be separated into pairs. For each pair, the above-described procedures are used to obtain any self and mutual partial inductances L_{mnp} between the pair.

5.3.3 Partial Inductance Calculation for A PWB with A Slot

An interesting application of the partial inductance is the investigation of the "Gap Inductance" on a printed wire board (PWB), where a gap cut on the ground plane is perpendicular to a microstrip transmission line [98]. The gap-inductance associated with this particular structure is one of the partial inductances involved [98]. To simplify the problem, only the gapped structure related to the extraction of the gap-inductance is shown in Fig.5.5. The problem is to find out the partial inductance between the two points at the cornners of the gap (Fig.5.5).

R.L.Hill *et al* has studied this structure using three different approaches ([98]). First, they used a coplanar strip transmission line to model the gap. However, the existing closed form of the characteritic impedance is only for a pair of symmetrical coplanar strips though the gapped structure is an asymmetric one. Thus, the inductance found from the characteristic impedance $L = \frac{Z_0 tan\beta l}{\omega}$ is assumed to be the upper bound for the partial inductance associated with the gap in the return plane.

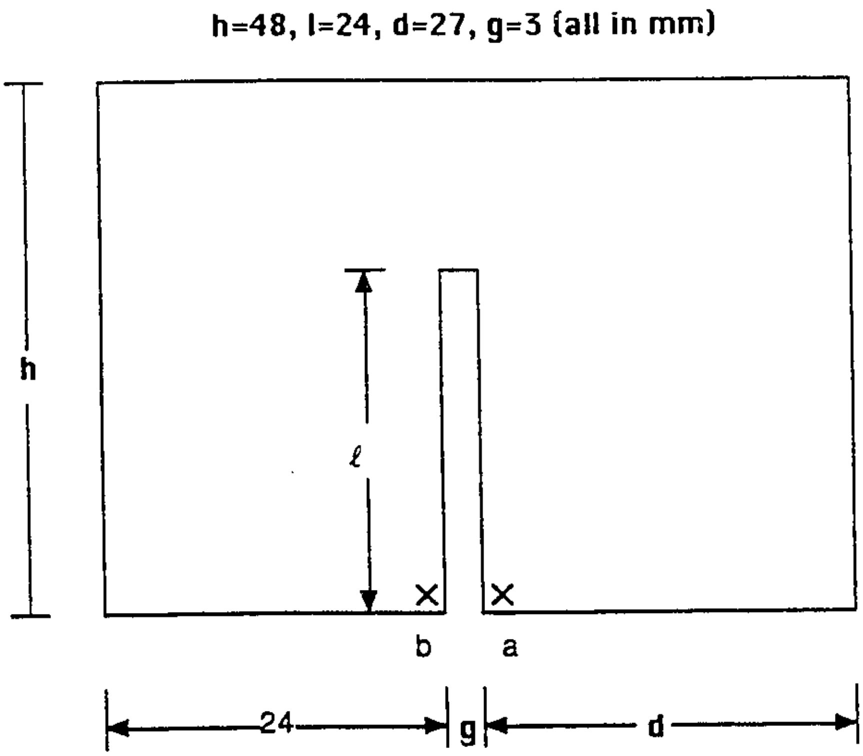

Figure 5.5: A gapped ground plane foe PWB, where "a" and "b" are two points between which the partial inductance will be determined.

To verify the theoretically derived inductance, Hill *et al* used other two experimental methods. With "Method 1", they measured the total inductances for two different PWB boards, one without the gap and the other with the gap. They assumed that the substraction of the two inductances would yield the gap-inductance. With "Method 2", a capcitor C is introduced to the gap, and then they measured the first resonance frequency of the modified structure. The associated inductance is given by $L = \frac{1}{4\pi^2 f^2 C}$. Both verifications provided good agreement with the theoretical value.

In this chapter, the same structure is studied with the numerical extraction techniques developed above. In the numerical procedures, integrals (Eqns.(5.6) (5.7)) have to be performed in the volume of the conductor. In particular, the integral routes can be chosen around one of the points "a" and "b". In principle, for the inductance calculation, one of the points either "a" or "b" will be the source of current and the other one the sink of current. Then, the integrating route should surrround either the source or the sink. Table 5.1 shows the numerical results obtained from four different integrating routes, two surrounding the source (Route 1, 2) and the other two surrounding the sink (Route 3, 4). Table 5.2 presents the comparison of the gap-inductances calculated with different methods.

About 7.8 percent error is found between the theoretical one [98] and the present one. There may be two major error sources. First, the numerical model is slightly asymmetric in the geometries. However, according to Hill's assumption, the asymmetric geometry should yield lower value of the inductance. Another source is related with the numerical calculations. In the numerical procedures, errors could be coming from mesh generation (coarse or fine), interpolation function for the field, and numerical integral. Nevertheless, our method has been testiffied against other methods [98], and acceptable results have been found even though different integrating routes are taken.

Table 5.1: Numerical results for gap-inductance

[Present]	Route 1	Route 2	Route 3	Route 4	Ave.
$L_p(nH)$	19.6	20.4	19.1	18.5	19.4

Table 5.2: Comparison between the several methods

	[98] Theory	[98] Method 1	[98] Method 2	[Present]
$L_p(nH)$	18.0	15.0	16.0	19.4

5.4 CONCLUSIONS

A computer simulation software is developed for deriving the partial inductance of the package reference planes. A systematic method to obtain and determine the self and mutual partial inductances is described. The method is simpler than the previously published one [96] since no inductance network is needed. The examples given in this chapter are limited to simple cases but more complicated problems are expected to be solved in the same fashion.

One application to the partial inductance extraction from a PWB board with a gap on it is demonstrated. the numerical results have been tested against other published data. Good agreement has been found. Therefore, it is proved that the numerical techniques involved in this chapter are reliable.

Chapter 6

TIME DOMAIN SIMULATION OF VLSI INTERCONNECT DISCONTINUITIES

6.1 INTRODUCTION

As clock frequency in high speed digital systems increases, the rise/fall time of drivers has dropped to tens of picoseconds with corresponding bandwidth expanding to several gigahertz for the interconnection systems. Interconnect junctions and discontinuities encountered in the high speed digital and microwave hybrid and monolithic circuits contribute to signal reflections, time delay, waveform distortion and crosstalk problems which can degrade the circuit and system performance. The same problems also happen in printed circuit boards (PCBs), single and multichip modules, and other packages. The parasitic effects associated with the discontinuities described above have become an important technical concern recently. It is essential that the electrical performance of interconnect discontinuities be predicable by using computer simulation techniques. Furthermore, optimization of the discontinuity structures would be a next feasible objective without any hardware trial and error.

Computer simulation process of interconnect discontinuities may be divided into two stages: first, modeling and extracting equivalent circuits that represent the discontinuities in a practical bandwidth; secondly, performing a suitable transient analysis with inclusion of the parasitic models. Typical discontinuity structures like bends and vias have been

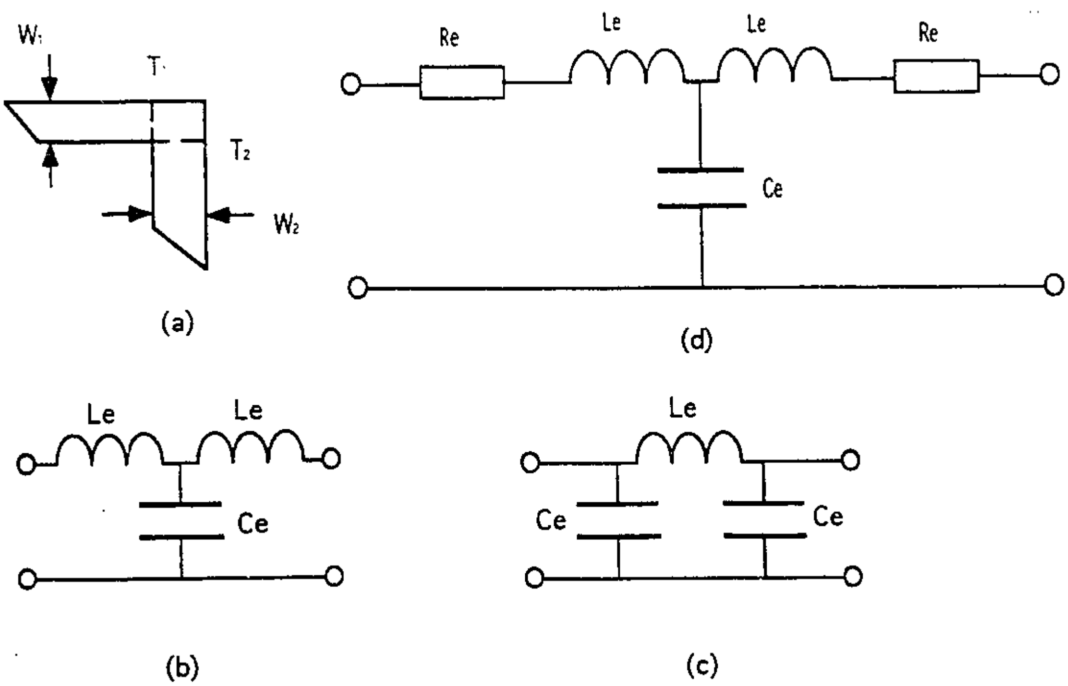

Figure 6.1: Equivalent circuits for a microstrip bend: (a) a right-angled bend; (b) LCL model; (c) CLC model; (d) RLCLR model.

studied by many authors [102] - [116] for years.

In the first stage of the simulation, either distributed or lumped element model can be applied. Taking a bend for example, Fig.6.1 shows equivalent circuits for modeling a right-angled bend. Basically, there are LCL [104] and CLC [106] models as shown in Fig.6.1 (b) (c) for the bend structures. However, other equivalent circuit models including Γ-type model [102] and hybrid models of distributed and lumped elements [105] [106] are still used in practice. With regard to the via structures, lumped element circuits are adopted to represent the vias through one or several layers of metallic planes (usually ground planes) [108] [113]. Equivalent circuits of vias resemble those of the bend structures shown in Fig.6.1.

In the second stage of the simulation, commercial simulators like SPICE [105] [106] may be resorted to. However, if the discontinuity is usd as an original physical model in the simulation, extraction procedure will not be necessary. A prevailing methodology for examining the transient response of a signal passing through the discontinuities is the adoption of the finite-difference time-domain (FDTD) method [107] [108] [114] [116], which is able to perform a full wave analysis. Other method like mode matching techniques [115] is also applicable.

It may be noted that most existing methodologies involved in the first stage have not taken into account the losses of discontinuities so far in the literature except for [116]. As signal rise time has dropped to tens of picoseconds, the time dependent losses in the conductors that make up the interconnects and discontinuities are becoming an important technical issue which needs special analysis [116] [117].

In this chapter, we adopt the LCL type of model to represent the discontinuities like bends and vias. However, the LCL model is extended to an RLCLR model (Fig.6.1 (d)) which takes into account the time dependent losses in the discontinuities. Approximate procedures are proposed to extract the lumped elements from a through hole via. The RLCLR model is then applied to transient analysis of both bend and via structures. In the transient analysis, the methodology described in the previous chapters and [117] will be adopted. Thus, the time dependent losses given as the time domain skin effect model is included in the transient process. Although the losses in the discontinuities are rather small compared with the losses in the lines, we still include these losses in the equivalent circuits as a general approach for any case where such losses are pronounced. For instance, several such vias are related in series connection or the materials that make up the vias are less conductive.

An important development in this chapter is the establishment of a mathematical interface between the discrete time domain signal and the equivalent lumped element circuit which represents the discontinuities. This mathematical interface represents explicitly the physical relationship between the interconnecting lines and the discontinuity. Therefore, it is possible to examine the transient response of the discontinuity in a simpler way without resorting to more complicated 3D numerical techniques. In addition, this interface would provide a potential to be used as a tool for sensitivity analysis and optimazation of the discontinuity structures. Without losing generality, all initial conditions are assumed to be zero.

6.2 LUMPED ELEMENT MODELS OF DISCONTINUITIES

Typical interconnect discontinuities such as bends and vias have long been treated with equivalent lumped element circuits for years. This technical treatment gives circuit designers great flexibility of using other simulators like SPICE. Providing a general approach to extract the lumped parameters from a wide range of discontinuity structures is out of the scope of this chapter. Review of the existing literature reveals that there have been already many technical papers concentrating on the extraction for bend structures while only very few for the via structures. Therefore, this section will be devoted to the extraction procedure for one of the most typical interconnect discontinuities, i.e., a through hole via.

A typical through hole via can be approximated by a cylindrical conductor. With this approximation, the lumped element circuit equivalent to a through hole via could be built up by an RLCLR model shown in Fig.6.1 (d). There are two steps to determine the equivalent inductance Le, resistance Re and capacitance Ce. First, an implicit time domain skin effect model [86] [118] suitable for a cylindrical conductor is used to obtain the equivalent inductance and resistance whose time dependent properties have been accounted for; Secondly, a simple but effective extraction procedure is applied to find out the equivalent capacitance.

6.2.1 Equivalent Inductance and Resistance

Consider a through hole via shown in Fig.6.2, where the via is represented by a solid round conductor. A skin effect model derived for the cylindrical type of conductors is provided in [86] [118]. The model is established based on the theory that the time dependent skin effect can be represented by an infinite number of parallel lumped parameters defined by

$$Re_n = \frac{1}{4} r_{dc} x_n^2 (1 + m^2 x_n^2) \tag{6.1}$$

$$Le_n = \frac{\tau}{x_n^2} Re_n \tag{6.2}$$

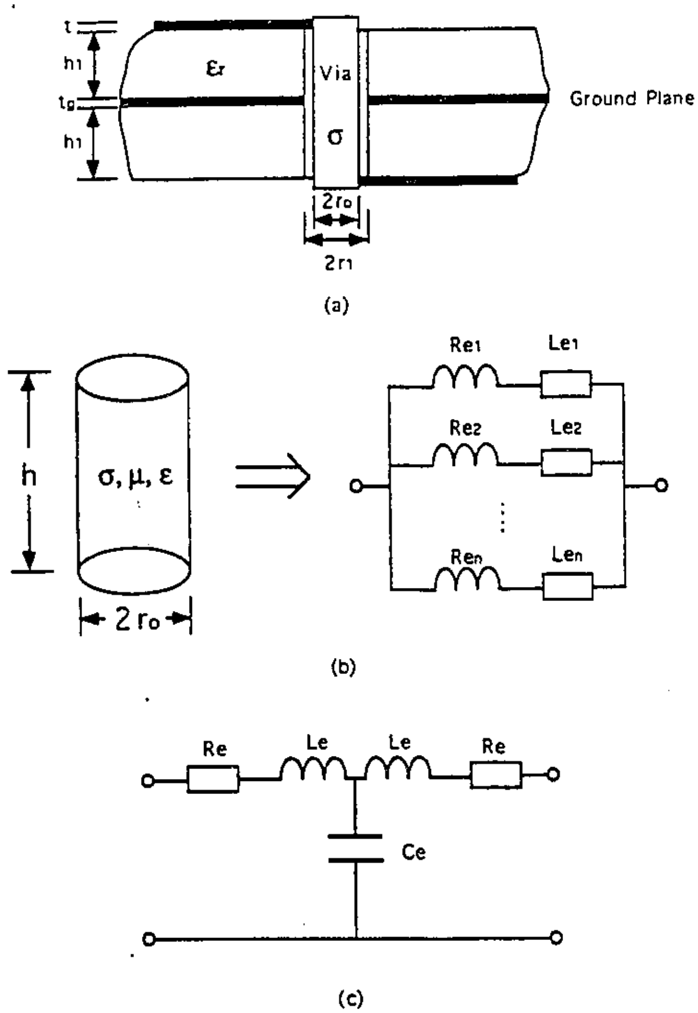

Figure 6.2: Equivalent inductance and resistance for a through hole via: (a) geometry of the via discontinuity; (b) partial equivalent circuit; (c) a full representation of the equivalent circuit.

where r_{dc} is the dc resistance of the cylinder; $\tau = \mu\sigma r_0^2$ is the time constant characterizing the transient skin effect; $m = L_{ext}/L_{dc}$ is the ratio between the external and internal (dc) inductances; and x_n are the roots of the following transcendental equation

$$J_0(x_n) - mJ_1(x_n) = 0. \tag{6.3}$$

It is noted that n, the number of element Re or Le, does not have to be very large since the lumped elements make a fast convergence. Practically, $n = 5$ is large enough to represent the time domain skin effect that happens in the cylindrical conductor [118]. However, a lumped element circuit shown in Fig.6.2 (b) with $n = 5$ is still inconvenient to be incorporated into the discontinuity analysis. A lumped element circuit with $n = 5$ needs to be further approximated to an equivalent circuit shown in Fig.6.2 (c), where the capacitance will be extracted through the procedure given in the next subsection. Numerical calculation shows that it is possible to make this approximation by only comparing between the total impedances calculated from a lumped element circuit with $n = 5$ (Fig.6.2 (b)) and from a simplified equivalent circuit. This simplified circuit, called one-element circuit, consists of one resistance in series connection with one inductance, whose values are determined by the following definitions of the impedances. The impedances for a 5-element circuit and a 1-element circuit are defined as $Ze_{(5-elmt)}(f)$ and $Ze_{(1-elmt)}(f)$, respectively.

$$Ze_{(1-elmt)}(f) = \alpha Re_{15} + j\omega\beta Le_1 \qquad (\omega = 2\pi f) \tag{6.4}$$

$$Ze_{(5-elmt)}(f) = Ze_1(f)//Ze_2(f)//Ze_3(f)//Ze_4(f)//Ze_5(f) \tag{6.5}$$

$$Re_{15} = Re_1//Re_2//Re_3//Re_4//Re_5 \tag{6.6}$$

$$Ze_i(f) = Re_i + j\omega Le_i \qquad (i = 1, 2, ..., n;\ n = 5) \tag{6.7}$$

where Re_i and Le_i are determined by Eqn.(6.1) - (6.3) with symbol "//" representing parallel connection of the resistances and impedances. α and β in Eqn.(6.4) are the adjusting factors that make the two representations of lumped element circuit agree well.

Fig.6.3 displays the equivalence of the real and imaginary parts of the total impedances from 5- and 1-element circuits for a given via structure ($r_0 = 0.1mm,\ h = 0.32mm,\ \sigma = 5.6 \times 10^7 S/m$). One may notice that the resistance in the lower frequency range is replaced by a constant resistance while at the higher frequencies ($f > 100MHz$) both resistances agree very well (Fig.6.3 (a)). In regard to the imaginary parts, the single element circuit provides excellent agreement with the five element circuit (Fig.6.3 (b)). Table 6.1 demonstrates the equivalent circuit parameters for the same via structure calculated above.

Table 6.1: The equivalent circuit parameters

Root No.	x_n	$Re_n(\Omega)$	$Le_n(H)$
$n = 1$	0.561	0.67×10^{-4}	1.5×10^{-10}
$n = 2$	4.126	0.15538	6.423×10^{-9}
$n = 3$	7.305	1.52178	2.007×10^{-8}
$n = 4$	10.46	6.39465	4.112×10^{-8}
$n = 5$	13.61	18.3165	6.958×10^{-8}

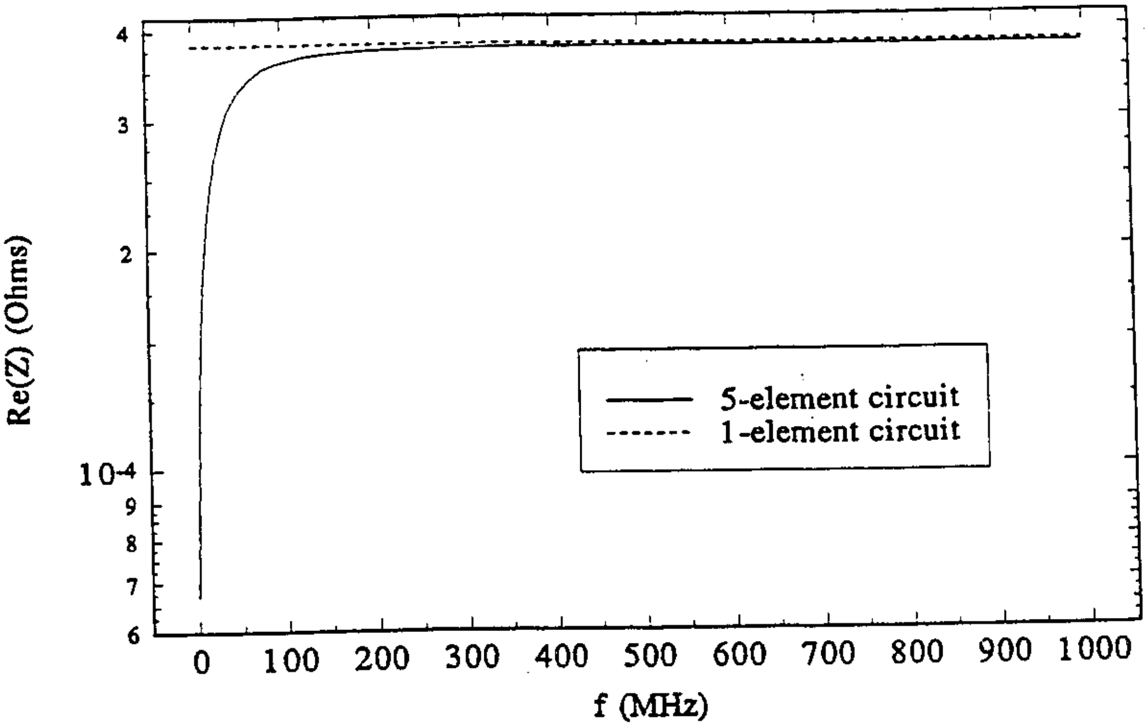

(a)

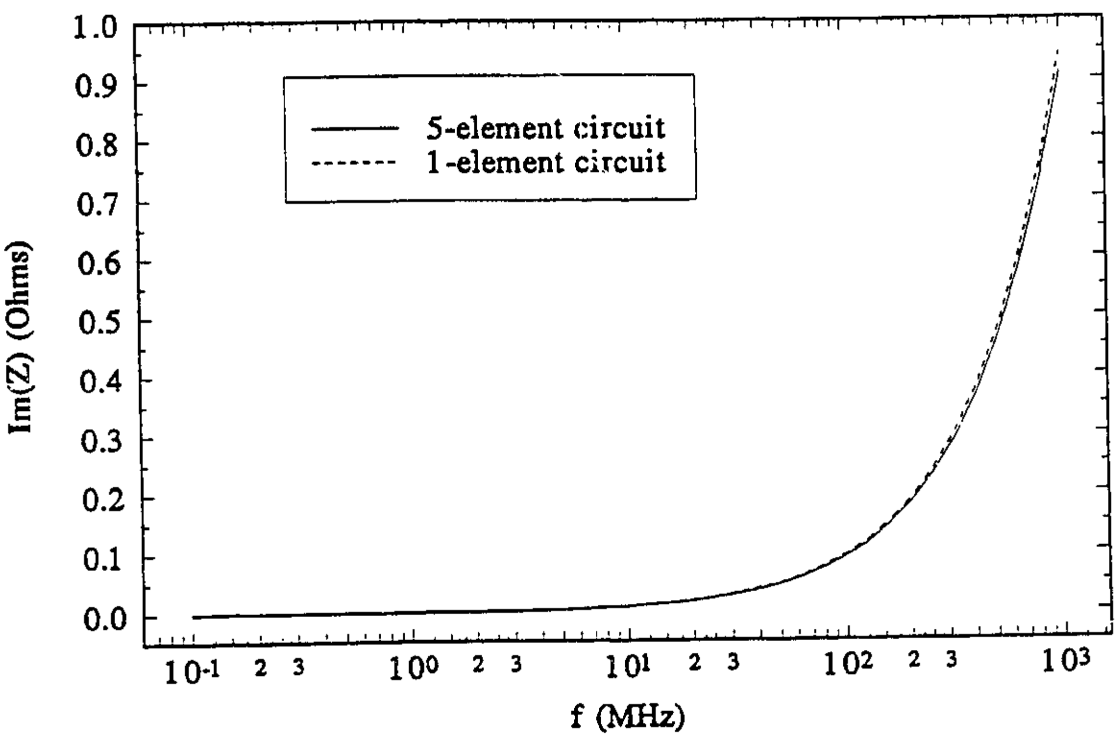

(b)

Figure 6.3: Comparing 5- and 1-element equivalent circuits: (a) real part of the total impedance; (b) imaginary part of the total impedance.

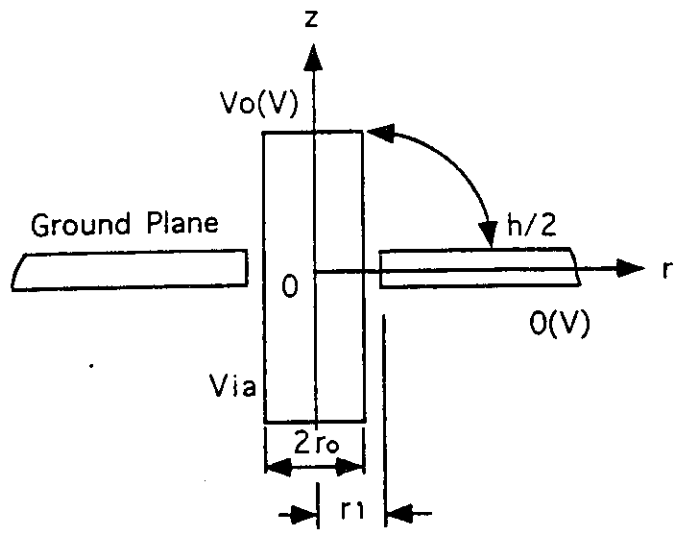

Figure 6.4: A structure for extraction of the equivalent capacitance.

6.2.2 Equivalent Capacitance

An exact extraction of the capacitance between the through hole via and the ground plane may involve extensive mathematical manipulations. We would think of some approximate modeling procedure through which the capacitance can be extracted with a simple but effective method.

First, consider a structure shown in Fig. 6.4 where the substrate is not included. To obtain the capacitance between the through hole via and the ground plane, a dc voltage source is imposed on both conductors. A partial capacitance for the upper part of the structure could be given by

$$C_p = \frac{Q}{V_0} \tag{6.8}$$

where

$$Q = \int_{r_1}^{h_1} \epsilon_0 \frac{V_0}{(r_1 - r_0) + \frac{\pi}{2}(r - r_1)} 2\pi r dr|_{h_1 = h/2} \tag{6.9}$$

$$\tag{6.10}$$

After performing the integration, we obtain

$$C_p = \frac{4\epsilon}{\pi}[ln(2(r_1 - r_0) + \pi(h_1 - r_1))^{2(r_0 - r_1)} + \pi h_1 + ln(2(r_1 - r_0) + \pi(h_1 - r_1))^{\pi r_1})$$

$$-ln(2(r_1 - r_0))^{2(r_0 - r_1)} - \pi r_1 - ln(2(r_1 - r_0))^{\pi r_1}]. \tag{6.11}$$

Then, the equivalent capacitance may be defined as

$$Ce = 2C_p + \delta C \tag{6.12}$$

where δC is a small amount of the partial capacitance between the via and the ground conductor within the thickness of the ground plane.

The approximate procedure described above assumes that the contribution from the substrate to the equivalent capacitance is ignored. However, this problem could be alleviated by introducing an empirical factor that compensates the substrate effect. Otherwise, more complicated mathematical process should be invoked.

6.3 MATHEMATICAL INTERFACE

It should be noted that above extraction procedure has accounted for the time dependent skin effect in the through hole via. Likewise, the transmission lines which are connected to the via should be considered as lossy interconnects with time dependent properties. An approach called Modified Method of Convolution-Characteristics (MMCC) has been proposed in [117], where a time domain skin effect model is incorporated into the transient analysis of VLSI interconnects.

In many cases, examination of the transient signal process through an interconnect via is performed with 3D finite difference time-domain (FDTD) methods. Optimization of the via structure with the FDTD approach would involve many numerical adjustments, which is not easy to be generalized to other structures. However, the method proposed in [117] provides a semi-analytical approach in which voltage and current vectors at any location of the multiconductor system can be explicitly expressed. This offers a better perspective to sensitivity analysis and optimization of the VLSI interconnect circuits.

In this section, a mathematical interface will be built up between the discrete time domain voltage and current outputs from a transmission line and the lumped element circuit representing the discontinuities. The voltage and current outputs from the interconnecting lines are obtained through the approach described in [117], whose solutions are analytically expressible in each time interval. This means that there is a direct mathematical link between these outputs and the equivalent circuit at every time step. However, to capture a whole transient response from an interconnect discontinuity, special mathematical techniques like time domain convolutions may be involved. The mathematical interface should represent a continuous physical relationship between the signals passing through the discontinuities via interconnecting transmission lines.

Specifically speaking, such a mathematical interface consists of two parts. First, the lumped element circuit is used as a terminal load to the interconnecting lines, where the incoming signal represented by its voltage and current to the discontinuity should preserve its time signature as it were terminated by a real discontinuity plus the transmission line connecting to the other side of the discontinuity. Secondly, the lumped element circuit with the incoming signal may act as a signal generator to the other side transmission line, where the time signature of the incoming signal is reasonably altered as it were going through a real discontinuity structure. In addition, the lumped element circuit which represents the discontinuity is served as a two-port network, to which exsiting circuit analysis techniques can be directly applied. The two parts of the mathematical interface are: 1) lumped element circuit as a terminal load; 2) lumped element circuit as a signal generator.

6.3.1 Lumped Element Circuit As A Terminal Load

As discussed in the first section, typical interconnect discontinuities such as bends and vias can be modeled using LCL or RLCLR circuit. Full approximate procedures concerning the extraction of the lumped parameters Le, Ce and Re for a through hole via is presented in the previous section. Basically, either a bend or a via may be represented by an RLCLR circuit. Thus, in this section we start with a general RLCLR model without distinction between the physical structures of the discontinuity. In other words, if the RLCLR circuit can model other discontinuities than bend or via, the mathematical interface provided here can also be applied.

Fig.6.5 shows an RLCLR circuit used as a terminal load to the interconnecting line. $v_2(t)$ and $i_2(t)$ in Fig.6.5 represent the discrete time domain voltage and current outputs from the transient analysis using the MMCC method [117], and Z_0 is the characteristic impedance of the interconnecting lines. It is essential to find out the relationship between the discrete outputs and the lumped element circuit (here, we avoid using SPICE simulator since we need to have explicit time domain expressions). It may start from the following relations:

$$i_2(t) = i_3(t) + i_4(t) \tag{6.13}$$

$$u_2(t) = Le\frac{di_2(t)}{dt} + i_2(t)Re + u_3(t) \tag{6.14}$$

$$u_3(t) = \frac{1}{Ce}\int_0^t i_3(t)dt \tag{6.15}$$

or

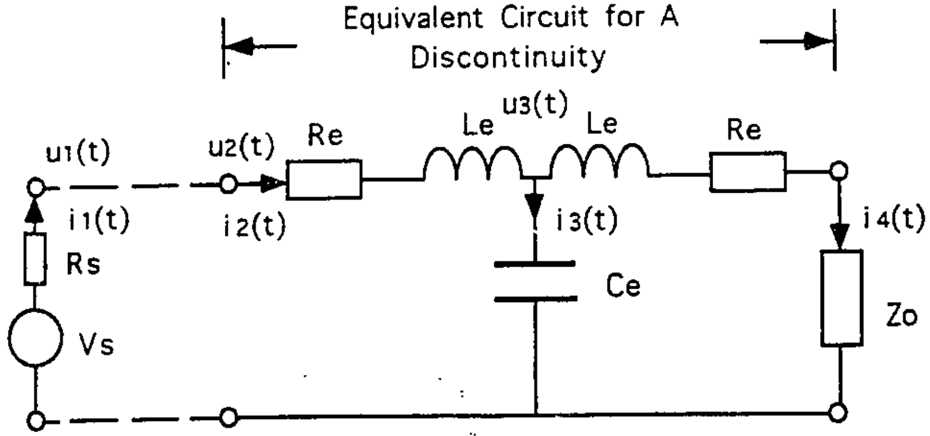

Figure 6.5: An RLCLR circuit modeling a discontinuity to terminate an interconnecting line.

$$u_3(t) = Le\frac{di_4(t)}{dt} + i_4(t)(Z_0 + Re). \tag{6.16}$$

From Eqns. (6.13) (6.15) (6.16), we have

$$\frac{1}{Ce}\int_0^t (i_2(t) - i_4(t))dt = Le\frac{di_4(t)}{dt} + i_4(t)(Z_0 + Re). \tag{6.17}$$

Using the first order approximations for the derivative and integral, Eqn.(6.17) becomes

$$\frac{1}{Ce}[\sum_{k=1}^{n} i_2(k\Delta t)\Delta t - i_4(n\Delta t)\Delta t - \sum_{k=1}^{n-1} i_4(k\Delta t)\Delta t] = \frac{Le}{\Delta t}[i_4(n\Delta t) - i_4((n-1)\Delta t)] - i_4(n\Delta t)(Z_0 + Re)$$

where $t = n\Delta t$.

Then

$$i_4(n\Delta t) = \frac{-1}{Z_1(\Delta t)Ce}i_2(n\Delta t)\Delta t + \frac{1}{Z_1(\Delta t)Ce}\sum_{k=1}^{n-1}[-i_2(k\Delta t) + i_4(k\Delta t)]\Delta t$$

$$-\frac{Le}{Z_1(\Delta t)\Delta t}i_4((n-1)\Delta t) \tag{6.18}$$

where

$$Z_1(\Delta t) = Z_0 + Re - \frac{\Delta t}{Ce} - \frac{Le}{\Delta t}. \tag{6.19}$$

The same treatment can be applied to $u_2(t)$ (Eqn.(6.14)), and it yields

$$u_2(n\Delta t) = Z_3(\Delta t) i_2(n\Delta t) + u_2((n-1)\Delta t) \tag{6.20}$$

where

$$Z_3(\Delta t) = Re + \frac{Le}{\Delta t} - \frac{Z_2(\Delta t)\Delta t}{Z_1(\Delta t)Ce} \tag{6.21}$$

$$Z_2(\Delta t) = Z_0 + Re + \frac{Le}{\Delta t} \tag{6.22}$$

$$u_2((n-1)\Delta t) = -\frac{Le}{\Delta t} i_2((n-1)\Delta t) - \frac{Le}{\Delta t}[1 + \frac{Z_2(\Delta t)}{Z_1(\Delta t)\Delta t}] i_4((n-1)\Delta t)$$

$$+\frac{Z_2(\Delta t)}{Z_1(\Delta t)Ce} \sum_{k=1}^{n-1} [-i_2(k\Delta t) + i_4(k\Delta t)]\Delta t \tag{6.23}$$

and

$$i_4((n-1)\Delta t) = -\frac{i_2((n-1)\Delta t)\Delta t}{Z_1(\Delta t)Ce} + \frac{1}{Z_1(\Delta t)Ce} \sum_{k=1}^{n-2} [-i_2(k\Delta t) + i_4(k\Delta t)]\Delta t$$

$$-\frac{Le}{Z_1(\Delta t)\Delta t} i_4((n-2)\Delta t). \tag{6.24}$$

Eqn.(6.20) represents the relationship between the voltage and current at the discontinuity, while the discontinuity has been replaced by the RLCLR circuit. This relationship can be further implemented into the analysis of the interconnecting lines as described in [117].

6.3.2 Lumped Element Circuit As A Signal Generator

Through the discontinuity, the transmitted signal could be thought of as a new signal source to the interconnecting lines immediately connected to the discontinuity. However, since the signal has been numerically discretized in the time domain, the new signal generator has to be a combination of the transmitted voltage/current and the RLCLR circuit. To construct such an equivalent representation, the concept of the Thevenin equivalent circuit will be adopted here.

According to the Thevenin equivalent, a complicated signal source can be replaced by an open circuit voltage u_{oc} and an equivalent internal resistance R_{eq}. Fig.6.6 illustrates the circuits of the signal source for the extraction of u_{oc} and R_{eq}. It is noted that the equivalent internal resistance is obtained from the ratio of open circuit voltage u_{oc} to short circuit current i_{sc}. u_{oc} and i_{sc} have to be solved separately.

A. Open Circuit Voltage:

From Fig.6.6 (a), we have

$$u_{oc}(t) = u_2(t) - i_{oc}(t) - Le\frac{di_{oc}(t)}{dt}. \tag{6.25}$$

To find out $i_{oc}(t)$ in the above equation, we would start from the Laplace domain.

$$i_{oc}(s) = \frac{u_{oc}(s)}{Re + sLe + \frac{1}{sCe}} \tag{6.26}$$

or

$$i_{oc}(s) = u_{oc}(s)G_2(s) \tag{6.27}$$

where

$$G_2(s) = \frac{1}{Le}\frac{sCe}{(s-s_1)(s-s_2)} \tag{6.28}$$

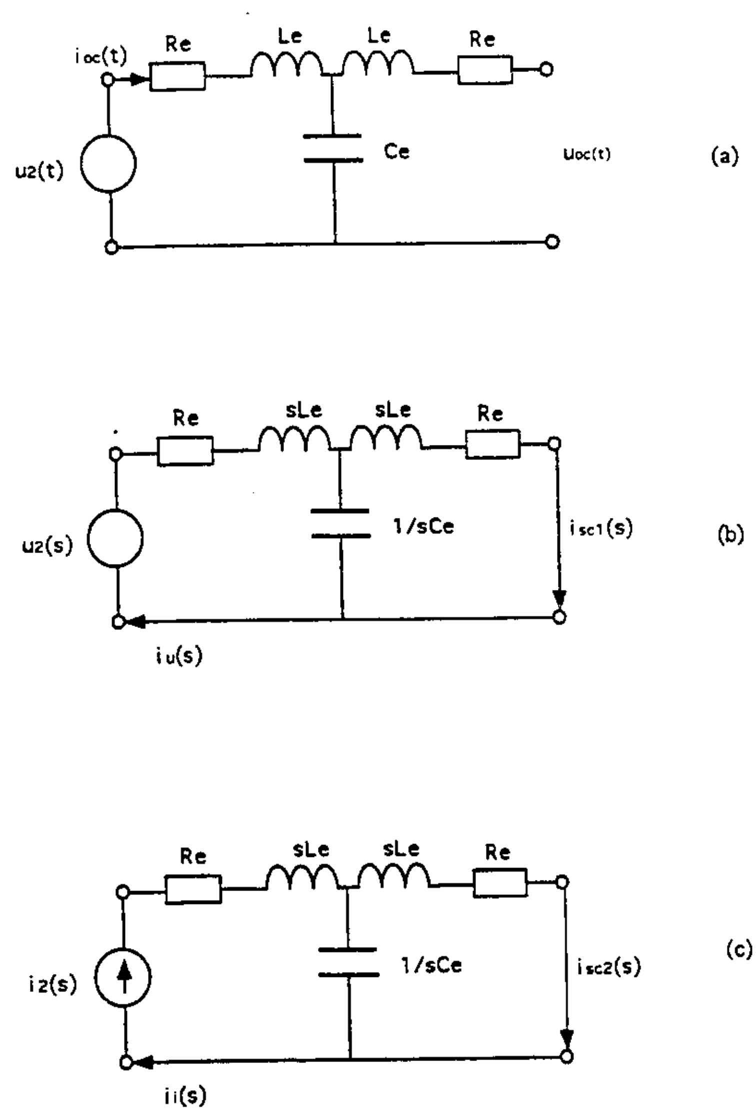

Figure 6.6: The transmitted signal and the RLCLR circuit to form a new signal source: (a) open circuit voltage; (b) short circuit current — case 1; (c) short circuit current — case 2.

s_1 and s_2 are the two roots, which are found from the denominator of Eqn.(6.26):

$$s_1 = p + qj, \quad s_2 = p - qj. \tag{6.29}$$

Then, after the inverse Laplace transform, we obtain a convolution form of the open circuit current:

$$i_{oc}(t) = \int_0^t u_2(\tau) G_2(t-\tau) d\tau \tag{6.30}$$

where

$$G_2(t) = \frac{1}{Le}[(\frac{qcos(qt) + psin(qt)}{q})e^{pt}]. \tag{6.31}$$

We notice that in Eqn.(6.25)

$$\frac{di_{oc}(t)}{dt} = \frac{d}{dt}\int_0^t u_2(t) G_2(t-\tau) d\tau$$

$$= \int_0^t u_2(\tau)\frac{d}{dt}G_2(t-\tau)d\tau + u_2(t)G_2(0)|_{G_2(0)=\frac{1}{Le}} \tag{6.32}$$

where

$$\frac{d}{dt}G_2(t) = \frac{1}{qLe}[2pqcos(qt) + (p^2 - q^2)sin(qt)]e^{pt}. \tag{6.33}$$

Then

$$u_{oc}(t) = -\frac{Re}{qLe}\int_0^t u_2(\tau)[qcos(q(t-\tau)) + psin(q(t-\tau))]e^{p(t-\tau)}d\tau$$

$$-\frac{1}{q}\int_0^t u_2(\tau)[2pqcos(q(t-\tau))+(p^2-q^2)sin(q(t-\tau))]e^{p(t-\tau)}d\tau. \quad (6.34)$$

Using the approximate treatment to the integral, we finally have the following closed form expression for the open circuit voltage at each time interval Δt:

$$u_{oc}(n\Delta t) = -\frac{Re}{qLe}\sum_{k=1}^{n} u_2(k\Delta t)[qcos(q(n-k)\Delta t)+psin(q(n-k)\Delta t)]e^{p(n-k)\Delta t}\Delta t$$

$$-\frac{1}{q}\sum_{k=1}^{n} u_2(k\Delta t)[2pqcos(q(n-k)\Delta t)+(p^2-q^2)sin(q(n-k)\Delta t)]e^{p(n-k)\Delta t}\Delta t. \quad (6.35)$$

B. Short Circuit Current:

In order to find out the short circuit current for the equivalent internal resistance, it would be better to start from the Laplace domain as shown in Fig.6.6 (b), where we have two different original sources $u_2(s)$ and $i_2(s)$. The contributions from the two sources will be considered separately. In the following derivations, $i_{sc1}(s)$ and $i_{sc2}(s)$ represent the short circuit currents originating from $u_2(s)$ and $i_2(s)$, respectively.

Using the mesh analysis techniques, we have

$$i_u(s)(sLe+Re+\frac{1}{sCe})+i_{sc1}(s)(\frac{-1}{sCe}) = u_2(s) \quad (6.36)$$

$$i_u(s)(\frac{-1}{sCe})+i_{sc1}(s)(sLe+Re+\frac{1}{sCe}) = 0. \quad (6.37)$$

Solving the above system of equations, it yields

$$i_{sc1}(s) = \frac{u_2(s)}{Le^2Ce[s^3+\frac{2Re}{Le}s^2+\frac{2Le+Re^2Ce}{Le^2Ce}s+\frac{2Re}{Le^2Ce}]} \quad (6.38)$$

or

$$i_{sc1}(s) = \frac{1}{Le} u_2(s) G_1(s) \tag{6.39}$$

where

$$G_1(s) = \frac{1}{(s - s_1)(s - s_2)(s - s_3)} \tag{6.40}$$

and s_i $(i = 1, 2, 3)$ are the three roots of the denominator of $i_{sc1}(s)$ (Eqn.(6.38)). The inverse transform of $i_{sc1}(s)$ will provide time domain solution of the short circuit current:

$$i_{sc1}(t) = \frac{1}{Le} \int_0^t u_2(\tau) G_1(t - \tau) d\tau \tag{6.41}$$

where

$$G_1(t) = \frac{e^{s_1 t}}{(s_1 - s_2)(s_1 - s_3)} + \frac{e^{s_2 t}}{(s_2 - s_1)(s_2 - s_3)} + \frac{e^{s_3 t}}{(s_3 - s_1)(s_3 - s_2)}. \tag{6.42}$$

Numerical implementation of the above convolution yields

$$i_{sc1}(n\Delta t) = \frac{1}{Le} \sum_{k=1}^{n} u_2(k\Delta t) G_1((n-k)\Delta t) \Delta t. \tag{6.43}$$

Considering another part of the short circuit current (Fig.6.6 (c)), we will have similar derivation procedure.

$$i_{sc2}(s)(sLe + Re) = i_c(s) \frac{1}{sCe} \tag{6.44}$$

$$i_2(s) = i_c(s) + i_{sc2}(s). \tag{6.45}$$

From the above system of equations $i_{sc2}(s)$ is solved as

$$i_{sc2}(s) = \frac{1}{LeCe} i_2(s) G_3(s) \tag{6.46}$$

where

$$G_3(s) = \frac{1}{(s - s_1)(s - s_2)} \tag{6.47}$$

and $s_1 = p + qj$ and $s_2 = p - qj$, and they are the roots of the following equation:

$$LeCes^2 + ReCes + 1 = 0.$$

The inverse transform of $i_{sc2}(s)$ gives

$$i_{sc2}(t) = \frac{1}{LeCe} \int_0^t i_2(\tau) G_3(t - \tau) d\tau \tag{6.48}$$

where

$$G_3(t) = \frac{1}{q} sin(qt) e^{pt}. \tag{6.49}$$

Using the same numerical procedure as we applied to $i_{sc1}(n\Delta t)$, we obtain

$$i_{sc2}(n\Delta t) = \frac{1}{qLeCe} \sum_{k=1}^{n} i_2(k\Delta t) sin(q(n-k)\Delta t) e^{p(n-k)\Delta t} \Delta t. \tag{6.50}$$

The total short circuit current will be the sum of the two currents derived above:

$$i_{sc}(t) = i_{sc1}(t) + i_{sc2}(t) \tag{6.51}$$

and the equivalent internal resistance will be determined by Eqns.(6.35) and (6.51) as

$$R_{eq}(t) = \frac{u_{oc}(t)}{i_{sc}(t)}. \tag{6.52}$$

6.4 APPLICATIONS TO VIA AND BEND STRUCTURES IN VLSI INTERCONNECTS

The mathematical interface built up in the previous section is a general technique to treat the physical relationship between the discrete time domain signals and the lumped element circuits. In principle, this approach is not limited to bend and via structures which can be modeled by LCL or RLCLR equivalent circuits. Any other combinations of the lumped equivalent circuits, such as CLC circuit (Fig.6.1 (b)), Γ-type model [102], and hybrid models of distributed and lumped elements [105] [106], can also be dealt with the same technique. The advantage of this technique is that it explicitly expresses the transient behavior of the signal passing through the discontinuities, which is not feasible by using FDTD approach or commercial simulators.

In this section, an indirect verification of the proposed mathematical interface is provided before the applications to discontinuity problems. The principle of this verification is that if the values of the lumped parameters (Le, Ce and Re) in the RLCLR circuit decreases, the waveform distortion of the signal passing through the circuit will become less. In other words, the signal pulse shape should be convergent to the original form as if there were no such RLCLR circuit introduced when the lumped parameters vanish.

The previous sections have provided the extraction procedures and interface techniques for discontinuity problems. After the verification, applications to realistic via and bend structures will be presented.

6.4.1 An Indirect Verification

The mathematical interface presented in the previous section is not limited to a single transmission line structure. It could be adopted in the modal analysis of multiconductor systems (with muti-discontinuities [104]). However, a single transmission line is the best structure to test the mathematical interface proposed in this chapter since we could easily avoid other error factors introduced by coupling effects. Up till now, there is no report on the waveform distortion of a trapezoidal pulse passing through an interconnect discontinuity in a single transmission line structure. There are two ways to implement the verification: numerical testing and experiment. For the former, it is naturally related and

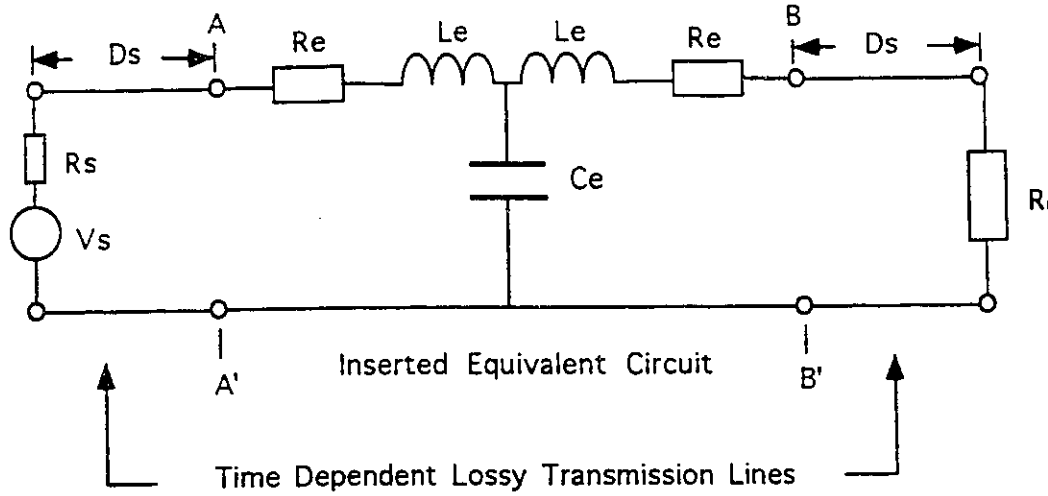

Figure 6.7: Transmission line system for numerical testing of the mathematical interface.

straightforward. However, for the latter, it rather depends on the facilities because there is a requirement for sensing the subtlety of the signal weveform. In this chapter, only numerical testing of the interface is provided.

Fig.6.7 displays a transmission line system for the numerical testing, where an RLCLR circuit is inserted in the middle of the line. It is evident that the inserted circuit will introduce distortion to the original signal. However, if the values of the parameters of the circuit are decreased towards zero, the distortion will become smaller or vanish.

Fig.6.8 and Fig.6.9 show the time domain responses at the sending end and receiving end of one uniform transmission line, respectively. The time dependent losses of the signal and ground conductors have been taken into account using the method proposed in [117]. Comparison with dc losses and lossless cases ([94]) is also illustrated. Both figures are related with a system ($R_s = 50\Omega$, $R_L = 50\Omega$, $L = 305.9nH/m$, $C = 103.9pF/m$, $D_s = 0.01m$) where no discontinuity is introduced. The transmission line in the system is a microstrip line with physical parameters being: the width of the strip $w = 0.2mm$, the thickness of the strip $t = 1.0\mu m$, the thickness of the substrate $h = 0.1mm$, the relative dielectric constant $\epsilon_r = 4.0$, and the conductivity of the signal and ground conductors $\sigma = 5.6 \times 10^7 S/m$. The rise time and fall time of the trapezoidal pulse are the same, i.e., $0.01ns$,

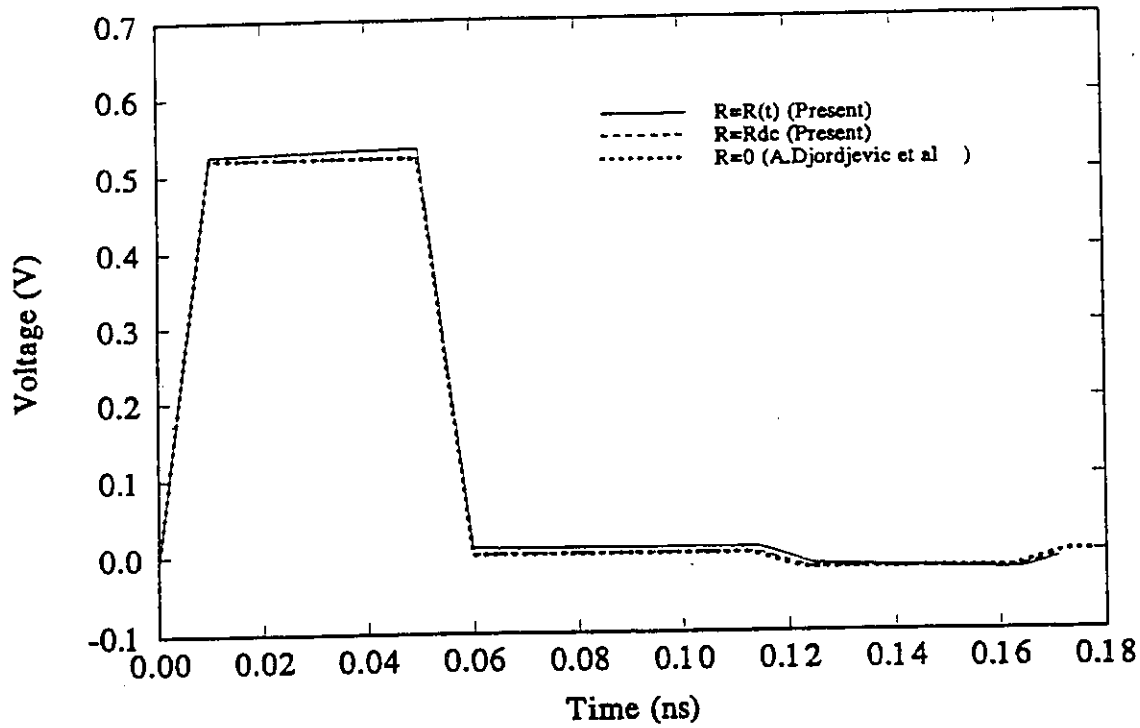

Figure 6.8: Time domain response at the sending end of a uniform transmission line without presence of the discontinuity.

Fig.6.10 and Fig.6.15 display the open circuit voltage $u_{oc}(t)$ and the equivalent internal resistance $R_{eq}(t)$ at location $B - B'$ in Fig.6.7. The transmission line system is the same as the one reported for Fig.6.8 and Fig.6.9.

One would observe that being shown in Fig.6.10 and Fig.6.15, as the circuit parameters deceases, the waveform of the open circuit voltage approaches the undistorted shape shown in Fig.6.9. This provides us an indirect verification of the present analysis. However, small ripples are observed on the trapezoidal pulse. This is due to the resonant frequency of the RLCLR circuit. Since the pulse contains frequency components up to tens of gigahertz, it is possible to excite proper resonance which exerts its influence on the pulse. In addition, the decaying rates of the ripples are rather small because of the low attenuation property of the RLCLR circuit.

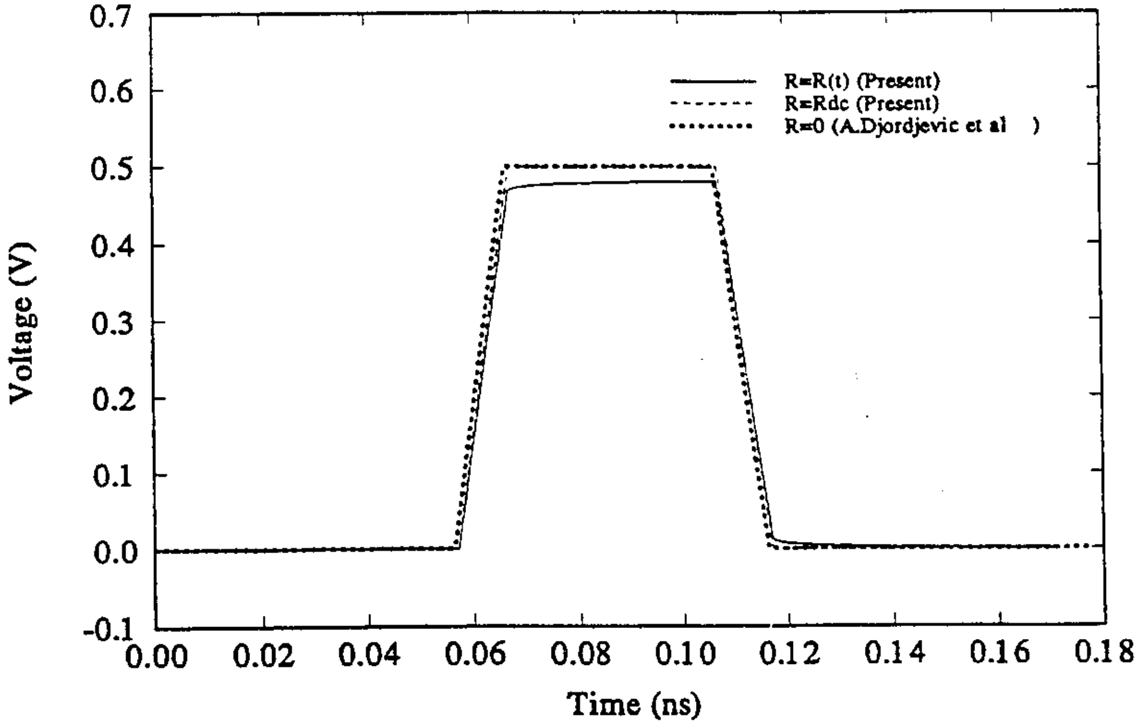

Figure 6.9: Time domain response at the receiving end of a uniform transmission line without presence of the discontinuity.

6.4.2 Application to A Through Hole Via

Consider a through hole via with the geometrical structure shown in Fig.6.2 (a), where the physical parameters are: $h_1 = 0.15mm$, $t = 0.01mm$, $r_0 = 0.1mm$, $r_1 = 0.12mm$, $\epsilon_r = 4.0$, $\sigma = 5.6 \times 10^7 S/m$. Its RLCLR lumped element representation is shown in Fig.6.2 (c) with lumped parameters being $Re = \alpha Re_{15}/2|_{\alpha=5.7} = 3.8175\times10^{-4}\Omega$, $Le = \beta Le_1/2|_{\beta=0.523} = 0.039nH$, $Ce = 0.015pF$. These parameters are extracted using the procedures described earlier. A full circuit representation of the via-interconnecting lines is illustrated in Fig.6.16. The total length of the transmission line is $2 \times D_s = 0.02m$, and the via is located at the middle $D_s = 0.01m$.

It would be interesting to look at the pulse arriving at the via location (Fig.6.17). The long dashed line represents the starting pulse in an "ideal" condition (no via is introduced). The short dashed line stands for the waveform reflected by the via at $D_s = 0.01m$, while the solid line is the transmitted pulse at the via location ($D_s = 0.01m$). As depicted in Fig.6.16, the other side of the transmission line is terminated by a linear resistive load ($R_L = 50\Omega$).

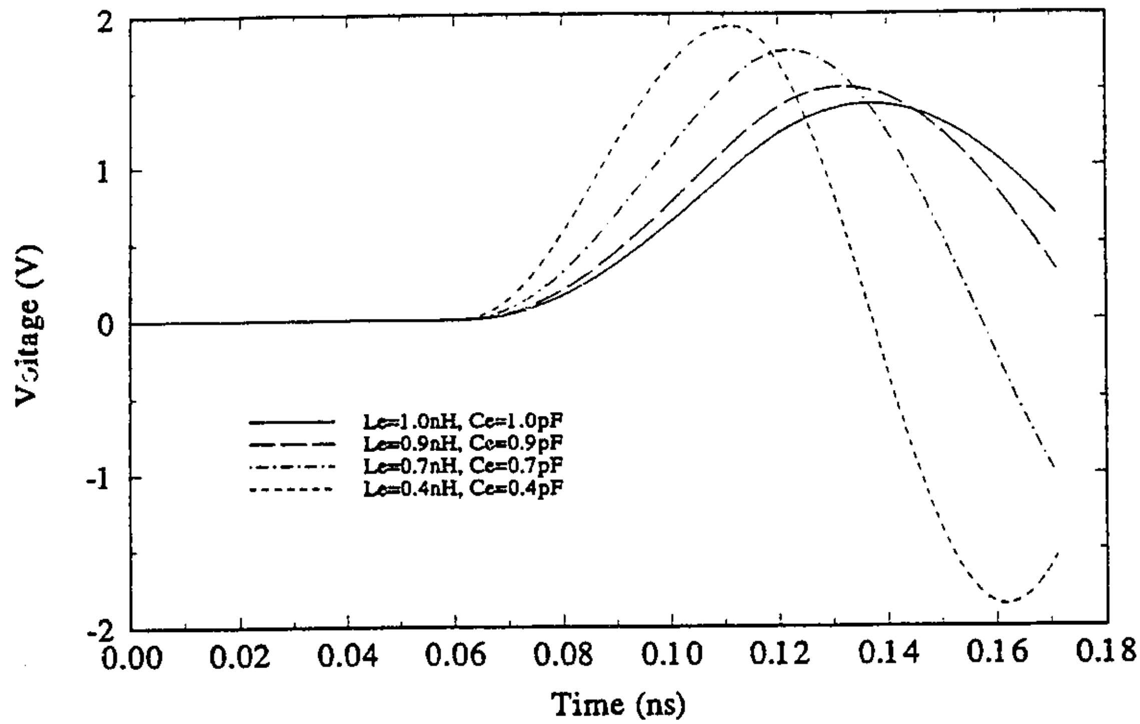

Figure 6.10: Equivalent open circuit voltage.

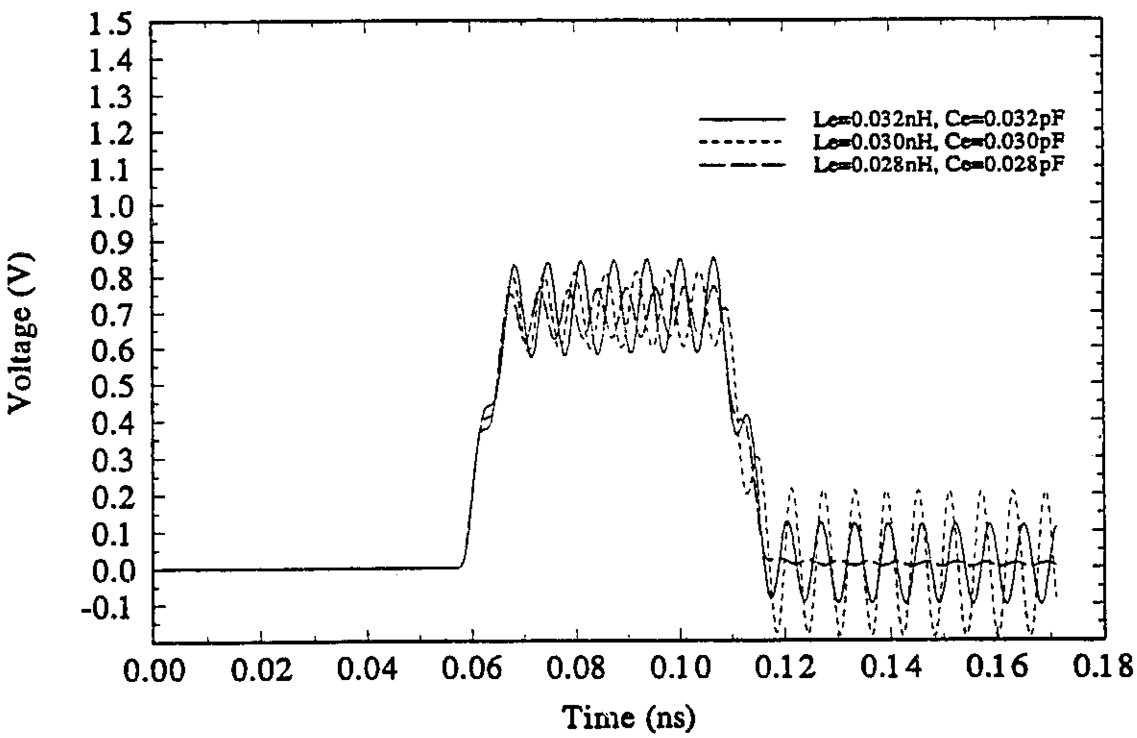

Figure 6.11: Equivalent open circuit voltage.

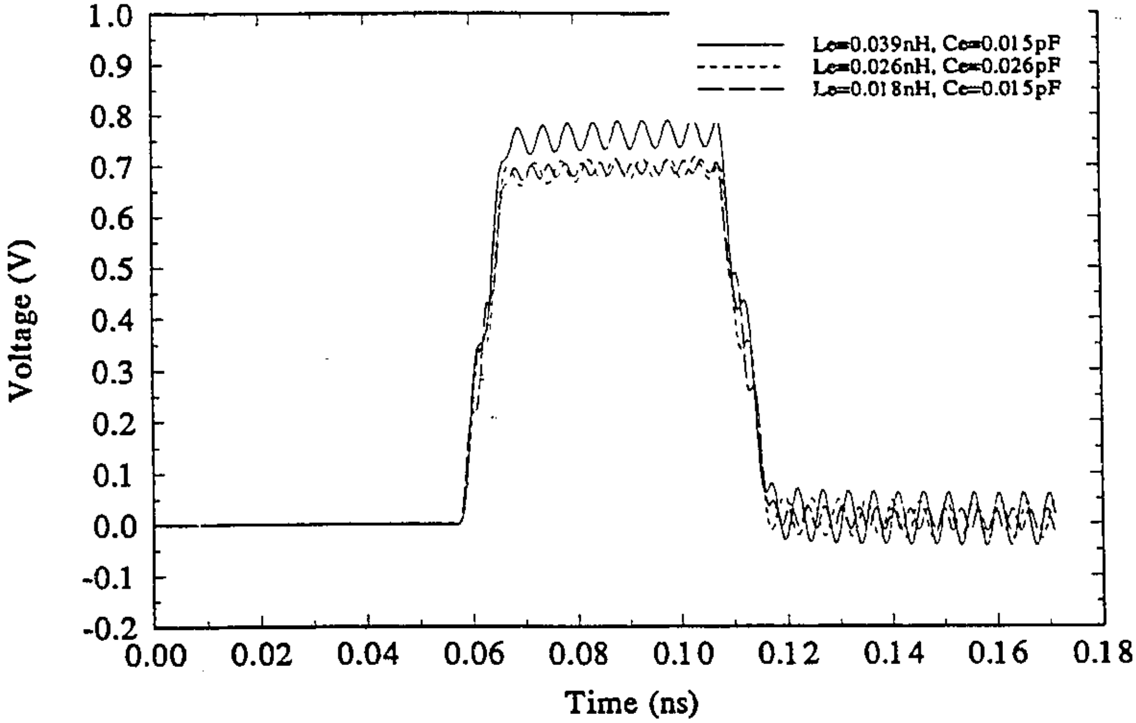

Figure 6.12: Equivalent open circuit voltage.

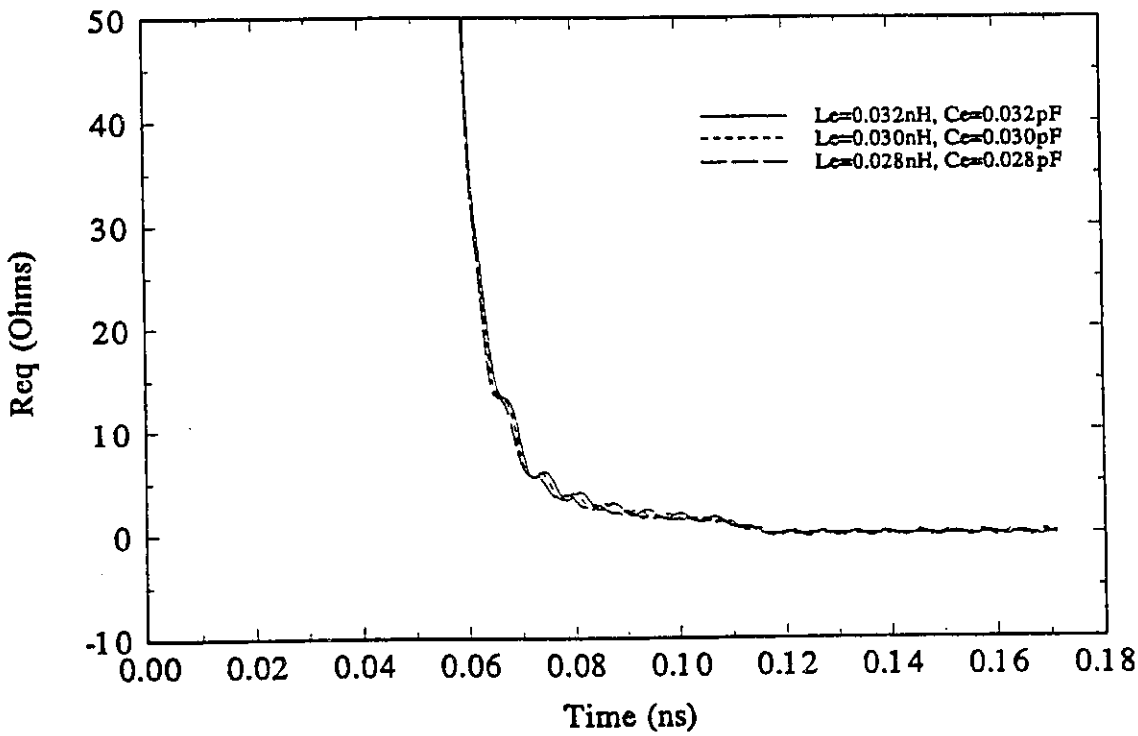

Figure 6.13: Equivalent internal resistance.

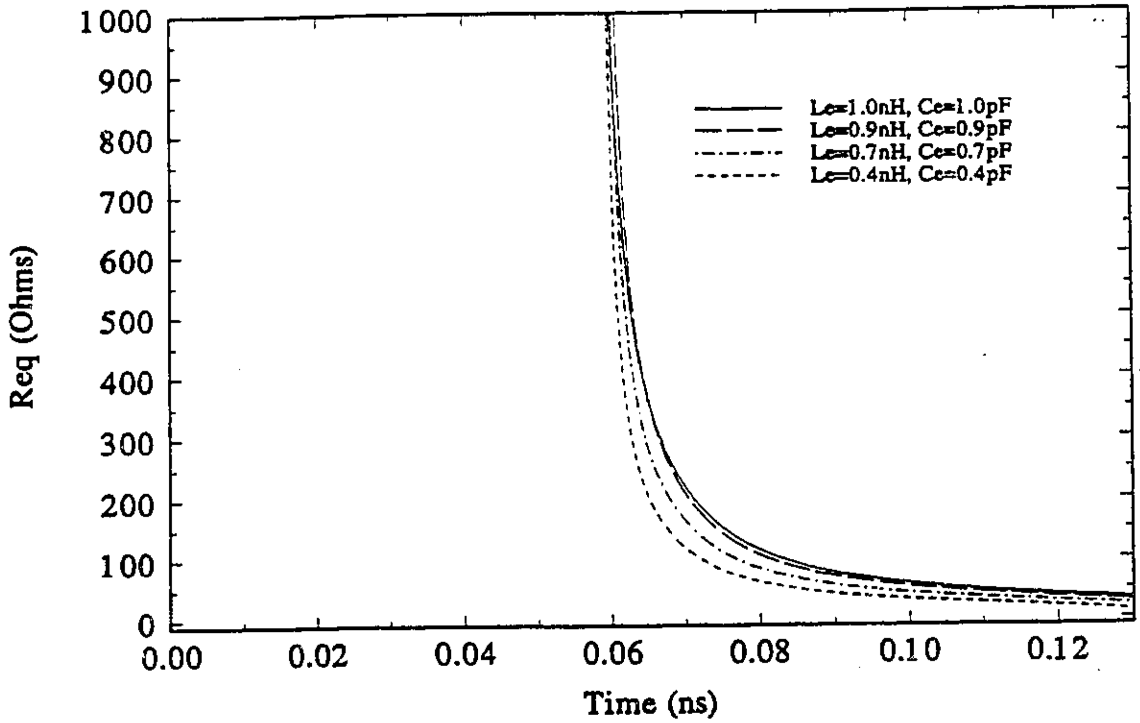

Figure 6.14: Equivalent internal resistance.

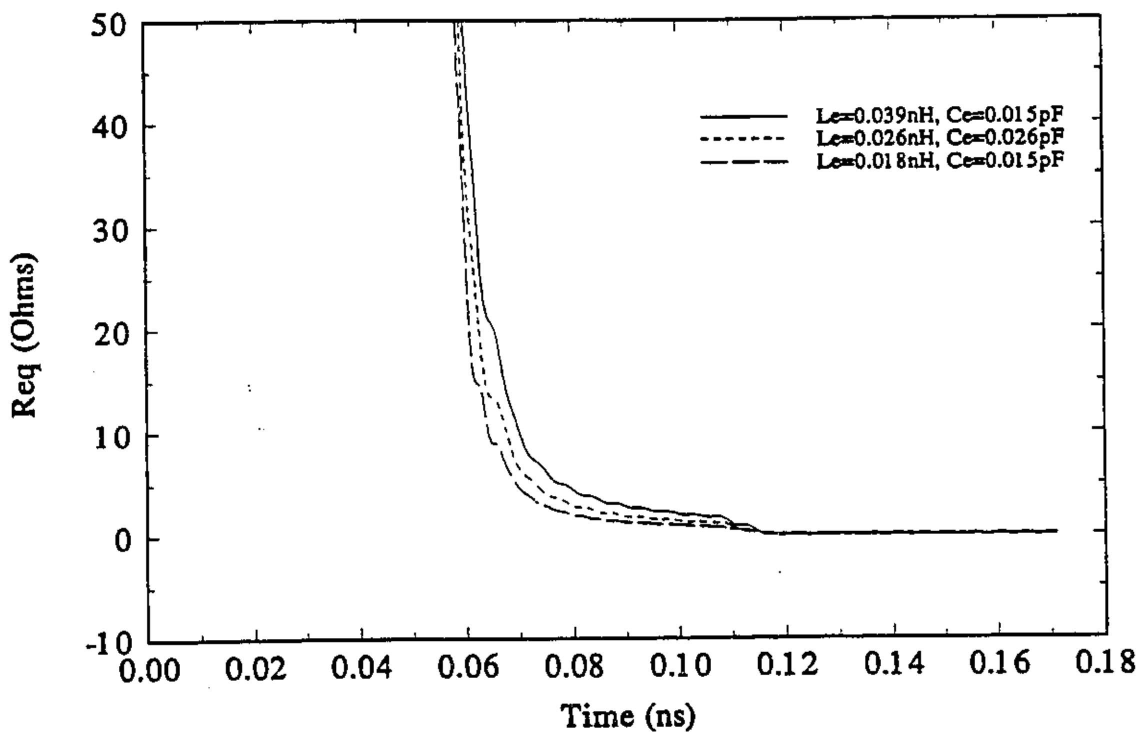

Figure 6.15: Equivalent internal resistance.

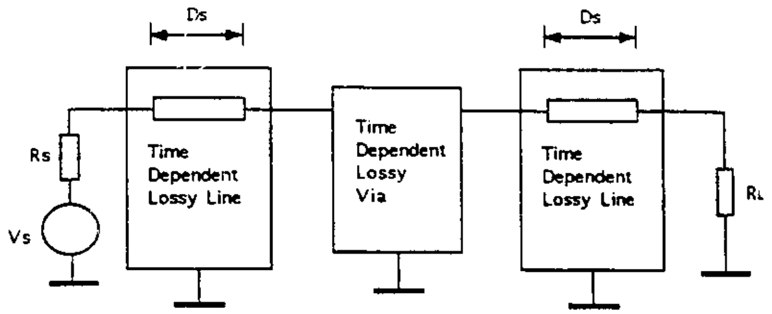

(a)

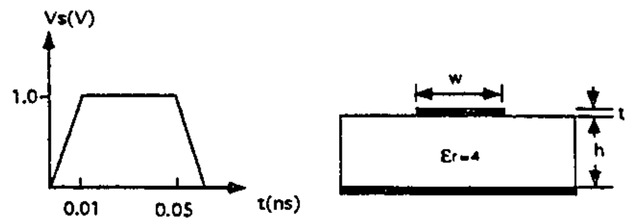

(b)

Figure 6.16: Circuit structure: (a) via-interconnecting lines circuit; (b) interconnecting line profile.

Fig.6.18 shows a comparison between the waveforms with and without the through hole via at the receiving end ($2 \times D_s = 0.02m$). It is noted that for the same termination load, the amplitude of the pulse transmitted through the via is lower than that of the pulse without the via. The cause of the small ripple has been stated earlier. One would also notice the skewed shape of the waveform at the receiving end. This is due to the time dependent losses which has been accounted for in the analysis [117].

6.4.3 Application to Bend Structures

If the bend structure is modeled using the LCL circuit as used in [104], the waveform distortion will be qualitatively the same as the one simulated in the via case. The only difference is the values of the circuit parameters.

Consider the same transmission line system as we studied for the through hole via. The via is replaced by a right-angled bend with $w_1 = w_2 = 0.2mm$ in Fig.6.1 (a). The equivalent inductance and capacitance for the right-angled bend may be extracted by the procedures described in [110] [111]. In our case, we have $Le = 0.018nH$ and $Ce = 0.015pF$. The equivalent open circuit voltage has been shown in Fig.6.12 (the long dashed line). The effects due to the equivalent resistance Re are minor since the resistance in that region is

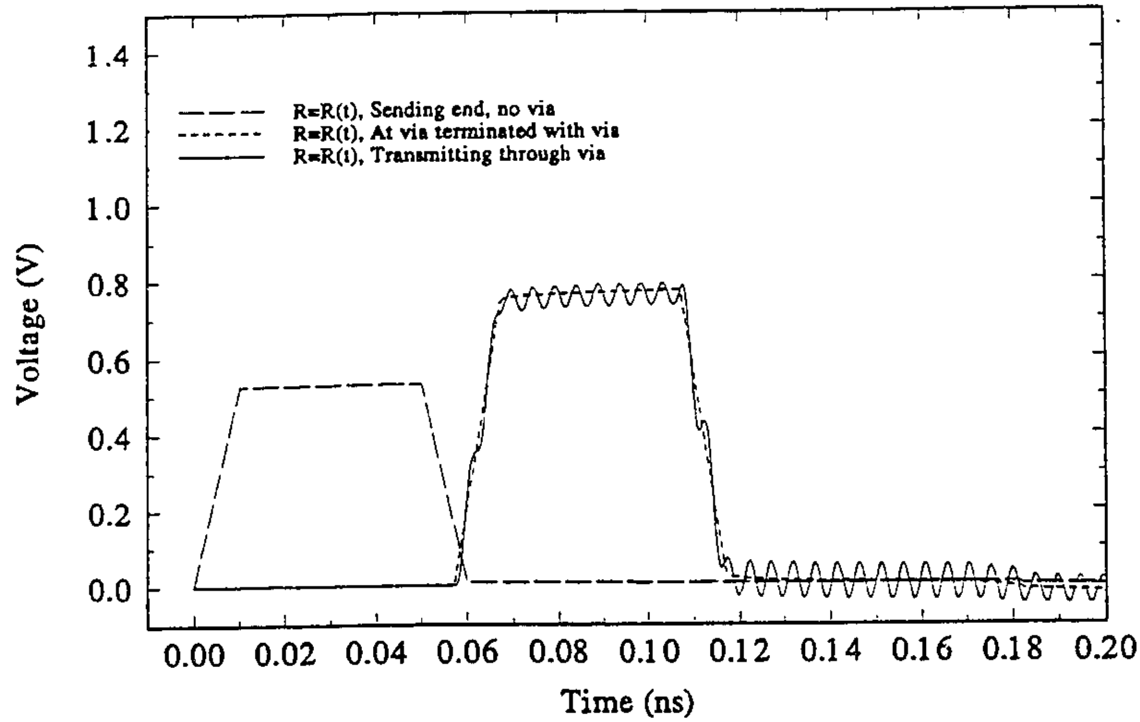

Figure 6.17: Waveforms of the pulse traveling through the via.

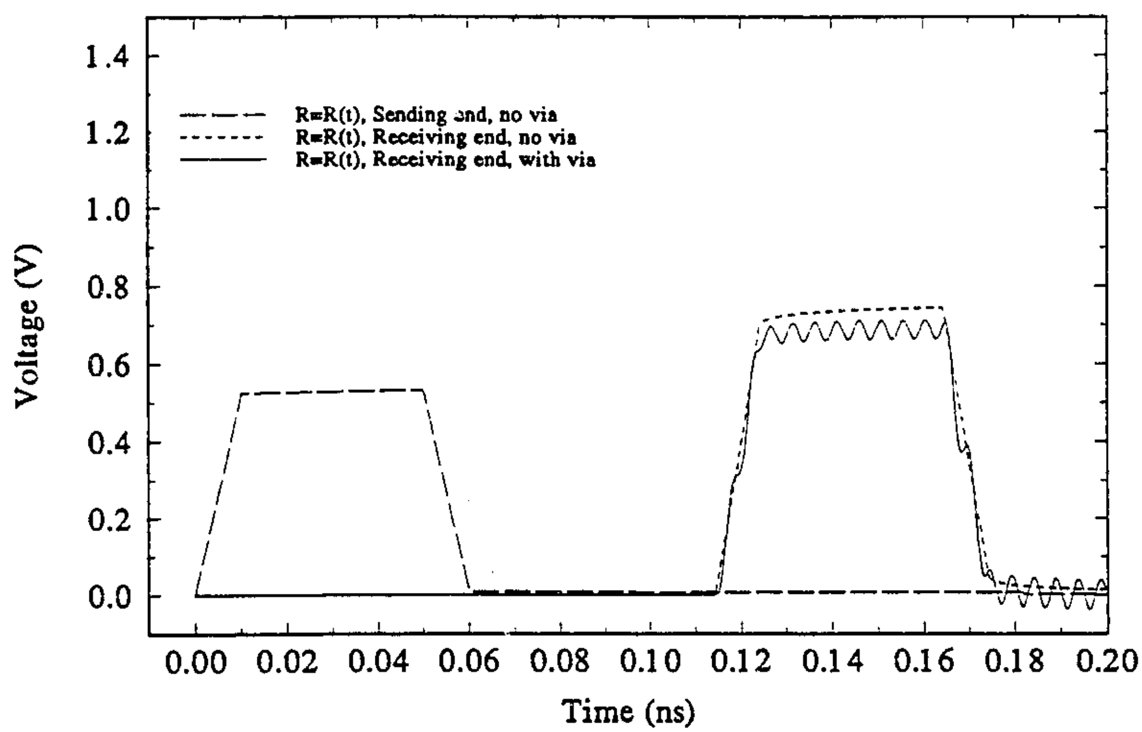

Figure 6.18: Comparison between waveforms with and without the via.

very small.

6.5 CONCLUSIONS

This chapter presents a semi-analytical approach to tackle the interconnect discontinuity problems encountered in the VLSI circuit designs. The "semi-analytical" means that the time domain response of the discontinuity is expressed in closed forms for each time interval (Δt) while the original signal is also given analytically at every Δt [117]. This is an advantage when sensitivity analysis or optimization is needed for a discontinuity structure. The mathematical interface presented in this chapter provides such easy facilities.

The extraction procedures for the lumped parameters of a through hole via are given with approximations. The approximations are based on the following assumptions: 1) the dielectric substrate contribution to the capacitance between the via and ground plane is ignored; 2) a very small amount of the capacitance (δC) between the via and the ground plane within the thickness of the plane is empirically compensated; 3) a one-element circuit is used to asymptotically represent a five-element circuit. However, there are quite a few numerical and analytical methods available to do the extraction job. To avoid the mathematical or numerical manipulations involved with these existing methods, the procedures presented in this chapter provides a simple way to estimate those lumped parameters. In addition, the time dependent losses included in the equivalent circuit of a through hole via may play an important role because the time dependent resistance of the via is very large at the very begining when the signal reaches it.

The mathematical interface is verified by an indirect approach. This indirect verification provides physically reliable information: 1) as the values of the lumped parameters, such as Le and Ce, decrease, the distortion introduced by these parameters becomes small; 2) time domain signals with very small rise time ($10ps$ for instance in this chapter) can excite resonance of a particular RLC circuit; 3) the resonance in a low loss circuit ($Re = 0.35m\Omega$) decays slowly. Fig.6.10 - Fig.6.12 provide consistent agreement with the above justification.

As a supplement work to the previous chapters, this chapter presents a technical insight in the VLSI discontinuity problems. Another alternative approach to build up the mathematical interface is the adoption of the nodal formulation [119], which is different from the mesh formulation used in this chapter. The sensitivity analysis can be performed based on the modified nodal admittance (MNA) matrix [17]. In principle, both nodal and mesh formulations for the RLCLR equivalent circuit would yield the same results.

Appendix A

ANALYTICAL SOLUTION OF A ONE-DIMENSIONAL TIME DOMAIN PROBLEM

The one-dimensional diffusion problem associated with boundary and initial conditions is given below:

$$\frac{\partial^2 H}{\partial x^2} - \mu\sigma \frac{\partial H}{\partial t} = 0 \tag{A.1}$$

$$H(0,t) = 0 \qquad (x = 0) \tag{A.2}$$

$$H(d,t) = f(t) \qquad (x = d) \tag{A.3}$$

$$H(x,0) = 0 \qquad (x \in [0,d]). \tag{A.4}$$

To solve the above problem, a reference function can be chosen as

$$r(x,t) = \frac{x}{d} f(t) \tag{A.5}$$

$$r(x,0) = \frac{x}{d} f(0) \tag{A.6}$$

which satisfies

$$r(0,t) = 0 \tag{A.7}$$

$$r(d,t) = f(t). \tag{A.8}$$

Thus a new homogeneous function is formulated as

$$V(x,t) = H(x,t) - r(x,t) \tag{A.9}$$

$$V(0,t) = 0 \tag{A.10}$$

$$V(d,t) = 0 \tag{A.11}$$

$$V(x,0) = H(x,0) - \frac{x}{d}f(0) = g(x). \tag{A.12}$$

Using the method of eigenfunction expansion, we have

$$V(x,t) = \sum_{i=1}^{\infty} a_n(t)\Phi_n(x) \tag{A.13}$$

where $\Phi_n(x)$ is the eigenfunction which can be written, according to the boundary conditions, as

$$\Phi_n(x) = sin(\frac{n\pi}{d}x). \tag{A.14}$$

The initial condition Eqn.(A.12) is satisfied if we have

$$g(x) = \sum_{i=1}^{\infty} a_n(0)\Phi_n(x) \tag{A.15}$$

where

$$a_n(0) = \frac{\int_0^d g(x)\Phi_n(x)dx}{\int_0^d \Phi_n^2(x)dx} = -\frac{\int_0^d \frac{x}{d}f(0)sin(\frac{n\pi}{d}x)dx}{\int_0^d sin^2(\frac{n\pi}{d}x)dx}\ . \tag{A.16}$$

From Eqns.(A.9) and (A.1), we obtain

$$\frac{\partial^2 V(x,t)}{\partial x^2} - \mu\sigma\frac{\partial V(x,t)}{\partial t} = -Q(x,t) \tag{A.17}$$

where

$$Q(x,t) = -\mu\sigma\frac{x}{d}f'(t). \tag{A.18}$$

Substituting Eqn.(A.13) in Eqn.(A.17) yields

$$\sum_{n=1}^{\infty}[\mu\sigma\frac{da_n(t)}{dt} + a_n(t)\lambda_n]\Phi_n(x) = Q(x,t) \tag{A.19}$$

where $\lambda_n = (\frac{n\pi}{d})^2 \quad (n = 1, 2, ...)$ is the eigenvalue of the following equation

$$\frac{d^2\Phi_n(x)}{dx^2} + \lambda_n\Phi_n(x) = 0. \tag{A.20}$$

Due to the orthogonality of $\Phi_n(x)$, we have

$$\frac{da_n(t)}{dt} + \frac{\lambda_n}{\mu\sigma}a_n(t) = \frac{1}{\mu\sigma}q_n(t) \tag{A.21}$$

where

$$q_n(t) = \frac{\int_0^d Q(x,t)\Phi_n(x)dx}{\int_0^d \Phi_n^2(x)dx}. \tag{A.22}$$

Multiplying Eqn.(A.21) with $e^{\frac{\lambda_n}{\mu\sigma}t}$and integrating from 0 to t yields:

$$a_n(t) = a_n(0)e^{-(\frac{n\pi}{d})^2\frac{1}{\mu\sigma}t} + e^{-(\frac{n\pi}{d})^2\frac{1}{\mu\sigma}t}\int_0^t q_n(\tau)e^{(\frac{n\pi}{d})^2\frac{1}{\mu\sigma}\tau}d\tau\ . \tag{A.23}$$

Finally we have

$$H(x,t) = V(x,t) + r(x,t) = \sum_{n=1}^{\infty} a_n(t)sin(\frac{n\pi}{d}) + \frac{x}{d}f(t) \tag{A.24}$$

where $f(t)$ is the excitation function on one of the boundaries.

Appendix B

INTRODUCTION TO THE METHOD OF CHARACTERISTICS

The set of partial differential equation describing TEM transmission lines (generally nonuniform and lossy ones) is written as [6]

$$-\frac{\partial v}{\partial z} = L\frac{\partial i}{\partial t} + Ri \tag{B.1}$$

$$-\frac{\partial i}{\partial z} = C\frac{\partial v}{\partial t} + Gv \tag{B.2}$$

where z is a physical distance along the transmission line, $0 < z < D_s$, L, C, R and G are inductance, capacitance, resistance and conductance per unit length specified as function of z, and $v = v(z,t)$ and $i = i(z,t)$ are the voltage and current, respectively.

By introducing a certain relationship $z = z(t)$, Eqns.(B.1) (B.2) can be transformed into two ordinary differential equations. First, we would evaluate the following derivatives:

$$\frac{d}{dt}v(z,t) = \frac{\partial v}{\partial z}\frac{dz}{dt} + \frac{\partial v}{\partial t} \tag{B.3}$$

$$\frac{d}{dt}i(z,t) = \frac{\partial i}{\partial z}\frac{dz}{dt} + \frac{\partial i}{\partial t}. \tag{B.4}$$

After substituting (B.3) (B.4) into (B.1) (B.2) and rearranging, we have

$$L\frac{\partial i}{\partial z}\frac{dz}{dt} - \frac{\partial v}{\partial z} = L\frac{di}{dt} + Ri \tag{B.5}$$

$$C\frac{\partial v}{\partial z}\frac{dz}{dt} - \frac{\partial i}{\partial z} = C\frac{dv}{dt} + Gv. \tag{B.6}$$

Combining the above two equations yields

$$\frac{d}{dt}(v + \sqrt{\frac{L}{C}}i) = -(\frac{G}{C}v + \frac{R}{\sqrt{LC}}i) + (\frac{\partial v}{\partial z} - \sqrt{\frac{L}{C}}\frac{\partial i}{\partial z})(\frac{dz}{dt} - \frac{1}{\sqrt{LC}}) \tag{B.7}$$

$$\frac{d}{dt}(v - \sqrt{\frac{L}{C}}i) = -(\frac{G}{C}v - \frac{R}{\sqrt{LC}}i) + (\frac{\partial v}{\partial z} - \sqrt{\frac{L}{C}}\frac{\partial i}{\partial z})(\frac{dz}{dt} + \frac{1}{\sqrt{LC}}). \tag{B.8}$$

To eliminate partial derivatives from the these two equations, we have to choose $z = z(t)$ such that

$$\frac{dz}{dt} = \frac{1}{\sqrt{LC}}, \quad i.e., \quad t = const + \int \sqrt{L(z)C(z)} \tag{B.9}$$

and

$$\frac{dz}{dt} = -\frac{1}{\sqrt{LC}}, \quad i.e., \quad t = const - \int \sqrt{L(z)C(z)}dz. \tag{B.10}$$

Then, we obtain two ordinary differential equations:

$$\frac{d}{dt}(v + \rho i) = -(\frac{G}{C}v + \frac{R}{L}\rho i) \quad for \quad t = const + \int \sqrt{L(z)C(z)}dz \tag{B.11}$$

$$\frac{d}{dt}(v - \rho i) = -(\frac{G}{C}v + \frac{R}{L}\rho i) \quad for \quad t = const - \int \sqrt{L(z)C(z)}dz \tag{B.12}$$

where

$$\rho = \sqrt{L(z)C(z)}. \tag{B.13}$$

It is important to note that although (B.11) and (B.12) include derivatives with respect to t, variables t and z are related by (B.9) and (B.10) so that a change in t has associated with a change in z. Relations (B.9) and (B.10) may illustrated in the $z-t$ plane by so called characteritic curves or characteristics. For uniform lines these curves are straight lines, i.e.,

$$t = const + z\sqrt{LC} \quad and \quad t = const - z\sqrt{LC}. \tag{B.14}$$

However, for nonuniform lines we have general curves. In order to make the general characteristics straight, let us introduce an electrical position along the line

$$y(z) = \int_0^z \sqrt{L(\eta)C(\eta)}d\eta. \tag{B.15}$$

Then the characteristic curves are again straight lines in the $y-t$ plane with the slope of +/- 45 degrees.

In order to avoid numerical approximations in determining the position and time of each new point in the $z-t$ plane, we will work with the electrical position $y = y(z)$ only. Then, the spatial discretization of the line can be defined together with the time step $t = \Delta t$ by dividing the total electrical length of the line into n sections (Fig.B.1):

$$\Delta y = y(D_s)/n = \Delta t. \tag{B.16}$$

On the z-axis we have corresponding points z_k, $k = 1, 2, ..., n+1$, nonuniformly distributed and

$$y(z_k) = (k-1)\Delta y = y_k. \tag{B.17}$$

Using the above discretization procedure, Eqns.(B.11) (B.12) may be approximated by difference equations

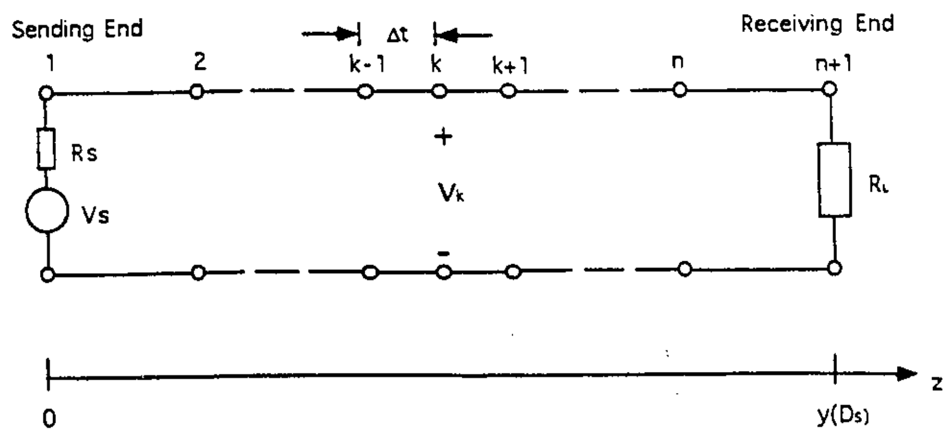

Figure B.1: Transmission line divided into n sections.

$$\Delta(v + \sqrt{\frac{L}{C}} i)|_{z_{k-1},t-\Delta t}^{z_k,t} = -(\Delta t \frac{G}{C} v + \frac{R}{L} \rho i)|_{average} \tag{B.18}$$

and

$$\Delta(v - \sqrt{\frac{L}{C}} i)|_{z_k,t-\Delta t}^{z_{k-1},t} = -(\Delta t \frac{G}{C} v - \frac{R}{L} \rho i)|_{average}. \tag{B.19}$$

The right-hand side of the above equations can be calculated in a number of ways. For instance, the value at the time instant t or an average value of the initial and final values at $t - \Delta t$ and t could be used. The second choice is called the "Trapezoidal Rule" and it is more accurate than the first choice. Details of the implementation of the numerical procedures are presented in Chapter 4.

Bibliography

[1] K.Miya, M.Uesaka and F.C.Moon, 'Finite-element analysis of vibration of toroidal field-coils coupled with Laplace transform,' *J. App. Mech. Trans. ASME*, Vol.49, pp.594-600, 1982.

[2] Han-Taw Chen, Tzer-Ming Chen and Cha'o-Kuang Chen, 'Hybrid Laplace transform/finite element method for one-dimensional transient heat conduction problems,' *Computer Meth. Appl. Mech. Eng.*, **63** vol.63, pp.83-95, 1987.

[3] C.-K.Chen and T.-M.Chen, 'New hybrid Laplace transform/ finite element method for three-dimensional transient heat conduction problem,' *Int. J. Num. Meth. Eng.*, vol.32, pp.45-61, 1991.

[4] F.H.Branin, "Transient analysis of lossless transmission lines," *Proc. IEEE (letters)*, vol.55, pp.2012-2013, Nov. 1967.

[5] F.-Y.Chang, 'Transient analysis of lossless coupled transmission lines in a nonhomogeneous dielectric medium," *IEEE Trans. on Microwave Theory Tech.*, vol.MTT-18, no.9, pp.616-626, Sep. 1970.

[6] V.Dvorak, "Computer simulation of signal propagation through a nonuniform transmission line," *IEEE Trans. on Circuit Theory*, vol.CT-20, no.5, pp.580-583, Sep. 1973.

[7] N.Orhanovic, P.Wang and V.K.Tripathi, "Generalized method of characteristics for time domain simulation of multiconductor lossy lines," *Proc. IEEE Symp. Circ. and Systems*, New Orleans, pp.2388-2391, May. 1990.

[8] V.K.Tripathi and N.Orhanovic, "Time domain characterization and analysis of dispersive dissipative interconnects," *IEEE Trans. on Microwave Theory Tech.*, vol.MTT-39, no.11, pp.938-945, Nov. 1992.

[9] N.Orhanovic, P.Wang and V.K.Tripathi, "Time-domain simulation of uniform and nonuniform multiconductor lossy lines by the method of characteristics," *IEEE Trans. on Computer-Aided Design of Integ. Cir. Sys.*, vol.12, no.6, pp.900-904, Jun. 1993.

[10] J.-F.Mao and Z.-F.Li, "Analysis of the time response of multiconductor transmission lines with frequency-dependent losses by the method of convolution-characteristics," *IEEE Trans. on Microwave Theory Tech.*, vol.MTT-40, no.4, pp.637-644, Apr. 1992.

[11] A.R.Djordjevic, T.K.Sarkar and R.F.Harrington, "Analysis of lossy transmission lines with arbitrary nonlinear terminal networks" *IEEE Trans. on Microwave Theory Tech.*, vol.MTT-34, no.6, pp.660-666, Jun. 1986.

[12] A.R.Djordjevic and T.K.Sarkar, "Analysis of time response of lossy multiconductor transmission line networks" *IEEE Trans. on Microwave Theory Tech.*, vol.MTT-35, no.10, pp.898-908, Oct. 1987.

[13] M.Cases and D.Quinn, "Transient response of uniformly distributed RLC transmission lines," *IEEE Trans. on Circuit Syst.*, vol.CAS-27, pp.200-207, Mar. 1980.

[14] A.J.Gourdis, "Transient analysis of uniform resistive transimission lines in a homogeneous medium," *IBM J. Res. Develop.*, vol.23, pp.675-681, Nov. 1979.

[15] A.J.Gourdis and C.S.Chang, "Coupled lossy transimission line characterization and simulation," *IBM J. Res. Develop.*, vol.25, pp.25-41, Jan. 1981.

[16] J.R.Griffith and M.S.Nakhla, "Time-domain analysis of lossy coupled transmission lines," *IEEE Trans. on Microwave Theory Tech.*, vol.MTT-38, no.10, pp.1480-1487, Oct. 1990.

[17] S.Lum, M.S.Nakhla and Q.-J.Zhang, "Sensitivity analysis of lossy coupled transmission lines," *IEEE Trans. on Microwave Theory Tech.*, vol.MTT-39, no.12, pp.2089-2099, Dec. 1991.

[18] D.H.Xie and M.S.Nakhla, "Delay and crosstalk simulation of high-speed VLSI interconnects with nonlinear terminations," *IEEE Trans. on Comput.Aided Design of Integ. Cir. Sys.*, vol.12, no.11, pp.1798-1811, Nov. 1993.

[19] L.Lu, M.S.Nakhla and Q.-J.Zhang, "A resetting algorithm for transient analysis of coupled transmission line circuits," *IEEE Trans. on Microwave Theory Tech.*, vol.MTT-42, no.3, pp.494-500, Mar. 1994.

[20] S.Lum, M.S.Nakhla and Q.-J.Zhang, "Sensitivity analysis of lossy coupled transmission lines with nonlinear terminations," *IEEE Trans. on Microwave Theory Tech.*, vol.MTT-42, no.4, pp.607-615, Apr. 1994.

[21] P.J.Leonard and D.Rodger, "Some aspects of two- and three-dimensional transient-eddy-current modelling using finite elements and single-step time-marching algorithms," *Proc. IEE, Pt.A.*, vol.135, no.3, pp.159-166, Mar. 1988.

[22] B.E.MacNeal, J.R.Brauer and R.N.Coppolino, "A general finite element vector potential formulation of electromagnetics using a time-integrated electric scalar potential," *IEEE Trans. on Magnetics.*, vol.26, no.5, pp.1768-1770, Sep. 1990.

[23] R.C.Mesquita and J.P.A.Bastos, "3D finite element solution of induction heating problems with efficient time-stepping," *IEEE Trans. on Magnetics.*, vol.27, no.5, pp.4065-4068, Sep. 1991.

[24] R.Albanese, E.Coccorrese, R.Martone, G.Miano and G.Rubinacci, "On the numerical solution of the nonlinear three-dimensional eddy current problem," *IEEE Trans. on Magnetics.*, vol.27, no.5, pp.3990-3995, Sep. 1991.

[25] I.A.Tsukerman, A.Konrad, G.Bedrosian and M.V.K.Chari, "A survey of numerical methods for transient eddy current problems," *IEEE Trans. on Magnetics.*, vol.29, no.2, pp.1711-1716, Mar. 1993.

[26] S.Celozzi and M.Feliziani, "Time domain finite element simulation of conductive regions," *IEEE Trans. on Magnetics.*, vol.29, no.2, pp.1705-1710, Mar. 1993.

[27] A.C.Cangellaris, C.C.Lin and K.K.Mei, "Point-matched time-domain finite methods for electromagnetic radiation and scattering," *IEEE Trans. on Antennas Propag.*, vol.AP-35, no.10, pp.1160-1173, Oct. 1987.

[28] A.C.Cangellaris, "Time-domain finite methods for electromagnetic wave propagation and scattering," *IEEE Trans. on Magnetics.*, vol.27, no.5, pp.3780-3785, Sep. 1991.

[29] J.Joseph, T.J.Sober, K.J.Gohn, and A.Konrad, "Time domain analysis by the point-matched finite element method," *IEEE Trans. on Magnetics.*, vol.27, no.5, pp.3852-3855, Sep. 1991.

[30] A.Konrad, R.Saldanha, S.Y.Lee and J.C.Sabonnadiere, "Application of the point-matched time domain finite element method to the analysis of transmission line transients," *J.Phys. III France*, vol.2, pp.2139-2154, Nov. 1992.

[31] J.O.Y.Lo and A.Konrad, "Time domain simulation of lossy planar networks," *IEEE Trans. on Magnetics.*, vol.29, no.2, pp.1717-1721, Mar. 1993.

[32] N.K.Madsen, R.W.Ziolkowski, "Numerical solutions of Maxwell's equations in the time domain using irregular nonorthogonal grids," *Wave Motion*, vol.10, pp.583-596, 1988.

[33] V.Shankar, A.H.Mohammadian and W.F.Hall, "A time-domain, finite-volume treatment for the Maxwell equations," *Electromagnetics*, vol.10, pp.127-145, 1990.

[34] N.K.Madsen and R.W.Ziolkowski, "A three-dimensional modified finite volume technique for Maxwell's equations," *Electromagnetics*, vol.10, pp.147-161, 1990.

[35] M.J.Tsuk and J.A.Kong, "A hybrid method for the calculation of the resistance and inductance of transmission lines with arbitrary cross sections," *IEEE Trans. on Microwave Theory Tech.*, vol.MTT-39, no.8, pp.1338-1347, Aug. 1991.

[36] N.S.Nahman, "A discussion on the transient analysis of the coaxial cables considering high-frequency losses," *IEEE Trans. on Circuit Theory,* vol.CT-9, no.6, pp.144-152, Jun. 1962.

[37] T.D.English, "Integrated transmission lines for magnetic thin film memories," *IEEE Trans. on Magnetics.,* vol.4, no.4, pp.272-276, Dec. 1965.

[38] C.L.Bertin, "Transmission-line response using frequency techniques," *IBM J. Res. Develop.,* vol.8, pp.52, 1964.

[39] E.F.Miersch and A.E.Ruehli, "Analysis of lossy coupled transmission lines," *IBM Technical Disclosure Bulletin,* vol.19, no.6, pp.2363-2365, 1976.

[40] C.S.Chang, "Electrical design of signal lines for multilayer oriented circuit boards," *IBM J. Res. Develop.,* vol.32, no.5, pp.647-657, Sep. 1988.

[41] C.R.Paul, "Modeling electromagnetic interference properties of printed circuit boards," *IBM J. Res. Develop.,* vol.33, no.1, pp.33-50, Jan. 1989.

[42] A.Deutsch, G.V.Kopcsay *et al*, "High-speed signal propagation on lossy transmission lines," *IBM J. Res. Develop.,* vol.34, no.4, pp.601-615, Jul. 1990.

[43] M.S.Lin, A.H.Engvik and J.S.Loos, "Measurement of transient response on lossy microstrips with small dimensions," *IEEE Trans. on Circuit Syst.,* vol.CAS-37, no.11, pp.1383-1393, Nov. 1990.

[44] P.Graneau, "Alternating and transient conduction currents in straight conductors of any cross-section," *J.Electron.,* vol.19, pp.41-59, 1965.

[45] P.Silvester, "Modal network theory of skin effect in flat conductors," *Proc. IEEE,* vol.54, no.9, pp.1147-1151, Sep. 1966.

[46] P.Silvester, "The accurate calculation of skin effect of complicated shape," *IEEE Trans. Power App. Sys.,* vol.PAS-87, pp.735-742, Mar. 1968.

[47] B.D.Popovic and Z.D.Popovic, "Method of determining power-frequency current distribution in cylindrical conductors," *Proc. IEE,* vol.119, no.5, pp.569-574, May 1972.

[48] G.Costache, "Finite-element solution of steady-state skin-effect problems in straight flat conductors," *COMPEL-Int. J. Comput. and Math. in Elec. and Electron. Eng.*, vol.2, no.2, pp.35-39, 1983.

[49] P.Waldow and I.Wolff, 'The skin-effect at high frequencies," *IEEE Trans. on Microwave Theory Tech.*, vol.MTT-33, no.10, pp.1076-1082, Oct. 1985.

[50] A.C.Cangellaris, "The importance of skin-effect in microstrip lines at high frequencies," *IEEE MTT-S Int. Microwave Symp. Dig.*, pp.197-198, 1988.

[51] Qingjian Yu and O.Wing, "Computational Models of transmission lines with skin effects and dielectric loss," *IEEE Trans. on Circuit and Syst. I: Fun. Theory and Appl.*, vol.CAS-41, no.2, pp.107-119, Feb. 1994.

[52] A.R.Djordjevic and T.K.Sarkar, 'Closed-form formulas for frequency-dependent resistance and inductance per unit length of microstrip and strip transmission lines," *IEEE Trans. on Microwave Theory Tech.*, vol.MTT-42, no.2, pp.241-248, Feb. 1994.

[53] A.Timotin, "Wave propagation on unifilar line with ground return," *Rev. Roum. Sci. Techn. - Electrotechnique et Energetique*, vol.15, no.2, pp.175-194, Bucarest, 1970.

[54] A.Timotin and A.Nicolae, "Skin-effect in shielded straight flat conductors," *Rev. Roum. Sci. Techn. - Electrotechnique et Energetique*, vol.17, no.1, pp.3-22, Bucarest, 1972.

[55] A.Timotin and A.Nica, "A method of numerical integration of the telegrapher's equation for transmission lines with losses," *Rev. Roum. Sci. Techn. - Electrotechnique et Energetique*, vol.23, no.1, pp.71-84, Bucarest, 1978.

[56] C.-S.Yen, Z.Fazarinc and R.L.Wheeler, "Time-domain skin-effect model for transient analysis of lossy transmission lines," *Proc. IEEE*, vol.70, no.7, pp.750-757, Jul. 1982.

[57] F.Durbin, 'Numerical inversion of Laplace transforms: an efficient improvement to Dubner and Abate's method,' *The Computer Journal*, vol.17, pp.371-376, 1974.

[58] J.N.Reddy, *An Introduction to the Finite Element Method*, McGraw-Hill, New York, 1985.

[59] Francis B.Hildebrand, *Method of Applied Mathematics*, Prentice-Hall, Englewood Cliffs, N.J., 1965.

[60] X.-D.Cai, G.I.Costache, 'Finite element analysis of a Triple-TEM cell,' to appear in *IEEE Trans. on EMC*, Nov. 1994 issue.

[61] R.F.Harrington, *Time-Harmonic Electromagnetic Fields*, McGraw-Hill, New York, 1965, Ch.7, p.345.

[62] H.-T.Chen and C.-K. Chen, 'Hybrid Laplace transform/ finite element method for two-dimensional transient heat conduction,' *J. Thermophysics*, vol.2, pp.31-36, 1988.

[63] T.-M.Chen, 'A modified hybrid Laplace transform/ finite element for transient heat conduction problems,' *Comp. Meth. App. Mech. Eng.*, vol.98, pp.261-272, 1992.

[64] F.B.J.Leferink, "A Triple-TEM cell: three polarizations in one setup," *Proc. 10th International Symposium on EMC,* pp.573-578, Zurich, 1993.

[65] D.Waser, "Radiated emissions test performance of the GHz TEM cell," 6ème *Colloque International et Exposition sur la Compatibilité Electromagnétique,* pp. 201-208, Lyon, France, June 2-4, 1992.

[66] J.C.Tippet and D.C.Chang, "Characteristic impedance of a rectangular coaxial line with offset inner conductor," *IEEE Trans. on Microwave Theory Tech.,* vol.MTT-26, no.2, pp.876-883, Nov. 1978.

[67] R.D.Leo, T.Rozzi, and L.Zappelli, "Rigorous Analysis of the GTEM cell," *IEEE Trans. on Microwave Theory Tech.,* vol.MTT-39, no.3, pp.488-500, March 1991.

[68] X.-D.Cai and J.-Y. Li, "Analysis of asymmetric TEM cell and its optimum design of electric field distribution," *Proc. IEE, Pt.H,* vol.136, no.3, pp. 191-194, Jun. 1989.

[69] R.J.Spiegel, W.T.Joines, C.F.Blackman, and A.W.Wood, "A method for calculating electric and magnetic fields in TEM cells at ELF," *IEEE Trans. on Electromagn. Compat.*, vol.EMC-29, no.4, pp.265-272, Nov. 1987.

[70] P.F.Wilson and M.T.Ma, "Simple approximate expressions for higher order mode cutoff and resonant frequencies in TEM cells," *IEEE Trans. on Electromagn. Compat.*, vol.EMC-28, no.3, pp.125-130, Aug. 1986.

[71] S.K.Das and B.K.Sinha, "Numerical solution of higher order mode cut-off frequencies in symmetric TEM cells using finite element method," *IEEE Trans. on Electromagn. Compat.*, vol.EMC-32, no.4, pp.264-268, Nov. 1990.

[72] J.-J. Zhang and J.-M. Fu, "Higher order mode cutoff frequencies in TEM cells calculated with TLM method," *IEEE Trans. on Electromagn. Compat.*, vol.EMC-30, no.4, pp.563-567, Nov. 1988.

[73] T.Tanaka T.Honma and I.Kaji, "A boundary-element analysis of TEM cells in three dimensions," *IEEE Trans. on Electromagn. Compat.*, vol.EMC-28, no.4, pp.179-184, Nov. 1986.

[74] M.L.Crawford, "Generation of standard EM fields using TEM transmission cells," *IEEE Trans. on Electromagn. Compat.*, vol.EMC-16, no.4, pp.189-195, Nov. 1974.

[75] D.A.Hill, "Bandwidth limitations of TEM cells due to resonances," *Journal of Microwave Power,* vol.18, no.2, pp.181-195, 1983.

[76] X.-D.Cai and G.I.Costache, "Theoretical modeling of longitudinal variations of electric field and line impedance in TEM cells," *IEEE Trans. on Electromagn. Compat.*, vol.EMC-35, no.3, pp.398-401, Aug. 1993.

[77] X.-D.Cai and G.I.Costache, "A Laplace domain finite element method (LDFEM) applied to diffusion and propagation problems," accepted by *Int. J. of Numerical Modelling - Electronic Network, Devices and Fields.*

[78] R.L.Khan and G.I.Costache, "Finite element method applied to modeling crosstalk problems on printed circuit boards," *IEEE Trans. on Electromagn. Compat.*, vol.EMC-31, no.1, pp.5-15, Feb. 1989.

[79] D.Hansen, P.Wilson, D.Koenigstein, and H.Garbe, "Emission and susceptibility testing in a tapered TEM cell," *Proc. 8th International Symposium on EMC*, pp.227-232, Zurich, 1989.

[80] X.-D.Cai and G.I.Costache, "An optimum engineering design approach of a Triple-TEM cell using finite element method" *Proc.International Symposium on EMC*, Sendai, Japan, pp.332-335, May 1994.

[81] R.L.Wigington and N.S.Nahman, "Transient analysis of coaxial cables considering skin effect," *Proc. IRE*, vol.45, pp.166-174, Feb. 1957.

[82] N.S.Nahman and D.R.Holt, "Transient analysis of coaxial cables using the skin effect approximation $A + B\sqrt{s}$," *IEEE Trans. on Circuit Theory*, vol.CT-19, no.5, pp.443-451, Sep. 1972.

[83] M.S.Lin, A.E.Engvik and J.S.Loos, "Measurements of transient response on lossy microstrips with small dimensions," *IEEE Trans. on Circuits and Systems*, vol.CS-37, no.11, pp.1383-1393, Nov. 1990.

[84] A.Timotin, "Longitudinal transient parameters of a unifilar line with ground return," *Rev. Roum. Sci. Techn. - Electrotechnique et Energetique*, vol.12, no.4, pp.523-535, Bucarest, 1967.

[85] E.S.Mok and G.I.Costache, "Skin-effect consideration on transient response of a transmission line excited by an electromagnetic pulse," *IEEE Trans. on Electromagn. Compat.*, vol.EMC-34, no.3, pp.320-329, Aug. 1992.

[86] G.I.Costache, S.K.Xavier and P.Bhartia, "Design suppressors for fast transients," *Proc. IEEE 1984 Int. Symp. on Electromagn. Compat.*, pp.729-731, 1984.

[87] W.T.Weeks, L.L.Wu, M.F.McAllister and A.Singh, "Resistive and inductive skin effect in rectangular conductors," *IBM J. Res. Develop.* vol.23, no.6, pp.652-660, Nov. 1979.

[88] G.I.Costache, "Finite element method applied to skin-effect problems," *IEEE Trans. on Microwave Theory Tech.*, vol.MTT-35, no.11, pp.1009-1013, Nov. 1987.

[89] F.Oberhettinger and L.Badii, *Tables of Laplace Transforms,* Spring-Varlag, 1973.

[90] F.Romeo and M.Santomauro, 'Time domain simulation of n coupled transmission lines," *IEEE Trans. on Microwave Theory Tech.,* vol.MTT-35, no.2, pp.131-137, Feb. 1987.

[91] D.S.Gao, A.T.Yang and S.M.Kang, "Modeling and simulation of interconnection delays and crosstalk in high-speed integrated circuits," *IEEE Trans. on Circuits and Systems,* vol.CS-37, no.1, pp.1-9, Jan. 1990.

[92] G.I.Costache, "Transient proximity effect and longitudinal transient parameters of a bifilar transmission line, *Rev. Roum. Sci. Techn. - Electrotechnique et Energetique,* vol.16, no.1, pp.111-124, Bucarest, 1971.

[93] A.Djordjevic, R.F.Harfington, T.Sarkar and M.Bazdar, *Matrix Parameters for Multiconductor Transmission Lines: Software and User's Manual*, Artech House, Norwood, 1989

[94] A.Djordjevic, T.Sarkar, R.F.Harfington and M.Bazdar, *Time-Domain Response of Multiconductor Transmission Lines: Software and User's Manual*, Artech House, Norwood, 1989

[95] C.R.Paul, *Introduction to Electromagnetic Compatibility,* John Wiley Sons, p.731, 1992.

[96] A.C.Cangellaris, J.L.Prince and R.Senthinathan, "Modeling of power/ground plane parasitics and investigation of their contribution to the effective inductance of V_{DD}/V_{SS} chip-package interface," *Proc. IEEE VLSI @ GaAs Chip Packaging Workshop,* p.32, Oct. 1991.

[97] M.A.Schmitt, K.Lam and L.E.Mosley *et al*, "Current distribution in power and ground planes of a multilayered pin grid array package," *Proc. 8th Int. Electronics Packaging Conference,* p.467, Nov. 1988.

[98] R.L.Hill, T.V.Doren, T.Hubing, J.Drewniak, "Common mode currents induced on wires attached to multilayer printed wire boards with segmented ground planes," *Proc. IEEE Int. Symp. EMC,* pp.116-120, Aug. 1994.

[99] X.-D.Cai, Redouanne Laroussi and G.I.Costache, *Computer Simulation of Partial Inductance of Package Reference (Power and Ground) Planes with FEM: Software and User's Manual,* Sponsored by Northern Telecom, June 1994.

[100] D.K.Cheng, *Field and Wave Electromagnetics,* Addison-Wesley, p.244, 1983.

[101] L.C.Shen and J.A.Kong, *Applied Electromagnetics,* Books/Cole Engineering Division, p.399, 1983.

[102] T.K.Sarkar, Z.A.Maricevic, J.B.Zhang and A.R.Djordjevic, "Evaluation of excess inductance and capacitance of microstrip junctions," *IEEE Trans. on Microwave Theory Tech.,* vol.MTT-42, no.6, pp.1095-1097, Jun. 1994.

[103] J.-M. Jong, L.A.Hayden and V.K.Tripathi, "Time domain characterization of coupled interconnections and discontinuities," *IEEE MTT-S Int. Microwave Symp. Dig.,* pp.1129-1132, May 1994.

[104] P.H.Harms and R.Mittra, "Equivalent circuits for multiconductor microstrip bend discontinuities," *IEEE Trans. on Microwave Theory Tech.,* vol.MTT-41, no.1, pp.62-69, Jan. 1993.

[105] J.-M. Jong, B.Janko and V.Tripathi, "Equivalent circuit modeling of interconnects from time-domain measurements," *IEEE Trans. on Comp. Hybrids, Manuf. Technol.,* vol.16, no.1, pp.119-126, Feb. 1993

[106] J.-M. Jong and V.Tripathi, "Time-domain characterization of interconnect discontinuities in high-speed circuits," *IEEE Trans. on Comp. Hybrids, Manuf. Technol.,* vol.15, no.5, pp.497-504, Aug. 1992.

[107] R.Mittra, W.D.Becker and P.H.Harms, "A general purpose Maxwell solver for the extraction of equivalent circuits of electronic package components for circuit simulation," *IEEE Trans. on Circuits and Systems-Fundamental Theory Appli.,* vol.39, no.11, pp.964-973, Nov. 1992.

[108] W.D.Becker, P.H.Harms and R.Mittra, "Time-domain electromagnetic analysis of interconnects in a computer chip package," *IEEE Trans. on Microwave Theory Tech.,* vol.MTT-40, no.12, pp.2155-2163, Dec. 1992.

[109] A.F.Thomson and A.Gopinath, "Calculation of microstrip discontinuity inductances," *IEEE Trans. on Microwave Theory Tech.*, vol.MTT-23, no.8, pp.648-655, Aug. 1975.

[110] B.Easter, "The equivalent circuit of some microstrip discontinuities," *IEEE Trans. on Microwave Theory Tech.*, vol.MTT-23, no.8, pp.655-660, Aug. 1975.

[111] A.Gopinath, A.F.Thomson and I.M.Stephenson, "Equivalent circuit parameters of microstrip step change in width and cross junctions," *IEEE Trans. on Microwave Theory Tech.*, vol.MTT-24, no.3, pp.142-144, Mar. 1976.

[112] P.A.Kok and D.D.Zutter, "Scalar magnetostatic potential approach to the prediction of the excess inductance of grounded via's and via's through a hole in a ground plane," *IEEE Trans. on Microwave Theory Tech.*, vol.MTT-42, no.7, pp.1229-1237, Jul. 1994.

[113] T.Wang, R.F.Harrington and J.R.Mautz, "Quasi-static analysis of a microstrip via through a hole in a ground plane," *IEEE Trans. on Microwave Theory Tech.*, vol.MTT-36, no.6, pp.1008-1013, Jun. 1988.

[114] S.Maeda, T.Kashiwa and I.Fukai, "Full wave analysis of propagation characteristics of a through hole using the finite-difference time-domain method," *IEEE Trans. on Microwave Theory Tech.*, vol.MTT-39, no.12, pp.2154-2159, Dec. 1991.

[115] R.Sorrentino, F.Alessandri, M.Mongiardo, G.Avitabile and Luca Roseli, "Full-wave modeling of via hole grounds in microstrip by three- dimensional mode matching technique," *IEEE Trans. on Microwave Theory Tech.*, vol.MTT-40, no.12, pp.2228-2234, Dec. 1992.

[116] E.Pillai and W.Wiesbeck, "Derivation of equivalent circuits for multilayer printed circuit board discontinuities using full wave models," *IEEE Trans. on Microwave Theory Tech.*, vol.MTT-42, no.9, pp.1774-1783, Sep. 1994.

[117] X.-D.Cai and G.Costache, "Time domain analysis of lossy interconnect with a novel skin effect model," submitted to *IEEE Trans. on Microwave Theory Tech.*,

[118] D.N.Ladd and G.Costache, "SPICE simulation used to characterize the cross-talk reduction effect of additional tracks grounded with vias on printed circuit boards," *IEEE Trans. on Circuits and Systems-II: Ana. Dig. Sig. Pro.,* vol.39, no.6, pp.342-347, Jun. 1992.

[119] J.Vlach and K.Singhal *Computer Methods for Circuit Analysis and Design,* Van Nostrand Reinhold Company, New York, 1983.

[120] R.Faraji-Dana, Y.L.Chow 'The current distribution and AC resistance of a microstrip structure," *IEEE Trans. on Microwave Theory Tech.,* vol.MTT-38, no.9, pp.1268-1277, Sep. 1990.

[121] E.Pettenpaul, H.Kapusta, A.Weisgerber, H.Mampe, J.Luginsland and I.Wolff, 'CAD models of lumped elements on GaAs up to 18GHz," *IEEE Trans. on Microwave Theory Tech.,* vol.MTT-36, no.2, pp.294-304, Feb. 1988.

[122] *Design Guidelines for Electronic Packaging Utilizing High -Speed Techniques,* ANSI/IPC-D-317, pp.33, 1990.